STUDIES

IN

NUCLEAR PHOTODISINTEGRATION

A Thesis
submitted for the degree of
Doctor of Philosophy
in the
Australian National University

by

H.J.Hay M.Sc.

1957

The experiments described in this thesis were performed at the Research School of Physical Sciences, the Australian National University, during the tenure of a scholarship awarded by the University. Some of the experiments were undertaken in collaboration with other people, and where the responsibility for portions of the work can be divided, the specific contributions were as follows:

(1) The measurement of the photoneutron cross section of tantalum was an extension of work in which Dr.J.H.Carver was engaged at the Cavendish Laboratory, Cambridge. He designed the Geiger counter, we conducted the irradiations together, and I was wholly responsible for the operation of the counter and reduction of the activation data. Calculation of the final results was undertaken independently.

(2) The proportional counter used in the study of the photodisintegration of carbon was provided by Dr.J.H. Carver. Some new photographic plate data, collected by Professor E.W.Titterton in the course of other experiments, was used in the interpretation of the results.

(3) For the investigation of the disintegration of neon I was joined by Dr.J.B.Warren from the University of British Columbia. The proportional counter was his, and I designed the gridded ionisation chamber with which most of the results were obtained.

The results of the experiments on tantalum and carbon have been published in the Philosophical Magazine, Ser.7.vol.44,p.1191 (1953) and vol.46,p.841 (1955).

With the exceptions already mentioned and apart from the usual discussions with other workers in the laboratory, this thesis embodies the results of my own work.

H. J. Hay.

ACKNOWLEDGEMENTS.

I wish to express my appreciation to Dr.J.H.Carver for his guidance and encouragement in the course of this work, to Mr.N.F.Bowkett for his able assistance in operating the H.T. set,and to Dr.F.C.Barker and Dr. P.B.Treacy for many helpful discussions. It is also a pleasure to record my gratitude to Dr.E.K.Inall for his advice and assistance with the design and assembly of the accelerator tube for the 600 kV generator at the Research School of Physical Sciences.

H.J.H.

TABLE OF CONTENTS.

	Page
CHAPTER 1. Introduction	1
CHAPTER 2. The Photodisintegration Process	
2.1 The Compound Nucleus	8
2.2 The Absorption Probability	10
2.3 Special Models for the Giant Resonance	12
2.4 Sum Rule Calculations	14
2.5 Direct Photodisintegration and the Compound Nucleus	19
2.6 Isotopic Spin Selection Rules	22
CHAPTER 3. Experimental Apparatus	
3.1 The Radiation Source	26
3.2 The Gamma Flux Measurement	28
3.3 The Tantalum Geiger Counter	32
3.4 The Methane Counter	35
3.5 The Nitrogen Counter	40
3.5.1 Gas purification and filling the counter	42
3.5.2 The pulse shape and electron mobility	44
3.5.3 Energy resolution in the presence of radiation	50
3.6 The Neon Counters	
3.6.1 The proportional counter	54
3.6.2 The gridded ionisation chamber	57
3.7 The Wall Effect in a Cylindrical Counter	62
CHAPTER 4. The Cross Section for $Ta^{181}(\gamma n)Ta^{180}$ at 17.6 MeV.	
4.1 Introduction	68
4.2 Irradiation of the Tantalum	71
4.3 Analysis of the Results	75
4.4 Conclusion	78

Page

CHAPTER 5. Cross Sections for the Reaction $C^{12}(\gamma,3\alpha)$ in the Energy Range 12 - 18 MeV.

5.1 Introduction 81
5.2 The Counter Experiment 82
5.3 The Cross Section at 17.6 MeV. 83
5.4 Photographic Plate Measurements 90
5.5 The Cross Sections at 14.8 and 12.3 MeV. 93

CHAPTER 6. The Reaction $N^{14}(\gamma\alpha)B^{10}$ at 17.6 MeV.

6.1 Introduction 97
6.2 Experimental Method 98
6.3 Experimental Results 101
6.4 Discussion of Results 110

CHAPTER 7. The Photodisintegration of Neon

7.1 Introduction 112
7.2 Possible Reactions in Neon 114
7.3 Experimental Results
7.3.1 For the 440 kV. resonance radiation 115
7.3.2 Non-resonant radiation, E_p=400-900 kV. 124
7.4 Discussion of Results 128

APPENDIX 1. The Wall Effect in a Cylindrical Counter 131

APPENDIX 2. A Note on the Maximum Voltage of a Cockcroft-Walton Generator under Load 137

STUDIES IN NUCLEAR PHOTODISINTEGRATION.

CHAPTER 1.

INTRODUCTION.

The transformations of nuclei following the absorption of photons would appear to have considerable advantages over the study of particle induced reactions for investigating nuclear structure. The chief features of the electromagnetic interaction are well understood, and the interaction is weak so that radiation may not disturb the nucleus under investigation as much as a particle reaction would. Hence one might hope that the photodisintegration process could be understood before other nuclear reactions. Unfortunately, there are difficulties on both the theoretical and experimental sides which rather offset these advantages. The processes are expected to depend very sensitively on the details of the charge and current distribution inside the nucleus. This distribution depends not only on the nucleon motions but also, for the case of exchange forces, on the motion of the charged meson cloud. The determination of the nucleon motion is hindered by our present ignorance concerning nuclear forces and by the

mathematical intractability of the many-body problem. A theoretical treatment of the exchange currents is even more difficult.

The development in recent years of betatrons and synchrotrons has provided intense gamma ray sources, and with their use the elucidation of the main features of photonuclear processes has advanced quickly. The excitation function for all photo-induced reactions in any given nucleus is unusual in that it displays a pronounced resonance. For all elements this resonance is about 6 MeV wide and the peak energy lies in the range 15-20 MeV; the peak energy slowly decreases with increasing atomic number while the cross section integrated over all energies increases. The discovery of this 'giant resonance' and the measurement of the energy and angular distributions of the reaction products has stimulated a considerable amount of theoretical work.

The essential results for the photodisintegration of the deuteron at energies up to 20 MeV have been described by the effective range calculations of Bethe and Longmire[1] and Austern[2], and the low energy photoeffect in Be^9 has been treated remarkably successfully by Guth and Mullin[3,4] using an independent particle model.

---

1. Bethe, H.A., and Longmire, C. Phys. Rev. 77:647 (1950).
2. Austern, N. Phys. Rev. 92:670 (1953).
3. Guth, E., and Mullin, C.J. Phys. Rev. 76:234 (1949).
4. Guth, E., and Mullin, C.J. Phys. Rev. 76:682 (1949).

Photodisintegration in other light nuclei can not be as well described as these two cases have been, but a useful unifying principle, the isotopic spin selection rule proposed by Radicati[5] and Gell-Mann and Telegdi[6], is applicable to nuclei of mass number up to about 20. Various models for the photoeffect in medium and heavy nuclei have been proposed, ranging from the independent particle (shell) model calculations of Burkhardt[7], Reifman[8], and Wilkinson[9], to the opposite extreme of the collective model, exemplified in the work of Goldhaber and Teller[10], Steinwedel and Jensen[11], Danos[12], and Ferentz, Gell-Mann and Pines[13]. Goldhaber and Teller's work was important because they were the first to emphasise the dipole nature of the large photonuclear cross sections found in the giant resonance. The sum rule calculations for the integrated cross section (e.g. Levinger and Bethe[14]), which use only the ground state wave functions, show that any specific model will fail unless it gives an integrated dipole cross section of about 0.06NZ/A MeV-barn.

---

5. Radicati, L.A., Proc. Phys. Soc. A66:139 (1953).
6. Gell-Mann, M. and Telegdi, V.L., Phys. Rev. 91:169 (1953).
7. Burkhardt, J.L., Phys. Rev. 91:420 (1953).
8. Reifman, A., Z. Naturforsch. 8a:505 (1953).
9. Wilkinson, D.H., Proceedings of the 1954 Glasgow Conference on Nuclear and Meson Physics, p.161.
10. Goldhaber, G. and Teller, E., Phys. Rev. 74:1046 (1948).
11. Steinwedel, H. and Jensen, J.H.D., Z. Naturforsch. 5a:413 (1950).
12. Danos, M., Ann. d. Phys. 10:265 (1952).
13. Ferentz, M., Gell-Mann, M. and Pines, D. Phys. Rev. 92:836 (1953).
14. Levinger, J.S. and Bethe, H.A. Phys. Rev. 78:115 (1950).

In general, the photodisintegration process in heavy elements is fairly well described by the statistical theory of the decay of a uniformly excited compound nucleus, although the anomalously large emission of high energy protons and their anisotropic angular distribution are not consistent with this description. These difficulties may be explained qualitatively by Courant's[15] theory of a direct photoeffect, though it fails quantitatively by a factor of about 20. The theory, based on shell-model wavefunctions, proposed by Wilkinson[9], gives a direct cross section which shows resonance features and removes this discrepancy, at the same time retaining the possibility of compound nucleus formation.

Experimentally, photodisintegration is a difficult subject to study, mainly because the interaction is weak and consequently the cross sections are small, about 100 mb even at their maximum. Monochromatic high energy gamma ray sources are usually (pγ) reactions, which have the disadvantage of low intensity and often the complication of several lines. High intensities of radiation are available from betatrons and synchrotrons, but the continuous spectrum makes accurate interpretation of the experiments much more difficult. The methods which are available for measurement of the energy and intensity

15. Courant, E.D. Phys. Rev. 82:703, (1951).

of the radiation at the very short wave lengths used are extremely crude compared to the methods of optical spectroscopy.

The most convincing evidence for the giant resonance has been obtained from (γn) cross sections which have been measured in many nuclei by activation techniques. The limitation to (γn) cross sections is not so important in heavy nuclei, where neutron emission is the most probable process, but with light nuclei the proportion of charged particle emission increases, so that detailed information is required about other photonuclear reactions such as (γp), (γd), $(\gamma \alpha)$, (γpn), etc. Because the charged particles must be detected in the presence of a high radiation background, the measurement of absolute yields and energy distributions is not always easy or certain.

The most widely applicable method for making these studies is the photographic emulsion, which gives good discrimination between the various emitted particles. Since the emulsion is continuously sensitive, it can be used with low intensity $(p\gamma)$ line sources; it is also useful with betatron sources because the energy of the incident photon may usually be deduced from measurements on the tracks. In both cases, the relative sensitivity of the emulsions used allows particle detection in a

high background of radiation and electrons. Two other important detecting instruments, namely the cloud chamber and the gas counter, cannot always be employed since relatively few nuclei are available in a suitable gaseous form. The cloud chamber has many of the advantages of the photographic emulsion when large gamma fluxes are available, and individual reactions can be studied in detail; the gas counter provides a very quick method of collecting large numbers of events for studying relative cross sections, its main shortcoming being that only the total energy release of a reaction is measured.

In this thesis will be described some studies of (γn), (γp) and $(\gamma \alpha)$ reactions induced by the 14.8 and 17.6 MeV radiations from the $Li^7(p\gamma)Be^8$ reaction. The (γn) cross section of Ta^{181} was investigated by measuring the Ta^{180} radioactivity in a Geiger counter constructed from tantalum. The $(\gamma \alpha)$ and (γp) reactions were detected in ionisation chambers containing methane, nitrogen or neon. The counter gas itself contained the isotope being studied, so that counting over all directions of emission was achieved. To provide sufficient stopping power a large mass of gas was necessary, which meant using high pressure counters. Variation of the pressure permitted discrimination between protons and alpha particles. With large gamma fluxes, many electrons

are ejected from the counter walls, hence fast counters operating by electron collection are required, and the presence of electronegative gases can not be tolerated. Even the commonly used gases argon, hydrogen, and methane at moderate pressures may show unpredictable effects and anomalies in the speed and completeness of ion collection, because of the presence of small amounts of normally harmless impurities. Each different gas which was used for the photodisintegration studies therefore required separate consideration and investigation of the conditions necessary for successful counter operation. Details of the counters will be given.

CHAPTER 2.

THE PHOTODISINTEGRATION PROCESS.

2.1. The Compound Nucleus.

The Bohr theory of the compound nucleus can be applied for a general description of the nuclear photo-effect at low energies, though some experimental data require the assumption of direct photo-ejection of nucleons from an irradiated nucleus.

Following the absorption of a quantum of energy E_γ, the excited nucleus may decay through different channels, and the cross section for emission of a particle 'a' can be written as

$$\sigma(\gamma, a) = \sigma_c(E_\gamma) G_a$$

where $\sigma_c(E_\gamma)$ is the capture cross section for photons of energy E_γ, and G_a, the branching probability for emission of the particle 'a' against competition from other modes of decay, is given by

$$G_a = \frac{\Gamma_a}{\sum_i \Gamma_i}$$

with Γ_i the partial width for emission of particle 'i'.

At low energies, below the binding energy of the least tightly bound nucleon, only scattering of the

gamma ray can occur. Above the threshold for emission of a particle, the cross section will rise with increasing energy, and its shape will depend on several factors, including:

(i) the capture probabilty $\sigma_c(E_\gamma)$,

(ii) the importance of competition from emission of other particles,

(iii) the effects of selection rules applying to the emission of the particular particle.

In light nuclei at moderate excitation the energy states of the compound nucleus are widely spaced relative to their widths, so it is expected that individual level properties will be important both in exhibiting resonance absorption effects for the formation of the compound nucleus, and in determining the energy and angular distributions of particles emitted to various states of the residual nuclei. In heavier nuclei, and for higher excitations, the widths of the compound levels are larger than the level spacings, so that many levels will contribute to the cross section at a given energy and it becomes possible to determine the branching probabilty from the expressions of the statistical theory (Weisskopf and Ewing[16]).

16. Weisskopf, V.F., and Ewing, D.H. Phys. Rev. 57:472 (1940).

2.2. The Absorption Probability.

At low energies, below about 25 MeV, where the gamma wave length is long compared to the nuclear size, classical radiation theory is applicable and shows that the main contributions to the absorption cross section will come from dipole and quadrupole transitions. Normally the electric dipole is expected to dominate, since the electric multipole intensity is greater than the magnetic multipole of the same order in the ratio $(\hbar/McR)^2$, which is of order 10^{-2}. However, the processes depend strongly on the mass and charge distributions inside the nucleus, and at low energies the electric dipole transitions may be forbidden, or at least severely reduced in probability. This is true for any nuclear model in which there exist strong correlations between the neutron and proton motions; for instance, in an alpha particle model the charge and mass centres coincide and so the electric dipole matrix elements vanish completely. Considerations such as these lead to the idea that at low energies, about 15 MeV, the main contributions to the capture cross sections come from electric quadrupole and magnetic dipole absorption, and above 15 MeV, when the photon energy is sufficient to disturb transient nucleon configurations, or disrupt an alpha-like structure, then

the electric dipole contribution will become effective resulting in a rapid rise in the cross section.

The rise to the characteristic giant resonance in all nuclei does in fact occur in the region 15-20 MeV, the general trend being toward lower energies as the mass number increases, so it is naturally interpreted as being due to the onset of electric dipole absorption. The fall of the cross section for emission of a particular particle could come about either from a genuine decrease in the absorption, or through a reduction in the probability for emission because of competition. In the case of (γn) reactions, competition will be expected when the $(\gamma 2n)$ threshold is exceeded, and Eyges[17] has shown that the peak (γn) cross section generally does occur at this energy. The relative importance of these two effects is not at all clear since every competing process cannot always be measured. In heavy nuclei neutron emission is dominant, and experiments on single and multiple neutron emission from tantalum indicate that competition cannot account for all of the decrease in the (γn) cross section.[18]

---

17. Eyges, L. Phys. Rev. 86:325 (1952).
18. See Chapter 4.

2.3. Special Models for the Giant Resonance.

To explain why different photodisintegration processes should have excitation functions of similar shapes and with peaks at such similar energies, Goldhaber and Teller[10] suggested a model in which there was an ordered dipole vibration within the nucleus. It was assumed that the excitation consisted of the protons moving in one direction against the neutrons moving in the opposite direction. The frequency would be high because of the strong binding between the protons and neutrons, and the width of the resonance would be due to transfer of energy from the ordered mode to other modes of nuclear motion. Several models were discussed, and calculations were carried through for the case of classical harmonic oscillations of protons and neutrons, as if they were two incompressible fluids which undergo relative displacement so that their surfaces no longer overlap. The total restoring force would then be proportional to the surface area, and for small displacements it was assumed proportional to the displacement. With not unreasonable choices of parameters and the simplifying assumption $N = Z = A/2$, the resonance frequency was found to be

$$\hbar\omega_0 = 40A^{-1/6}$$

in fair agreement with experimental results. The

integrated cross section for photon absorption was

$$\int_0^\infty \sigma \, dE = \frac{\pi^2 e^2 h}{2Mc} A = 0.015A \text{ MeV-barns.}$$

There are two main objections to this model: it is not clear why the neutrons and protons should have the nature of incompressible fluids, and there are two arbitrary parameters in the theory. The parameters, which appear in the coefficient of $A^{-1/6}$ in the expression for the resonance frequency, are related to the surface term in the empirical binding energy formula; the connection has been discussed by Present[19]. The width of the resonances, which can not be calculated explicitly, is considered to be due to the transfer of energy by coupling between the ordered dipole vibration and other modes of nuclear motion. With weak coupling only those gamma ray absorbing levels near the dipole resonance energy would be important.

Calculations have been made for other similar models, and the theory extended to higher order vibrations by Steinwedel and Jensen[11] and Danos [12]. The quadrupole resonance would be expected at 1.6 times the energy with only 8% of the integrated cross section of the dipole resonance. The higher orders make only small

19. Present, R.D. Phys. Rev. 77:355 (1950).

contributions to the cross section, and probably the peaks due to them could not be seen, though they may contribute to the high energy side and the tail of the dipole resonance. The $C^{12}(\gamma n)$ and $O^{16}(\gamma n)$ resonances, measured by Sagane[20], have tails extending up to 50 MeV, and measurements to higher energies by Jones and Terwilliger[21] indicate that for tantalum the cross section is flat from 30 to 80 MeV.

2.4. Sum Rules.

The integrated cross section for electric dipole absorption has been calculated by Levinger and Bethe[14], for no specific nuclear model, by using the sum rules for the matrix elements of the ground state wave function. The derivation needs only the quantum-mechanical expression for the commutator between the momentum and position operators. The displacement of the nucleons should be measured from the centre of mass of the nucleus, which makes it necessary to introduce an effective charge eN/A for protons, and -eZ/A for neutrons (Bethe[22]). For ordinary forces the integrated cross section for dipole absorption is

$$\int_0^\infty \sigma dE = 0.060\ NZ/A\ \text{MeV-barns}$$

20. Sagane, R. Phys. Rev. 84:587 (1951).
21. Jones, L.W., and Terwilliger, K.M. Phys. Rev. 91:699 (1953)
22. Bethe, H.A. Rev. Mod. Phys. 9:71 (1937).

which reduces to the Goldhaber-Teller result for $N = Z = A/2$. Feenberg[23] first showed that the sum rules are modified for exchange forces, Siegert[24] estimated that they would roughly double the integrated cross section, and Levinger and Bethe included the fraction, x, of the n-p exchange force as a parameter in the calculation. Assuming no correlation effects between nucleons (Hartree approximation), neglecting surface effects, and considering central forces only, for a square well and nuclear radius $r = 1.5\ 10^{-13} A^{1/3}$ cm, the above expression becomes

$$\int_0^\infty \sigma\, dE = 0.060\ \frac{NZ}{A}(1+0.8x)\ \text{MeV-barns.}$$

The n-p scattering experiments at high energies indicate that x lies between 0.5 and 0.7[25,26]. The neglect of the surface effect and the presence of other forces (e.g. spin-orbit coupling) will modify slightly the coefficient 0.8. Apart from this, the value for the integrated cross section is independent of the nuclear model. Frankel[27] has investigated the effect of spin-orbit interaction, finding that it has no effect on the integrated cross section, and less than a few tenths of

---

23. Feenberg, E. Phys. Rev. 49:328 (1936).
24. Siegert, A.J.F. Phys. Rev. 52:787 (1937).
25. Christian, R.S., and Hart, E.W. Phys. Rev. 77:441 (1950).
26. Kelly, E.L., Leith, C.E., Segre, E., and Wiegand, E.C. Phys. Rev. 79:96 (1950).
27. Frankel, S. Phys. Rev. 99:169 (1955).

an MeV on the average energy of absorption.

Sum rule calculations can also be used to give moments of the photon absorption curve, thus making it possible to estimate the mean energy of absorption. This further calculation requires a knowledge of the ground state wave function, which was unnecessary for the calculation of the integrated cross section, except for estimating the coefficient 0.8 for the effects of exchange forces. Levinger and Bethe defined two energies, the mean energy

$$\overline{E} = \int_0^\infty E\sigma dE \Big/ \int_0^\infty \sigma dE ,$$

and the harmonic mean energy

$$E_H = \int_0^\infty \sigma dE \Big/ \int_0^\infty \frac{\sigma dE}{E} .$$

For ordinary forces, with no correlations between nucleons, $\overline{E}$ is independent of A, and E_H is proportional to $A^{-2/3}$. The effect of exchange forces is to increase both mean energies, the values obtained being of the right order of magnitude but below the experimentally observed peak energies. The calculations do not give a detailed account of the shape of the absorption curve; it could be very broad or have a sharp maximum.

It is thought that the poor agreement between the calculated and observed energies is due to neglect of

correlations among the nucleons, and correlations are always present because of the Pauli exclusion principle. If an alpha particle model is used, then E_H is brought into better agreement with experiment. An alpha particle model cannot be used for all nuclei, but in cases where it can be applied, the sum rule predicts that electric dipole transitions are forbidden. However, at energies approaching 20 MeV (the energy of radiation from the reaction $T(p\gamma)He^4$) the alpha particles themselves could be disrupted and dipole transitions become possible. Although Weisskopf[28] considered the photodisintegration process in terms of quadrupole transitions, the sum rule calculations show that these transitions are only able to account for some 6-8% of the integrated dipole cross section. Blatt and Weisskopf[29], for instance, point out that in any nuclear model involving collective motion of the nucleons, or of nucleon sub-units, the electric dipole transitions may be suppressed, so that at energies below the giant resonance the absorption could be largely due to magnetic dipole and electric quadrupole interactions. At energies of 15 to 20 MeV, high enough to

28. Weisskopf, V.F. Phys. Rev. 59:318 (1941).
29. Blatt, J.M., and Weisskopf, V.F. 'Theoretical Nuclear Physics', Wiley (1952) pp. 651-659.

destroy particle correlations, electric dipole transitions start to occur with an intensity rising to several orders of magnitude greater than other transitions.

Measurements of neutron[30,31] and proton[32] yields show that individually neither is a smooth function of atomic number, especially for the light elements, but that their sum is, so that competition between neutron and proton emission can explain the fluctuations. For $Z > 40$ there are more neutrons than can be accounted for by (γn) reactions alone, and threshold considerations show that the increase must be due to multiple particle emission from $(\gamma, 2n)$, (γ, pn) type reactions[33]. The neutron multiplicity can be calculated by successive applications of the statistical evaporation theory. Levinger and Bethe[34] have interpreted the neutron yield measurements for $Z > 29$ in terms of multiple particle production, deriving for the integrated photo cross section

$$\int_0^\infty \sigma \, dE = 0.14 \frac{NZ}{A} \text{ MeV-barns.}$$

Although this is somewhat larger then the theoretical relation, they consider there is no clear discrepancy between theory and the experimental results.

30. Price, G.A., and Kerst, D.W. Phys.Rev. 77:806 (1950).
31. Terwilliger, K.M., Jones, L.W., and Jarmie, W.N. Phys.Rev. 82:820 (1951).
32. Mann, A.K., and Halpern, J. Phys.Rev. 82:733 (1951).
33. Cameron, A.G.W. Phys.Rev. 82:272 (1951).
34. Levinger, J.S., and Bethe, H.A. Phys.Rev. 85:577 (1952).

2.5. Direct Photodisintegration and the Compound Nucleus.

The idea of a compound nucleus formed by absorption of a photon then decaying by evaporation of nucleons, gives the main features of the photodisintegration processes for heavy nuclei. The rapid increase in level density with increasing excitation of the nucleus means that emission of low energy nucleons is favoured. Hence the energy distribution of photoneutrons is similar to that of a Maxwellian spectrum for which the characteristic temperature is that of the residual nucleus. However, for charged particles the effect of the Coulomb barrier must also be considered; for moderate excitation of high Z nuclei the emission of photoprotons is reduced, because very few have sufficient energy to overcome the barrier. The energy spectra and the relative probabilities of emission to be expected can be calculated by repeated applications of the equations of the statistical theory. A basic assumption about the compound nucleus, that it exists long enough for the excitation energy to be shared among all the nucleons and statistical equilibrium to be established, implies that the angular distribution of the emitted particles will most probably be isotropic[35].

35. Wolfenstein, L. Phys. Rev. 82:690 (1951).

Detailed studies of the energy distributions of photoprotons have been made by Curtis, Hornbostel, Lee and Salant[36] for rhodium, Diven and Almy[37] for silver, and Byerly and Stephens[38] for copper. In each case they found the yield of high energy protons was much larger than predicted by statistical theory. In addition, these protons were distinguished by a non-isotropic angular distribution having a maximum at right angles to the photon direction. Similar results have been found for fast photoneutrons by Byerly and Stephens in copper, and Poss[39] in bismuth, lead and tungsten.

Changes in the level density formula, nuclear temperature, and nuclear radius have been used by Schiff[40] and Diven and Almy in attempts to explain the departures from the normal compound nucleus expectations, but with little success. The anomalous results can be explained by postulating the direct ejection of nucleons from an irradiated nucleus. Calculations with this idea were first carried out by Courant[15] for an independent particle model of the nucleus, in which the Z protons occupy the Z lowest states in a square potential well. The

---

36. Curtis, N.W., Hornbostel, J., Lee, D.W., and Salant, E.O. Phys.Rev. 77:290 (1950).
37. Diven, B.C., and Almy, G.M. Phys.Rev. 80:407 (1950).
38. Byerly, P.R., and Stephens, W.E. Phys.Rev. 83:54 (1951).
39. Poss, H.L. Phys.Rev. 79:539 (1950).
40. Schiff, L.I. Phys.Rev. 73:1311 (1948).

absorption probability was calculated between this initial state and a final state in which one of the protons was raised into the continuum, the others remaining undisturbed. It is implied that the total photon absorption is due to a combination of absorption by individual neutrons and protons. The cross sections obtained were one or two orders of magnitude smaller than the experimental results require, but were very much larger than the statistical model predicted. Courant considered the disagreement was due to the crudity of the model; increases in the cross section would be obtained by using more complicated well shapes, taking account of exchange forces, and using the newer value for the nuclear radius, $1.2\ 10^{-13} A^{1/3}$ cm. The angular distributions for the interaction were independent of the exact shape of the nuclear potential, depending only on the angular momentum of the proton before and after emission. They differed for the transitions $l \rightarrow (l+1)$ and $l \rightarrow (l-1)$, but were of the general form $a+b\sin^2\theta$.

While the direct photonuclear effect is certainly dominant at high energies, it may also be important at low energies where the conventional compound nucleus explanation is so successful. The two ideas can be reconciled in the following way: the immediate emission of a nucleon need be only a small part of the total emission, because after absorbing a photon the nucleon

may not only be emitted but may also radiate or collide with other nucleons, thereby sharing its energy and forming a compound nucleus which decays in the normal way.

The success of the modified direct photoeffect postulate for describing the characteristics of the emission of high energy nucleons while retaining the possibility of compound nucleus formation, has been considerably extended by the calculations and suggestions advanced by Wilkinson[9]. Shell model wave functions were used for the initial and final states of the nucleus and shell model selection rules determined the allowed transitions. This model not only gave a direct cross section which was the required order of magnitude larger than that obtained by Courant, but also predicted the existance of a giant resonance with an integrated cross section which almost exhausted the dipole sum. The theory gave a variation of the resonance energy with mass number which, although 30% low in absolute value, showed the correct trend especially in the region of magic numbers, and the width of the resonance was also predicted very reasonably.

2.6. Isotopic Spin Selection Rules.

The concept of isotopic spin and the assumption of the charge independence of nuclear forces lead to selection rules which are potentially of great interest

in certain photodisintegration processes in light nuclei.

For nuclei with $Z \leq 10$, Radicati[5] showed that the total isotopic spin T should be a good quantum number, since the nuclear wave functions are little affected by the Coulomb repulsion between protons and the neutron-proton mass difference. As the electromagnetic interaction of nucleons is charge dependent, the total isotopic spin need not be conserved, but Radicati[41] has shown that definite selection rules determine the change in T for such processes. The rules can be summarised as:

(i) For all multipolarities, $\Delta T=0,\pm 1$ when $T_Z=\frac{N-Z}{2}\neq 0$

(ii) For electric dipole transitions only, $\Delta T=\pm 1$ when $T_Z=0$, otherwise as in (i).

If we integrate over all gamma energies, the main contribution to the photodisintegration cross section must come from electric dipole transitions. When the target nucleus is self-conjugate, i.e. $T_Z = 0$, this cross section cannot become large until T = 1 states in the compound nucleus can be excited. For (γn) and (γp) processes this happens for energies below the giant electric dipole resonance and the absorption is not inhibited. But when we are interested in the emission of T = 0 particles, such as deuterons or alpha particles,

41. Radicati, L.A. Phys. Rev. 87:521 (1952).

not only must the photon energy be enough to excite a T = 1 state in the compound nucleus, but the particle emission can only take place when there is enough energy to leave the residual nucleus also in a T = 1 state.

For even-even nuclei, in which $T_z=0$, the lowest T = 1 state is at a fairly high excitation W and the ground state has $J = 0^+$, Gell-Mann and Telegdi[6] have combined the usual conservation laws with the isotopic spin rules, and deduced the following rules for photon absorption:

(i) For $E_\gamma < W$, all absorption is either M1 via a state 1^+, T = 0, or E2 via a state 2^+, T = 0.

(ii) For $E_\gamma > W$, absorption to a T = 1 state can be M1, E2, or E1, but can result in deuteron or alpha particle emission only if there is sufficient energy to leave the residual nucleus in a T=1 state.

(iii) At any energy, (γd) or $(\gamma \alpha)$ reactions which leave the residual nucleus in a T = 0 state must proceed as in (i).

(iv) In particular, a $(\gamma \alpha)$ transition to the ground state of the residual nucleus may proceed only by E2 absorption through a state with T = 0, $J = 2^+$.

(v) The (γn) and (γp) cross sections must, for each residual state, be identical as functions of energy and angle, except to the extent that there is interference between transitions with $\Delta T = 0$ and other allowed transitions.

Because of impurity of the charge states, due to Coulomb forces and the neutron-proton mass difference, there will be a small probability of deuteron or alpha particle emission to a T = 0 state following M1, E2, or E1 absorption to a T = 1 state, Competition from neutron or proton emission would probably be strong enough to suppress this type of process.

CHAPTER 3.

EXPERIMENTAL APPARATUS.

3.1. The Gamma Ray Source.

Radiation was generated by bombarding an evaporated layer of metallic lithium with a resolved proton beam of up to 500 μA from the A.N.U. 1.2 MeV cascade generator. At all proton energies a mixture of radiations is produced from the $Li^7(p\gamma)Be^8$ reaction, the main components being due to radiative capture leading to the ground state of Be^8 and to the state of width about 2 MeV centred at 3 MeV, for which the Q values are 17.2 and 14.2 MeV respectively. Transitions to higher levels in Be^8 may also occur, but do so with intensities only 1% or 2% of the high energy transitions[42], so the radiation is usually undetectable. Both of the high energy lines are resonant at a proton energy of 440 keV, the mean photon energies being 17.6 and 14.8 MeV, and are individually isotropic at this energy. At other energies the angular distributions and relative intensities of the gamma rays alter[43,44,45]. Stearns and McDaniel[46], using

42. Inall,E.K. Phil.Mag.Ser.7,45:768 (1954).
43. Campbell,J.G. Aust.J.Phys.9:156 (1956).
44. Devons,S.,and Hine,M.G.N. Proc.Roy.Soc.199A:56,73 (1949).
45. Kraus,A.A.Jr. Phys.Rev.93:1309 (1954).
46. Stearns,M.B.,and McDaniel,B.D. Phys.Rev.82:450 (1951).

a pair spectrometer, measured the variation of intensity with angle at proton energies of 500 keV (thick target) and 1150 keV (250 keV target thickness); their results are summarised in Table 3.1. It will be seen that at

Table 3.1. Relative abundance of the $Li^7(p,\gamma)Be^8$ γ-rays.

	Angle	I_{14}	I_{17}	Intensity ratio
E_p = 500 keV	0°	1.00±.07	1.00±.07	1.70±.20
440 keV res.	35°	.97±.07	1.03±.07	1.80±.20
radiation	70°	.98±.07	.99±.07	1.72±.20
E_p = 1150 keV	0°	1.00±.05	1.00±.05	.62±.09
non-resonant	35°	.74±.06	.69±.06	.58±.10
radiation	75°	.77±.06	.56±.05	.45±.08

75° to the incident beam direction the abundance ratio changes by nearly 4 times; this change can be used to separate the effects of the two lines in experiments where the detector is insensitive to the energies of the photodisintegration products. At other proton energies no detailed information is available regarding the ratio of the high energy radiations. There may, in fact, be unsuspected errors in Stearns and McDaniel's results at 1150 keV, since the angular distribution for the total radiation deduced from their measurements does not agree with the angular distribution measured directly by Kraus[45].

At an incident energy of about 550 keV, excitation of the 477 keV level in Li^7 becomes possible by inelastic scattering of the protons; Kraus's results show that there is a copious yield of radiation from this reaction

at energies above 850 keV.

The absolute yield of high energy photons, according to the data of Fowler and Lauritsen[47], from a fresh clean lithium target at the 440 keV resonance is 1.9×10^{-8} gammas per proton (i.e. 1.2×10^{5} gammas per μC.), rising to 2.6×10^{-8} gammas per proton at 850 keV for a thick target.

3.2. The Gamma Flux Measurement.

The radiation was monitored by a thick walled brass Geiger counter of the type calibrated by Barnes, Carver, Stafford and Wilkinson[48]. Their counter efficiency for the $Li^7(p\gamma)$ resonance radiation was 2.5 counts/photon/cm^2 ($\pm$10%) for an active length of 8 cms. The efficiency of this type of counter will not depend critically on the exact composition of the brass, and as the present counter was constructed with the same pattern and dimensions, except for an active length of only 7.5cms, its efficiency was taken to be 2.35 counts/photon/cm^2 ($\pm$12%). Generally the flux observed for a given charge was only a fraction, 1/3 to 1/2, of that corresponding to the yield data of Fowler and Lauritsen; only when the target had been freshly laid down and had not become oxidised or otherwise contaminated was the full yield obtained.

47. Fowler, W.A., and Lauritsen, C.C. Phys.Rev. 76:314 (1949).
48. Barnes, C.A., Carver, J.H., Stafford, G.H., and Wilkinson, D.H. Phys.Rev. 86:359 (1952).

The consistency of operation of the Geiger counter was checked by means of a small Co^{60} gamma ray source giving about 2000 counts/min. The sensitivity of the counter during 3 years did not deviate from the average by more than 1%, due allowance being made for the Co^{60} decay (Fig.3.1). Short term variations in the counting rate were observed, with a magnitude up to five times the standard error for 10,000 counts. They appeared to be caused by changes in the gain of the electronic equipment and sometimes persisted for several hours.

When the proton energy was raised above 600 keV in order to alter the quality of the radiation, a NaI scintillation counter was used to permit discrimination against the low energy radiation from inelastic scattering of protons. For the experiments $Ta^{181}(\gamma n)Ta^{180}$ and $Ne^{20}(\gamma p)F^{19}$ in which the non-resonant radiation was used, a relative determination of the flux was sufficient since the absolute yields at lower energies were determined with the Geiger counter.

Background counts made with the beam stopping on a clean copper disc in place of the lithium target showed that very few counts were due to X-rays from the accelerator, the counting rate remaining at 32 counts/min. whether the H.T.set was operating or not. The target was normally run quite hot as a precaution against the

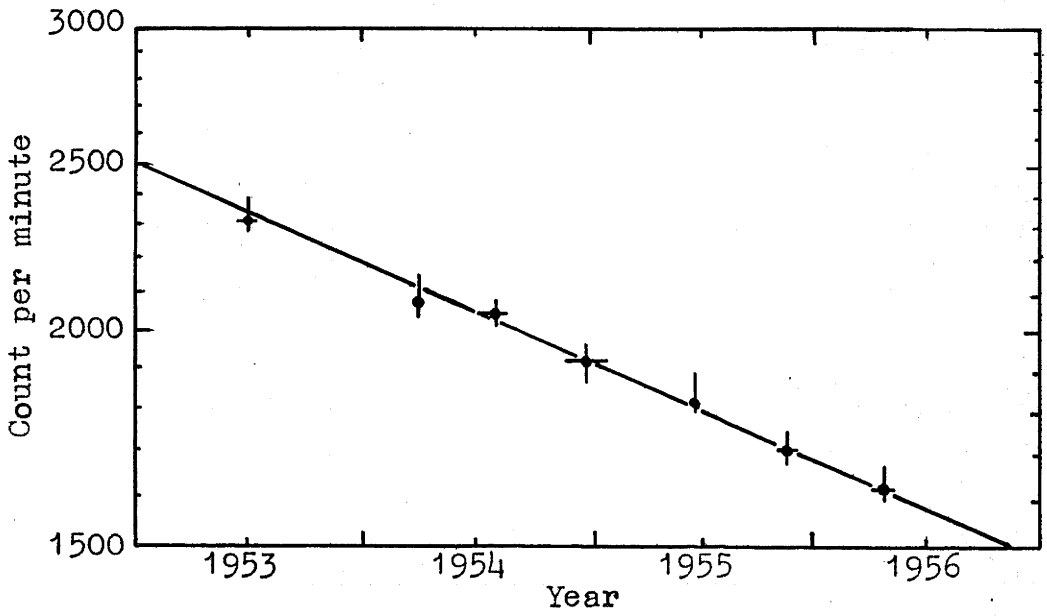

Fig.3.1 Thick walled brass Geiger counter sensitivity.

The count rate for a Co^{60} source in a standard position is compared with the 5.3 year half-life of Co^{60}. The plotted points show the mean rate during the period indicated by the horizontal bars. The vertical lines show the limits of the short term variations.

deposition of pump oil which would yield radiation from the $C^{12}(p\gamma)N^{13}$ reaction; after a run there was never evidence of any significant amount of 10 minute positron activity from the build-up of N^{13}.

The radiation is accompanied by neutrons, which arise from two sources. The first is from the action of the alphas, from $Li^7+p\rightarrow 2\alpha$, on the lithium of the target. The cross sections for the secondary Li^6 and $Li^7(\alpha n)$ reactions increase with increasing alpha energy, so the effect is greater at high proton energies. The neutron intensity is proportional to the square of the target thickness, whereas the gamma yield increases linearly with thickness, hence the relative neutron intensity can be reduced by using thinner targets. The second source of neutrons is photonuclear reactions in the target and other materials nearby; this source strength will be reduced by making the target mountings from the minimum amount of material. Since the $(n\alpha)$ reactions in Ne^{20} and N^{14} are relatively prolific, checks were made with a neutron sensitive scintillation counter (Hornyak button) and showed that the number of fast neutrons coming from the target regions was undetectable at the 440 keV resonance. A yield of 1 neutron/μC. (cf. 10^5 gammas/μC.) should have been easily observed.

3.3. The Tantalum Geiger Counter.

The counter, shown in Fig.3.2, had a cylindrical tantalum cathode, 1 inch in diameter and 4 inches in length. A tungsten wire of diameter 0.005" (kept taut by a tungsten spring) was taken through a glass capillary tube and along the axis of the counter, terminating in a glass bead at the other end of the counter. The body and ends of the counter were made from tantalum foil 0.010" thick, and along the axis of the counter were 9 equally spaced annular discs, also of tantalum, having 3/8" diameter holes at their centres. This method of construction exposed a large surface of tantalum within the counter and so improved the detection efficiency without requiring a complicated arrangement of several beta-counters, and it also ensured that the same geometrical arrangement could be easily repeated for all of the measurements.

After the counter had been evacuated and outgassed, it was filled to a pressure of 10 cms Hg with argon containing 10% of ethyl alcohol. It was operated as a Geiger counter, the plateau commencing at 910 volts and extending to 1030 volts, with a slope of 17% per 100 volts (Fig.3.3). Because of the steep plateau, presumably due to the shielding effect of the discs along the axis, it was necessary to operate the counter from a battery high

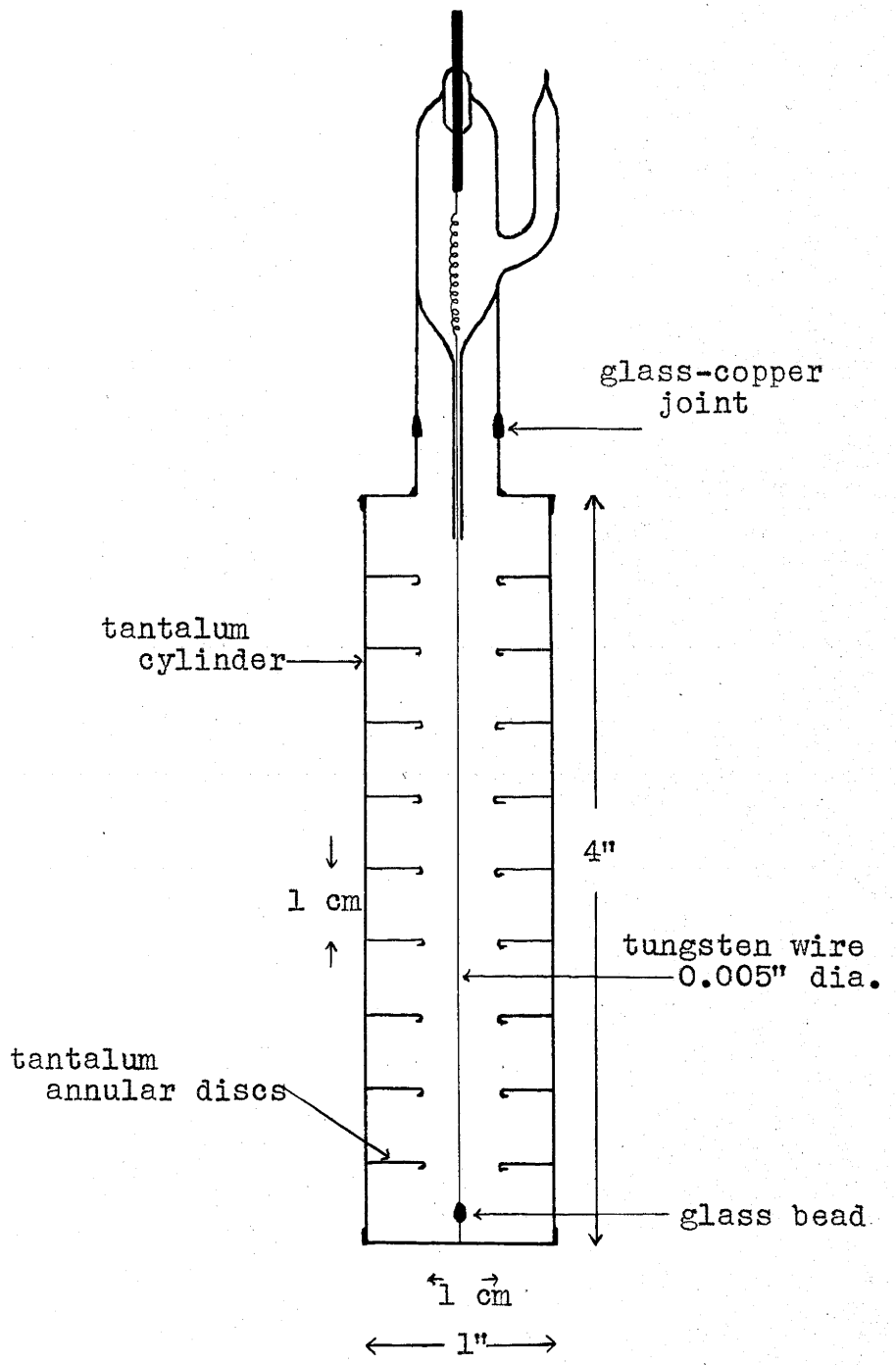

Fig.3.2 The tantalum Geiger counter.

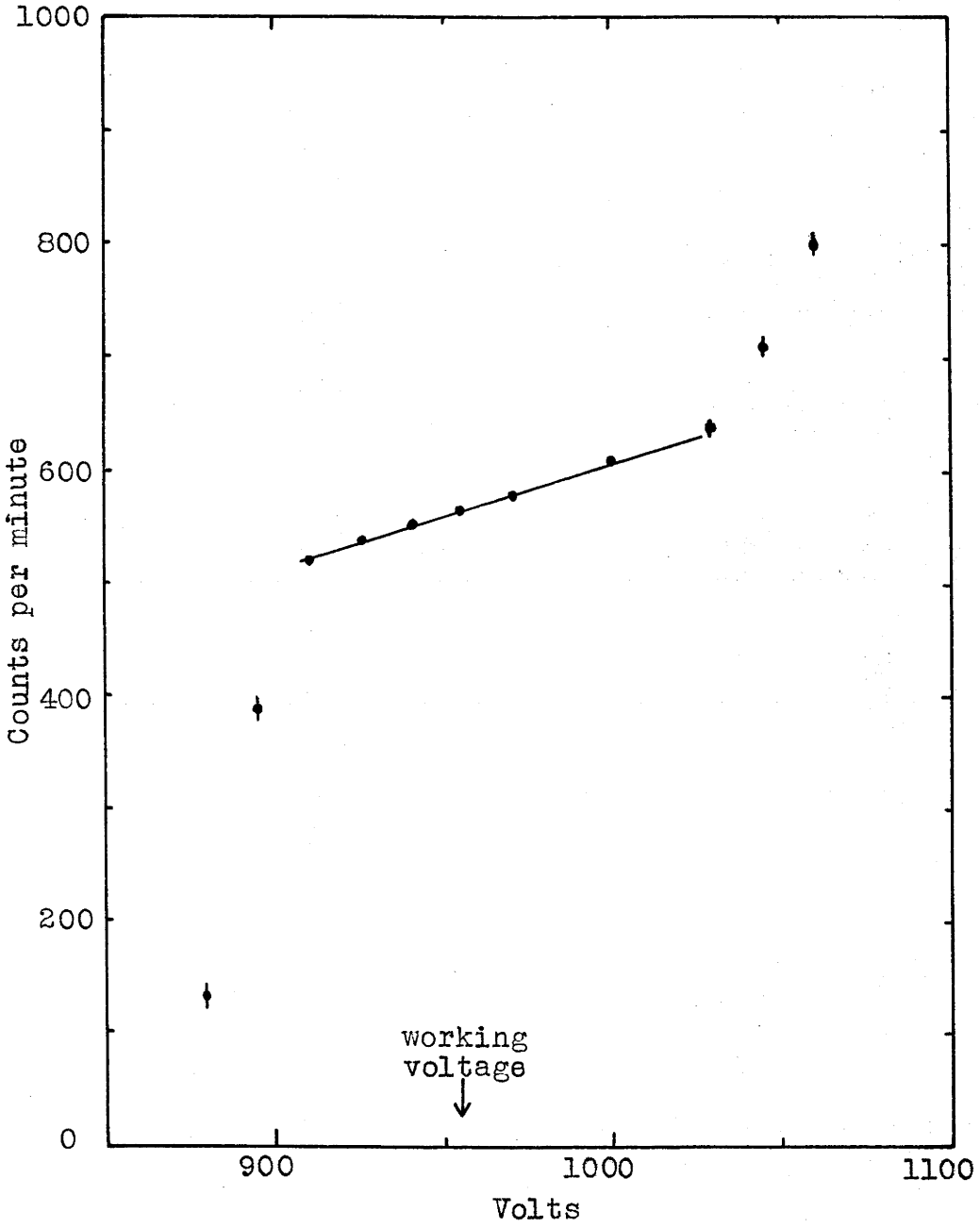

Fig.3.3 Tantalum Geiger counter plateau.
At 955v. the slope is 17½% per 100v.

voltage supply. The stability was frequently checked with a Co^{60} γ-ray source in a standard position. During the first two weeks of operation the standard count rate, at the working voltage of 955 volts, increased by 7% and thereafter it did not fluctuate by more than ±3%.

The additional counting rate resulting from irradiation was small (~30/minute), necessitating a careful measurement of the counter background. The natural background was 55 counts/minute, which became reduced to 25 counts/minute when the counter was shielded by 6" of lead. The background rate varied with voltage in the same manner as the standard Co^{60} counting rate.

3.4. The Methane Counter.

The counter, Fig.3.4, was cylindrical, of length 30 cm. and internal diameter 9.1 cm. A tungsten wire of diameter 40μ was taken through a Kovar-glass seal inside a 1.5 mm. diameter copper capillary tube, hung along the axis of the counter, and was kept taut by a nickel weight; 18 cm. of wire was exposed within the counter. The outer pressure chamber was made from stainless steel 1/16" thick and lined with a graphite cylinder and end-plates, also 1/16" thick, which formed the cathode surfaces of the counter. This lining prevented charged particles produced in the steel walls from entering the sensitive region. The only important

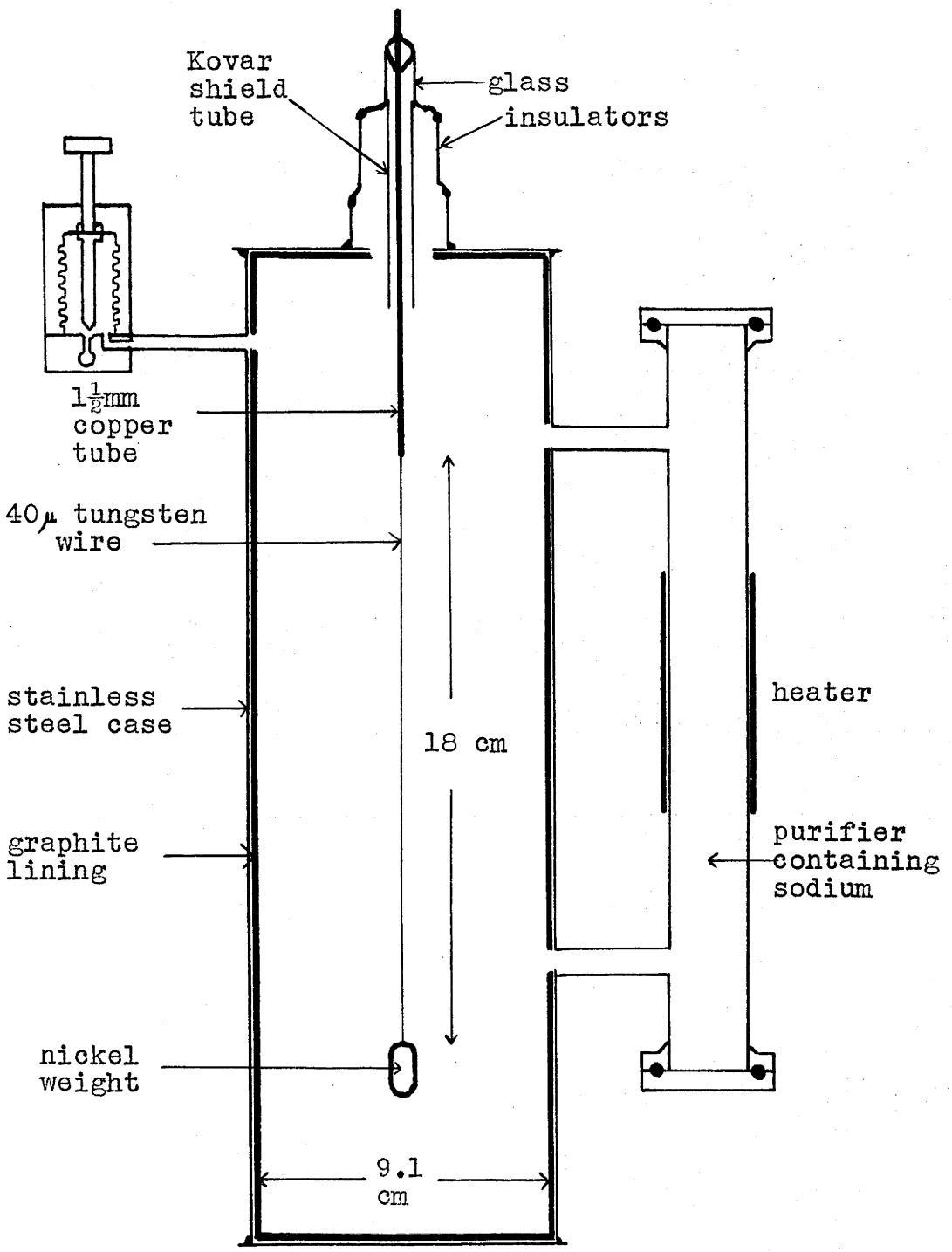

Fig.3.4 Diagram of the methane chamber.

reaction occurring in the graphite at energies up to 18 MeV was the reaction under study viz. $C^{12}(\gamma 3\alpha)$. Consideration of the maximum depth at which a photo-disintegration event could occur, and still lead to the dissipation of more than 5 MeV in the active volume, showed that less than 0.1% of the pulses observed in the experiment were due to reactions occurring in the graphite walls. Attached to the main chamber was a purifier through which the gas could be circulated by convection. It contained evaporated sodium metal which reacts strongly with water vapour and oxygen, the two most objectionable of the common electronegative counter gas contaminants, but does not react with methane. Gas could be pumped in and out of the counter through two needle valves, the moving parts of which were enclosed in bronze sylphon bellows to prevent grease from coming into contact with the gas.

The filling procedure was as follows: the air in the counter was replaced by methane and a pellet of sodium dropped into the purifier. The methane was then pumped out until a pressure of 10^{-4}mm.Hg was obtained, then the sodium was evaporated onto the walls of the purifier tube. Pumping was continued for half a day, the chamber being outgassed by frequent heating with a flame. Methane was then allowed to pass slowly through

a copper coil immersed in solid carbon dioxide and acetone to freeze out water vapour, and was admitted to the counter until the pressure reached 2.38 standard atmospheres.

At this pressure and at the working voltage of 2.4 kV the gas multiplication of the counter was found to be 3 times (Fig.3.5). The counter pulses, produced by polonium 5.3 MeV alpha particles, were observed on an oscilloscope to have rise times between 10 and 100 microseconds - rather longer and with a greater spread than expected. According to measurements by English and Hanna[49] of electron mobilities in methane, both the rise times and the spread, due to electron straggling and radial extension of the alpha particle tracks, were expected to be about 3 microseconds; this difference was not investigated at the time and was not understood. (However, a possible explanation could be the formation of negative ions. During later observations in which the filling gas was nitrogen, similar very long rise times were found. The cause was oil vapour which had entered the counter from an incompletely cleaned Bourdon pressure gauge. The oil would not be removed by circulation over sodium.) To handle the long pulses satisfactorily,

49. English, W.N., and Hanna, G.C. Can.J.Phys. 31:768 (1953).

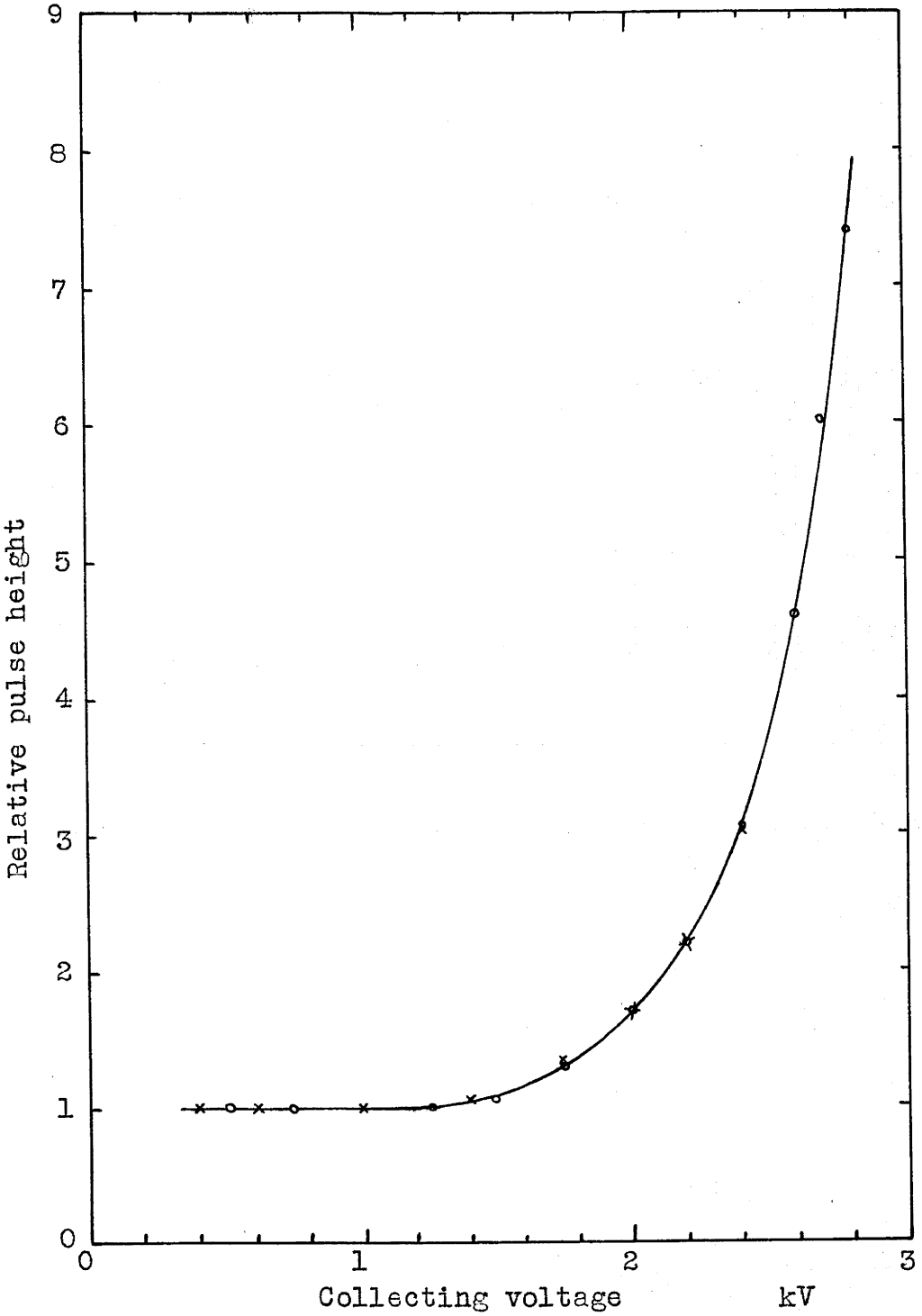

Fig.3.5 Pulse height from the methane proportional counter.

o on 2/12/54 × on 9/1/55

rise and clipping time constants of 80 μsec. were used in the amplifier; this value gave the best compromise between the lack of uniformity in pulse height and difficulties due to gamma ray 'pile-up'.[50] The output of the amplifier was recorded in a 120 channel pulse amplitude analyser.

An energy calibration for the counter was obtained using the spectrum of alpha particles from ThX and its daughter products which decay with a half-life of 3.64 days. A small amount of polonium was included in the counter to give a continuous check on the calibration. The energy scale, shown in Fig.3.6, was found to be linear within 1%.

3.5. The Nitrogen Counter.

The counter was the one which had been used with a methane filling to study the photodisintegration of C^{12}, and its construction is described in the previous section.

When gas counters are to be used for the study of photodisintegration with 18 MeV radiation, two conflicting requirements immediately arise. These are: (i) the necessity to have a large amount of gas i.e. a large counter or high pressure, or both, so that there is

---

50. See Section 3.5.3

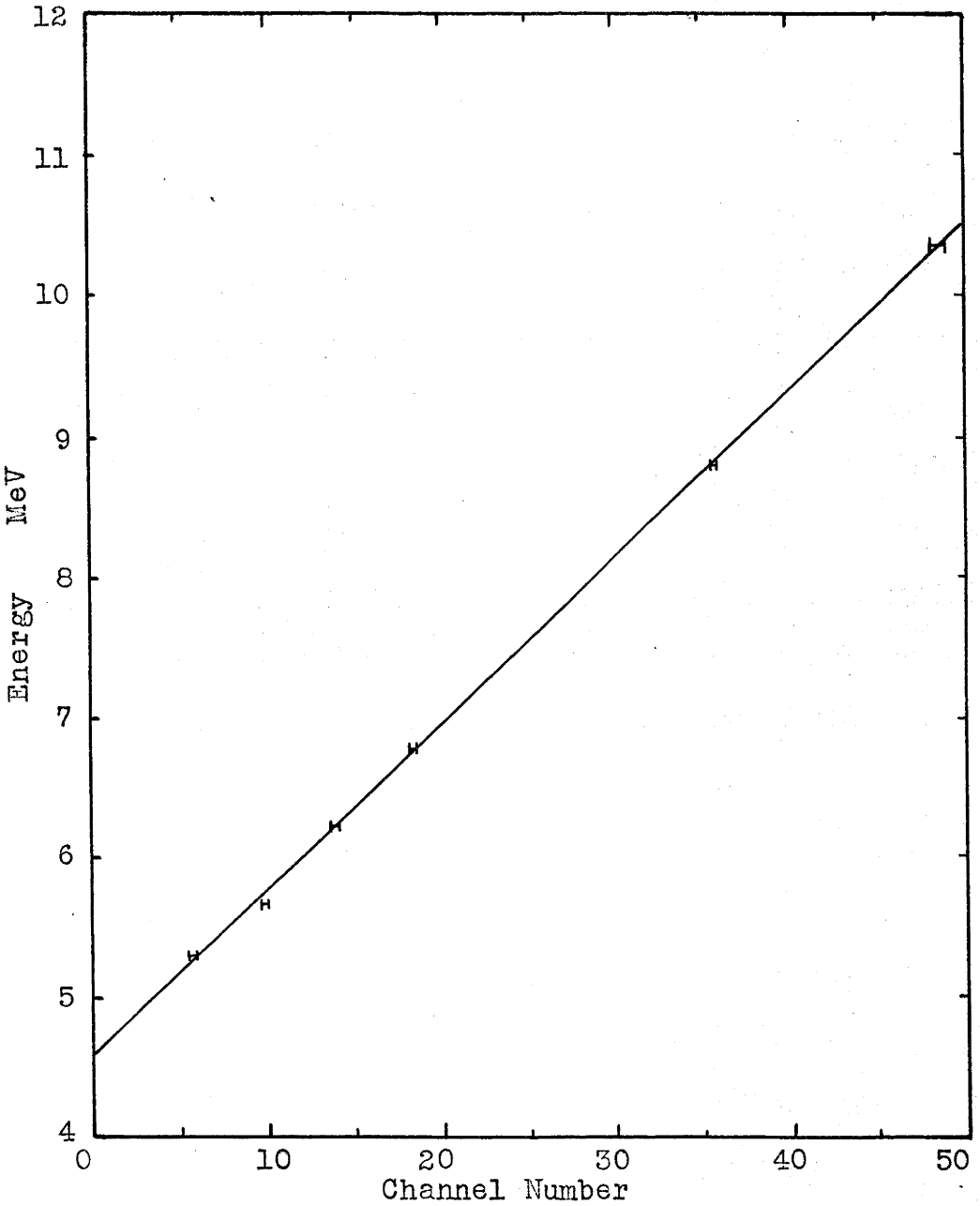

Fig.3.6 Energy scale for the methane counter. Calibration points:
Zero at channel -39
Po^{210} 5.30 MeV
ThX 5.67 6.07,6.11,6.28 6.77 8.78 MeV
$C^{12}(\gamma,3\alpha)$ 10.35 MeV

sufficient stopping power for the observation of particles with energies up to about 10 MeV, and (ii) the need for fast electron collection, so that large gamma fluxes can be used to give reasonable counting rates from the low cross section reactions, without destroying the energy resolution of the counter by electron pile-up. Rapid and complete collection of electrons is more difficult in molecular gases, such as hydrogen and nitrogen, at a few atmospheres pressure and low X/p than it is in the noble gases such as argon, so that purification becomes much more important than it is at low pressures.

For the investigation of the $(\gamma\alpha)$ reaction in nitrogen, stopping power considerations led to the choice of 3 atmospheres as the working pressure, and in order to determine the optimum operating conditions the speed and resolution of the counter were investigated in some detail as functions of collecting voltage (limited to 4 kV) and gamma ray flux.

3.5.1. Gas purification and filling of the counter.

The method described in Section 3.4. for introducing the gas into the counter failed to give satisfactory electron collection in nitrogen, which requires a much higher degree of freedom from electronegative gas contamination than methane does when pressures above

atmospheric are used. For nitrogen at 3 atmospheres pressure and with 4 kV applied to the counter, a rough calculation using the method and data given by Wilkinson[51], suggested that 1 part in 10^6 of oxygen or water vapour could cause up to 1½% loss of electrons by attachment to form negative ions. The filling procedure described below was found to give reproducible and reasonably fast counting conditions with nitrogen.

The chamber was pumped, with frequent flame heating, until the pressure did not rise above 10^{-3} mm.Hg in 16 hours after the chamber had been isolated from the pumps. Medical grade nitrogen, containing less than 1 part in 10^5 of oxygen, was then passed through tubes coated with evaporated sodium and condensed at atmospheric pressure in a coil immersed in liquid air. From this coil most of the nitrogen was evaporated and condensed in a second cooled coil, whence it was re-evaporated into the counter until the desired pressure was reached.

After isolating the counter from the filling system, the purifier attached to the side was heated to circulate the gas over the sodium until the pulses from an alpha particle source had attained a constant height. The initial cleaning up time was usually about 12 hours, and

---

51. Wilkinson, D.H. 'Ionisation Chambers and Counters', C.U.P. (1950) p.42.

after this it was necessary to operate the purifier for an hour or so daily, otherwise the pulse height began to decrease. The very persistent leak during pumping and the continual purification which was found necessary may have been due to slow outgassing of the 1/16" thick graphite lining in the counter.

3.5.2. The pulse shape and electron mobility in the counter.

Pulses from the 5.30 MeV alpha particles of Po^{210} were used to study the characteristics of the counter. The source was mounted on the wall, opposite the centre of the wire, behind a magnetically operated shutter so that the source could be covered during the photo-disintegration runs, but was still available as a convenient calibration check. Its strength was 20 disintegrations/second, and only those particles which were emitted within a cone of semi-angle 75° could enter the counter.

The variation of pulse height with voltage is shown in Fig.3.7. It is seen that ionisation chamber saturation was achieved at about 1000 volts, gas multiplication had commenced below 2000 volts, and was 3 times at 4000 volts.

The shapes and speeds of the pulses have been compared with calculations based on the analysis of

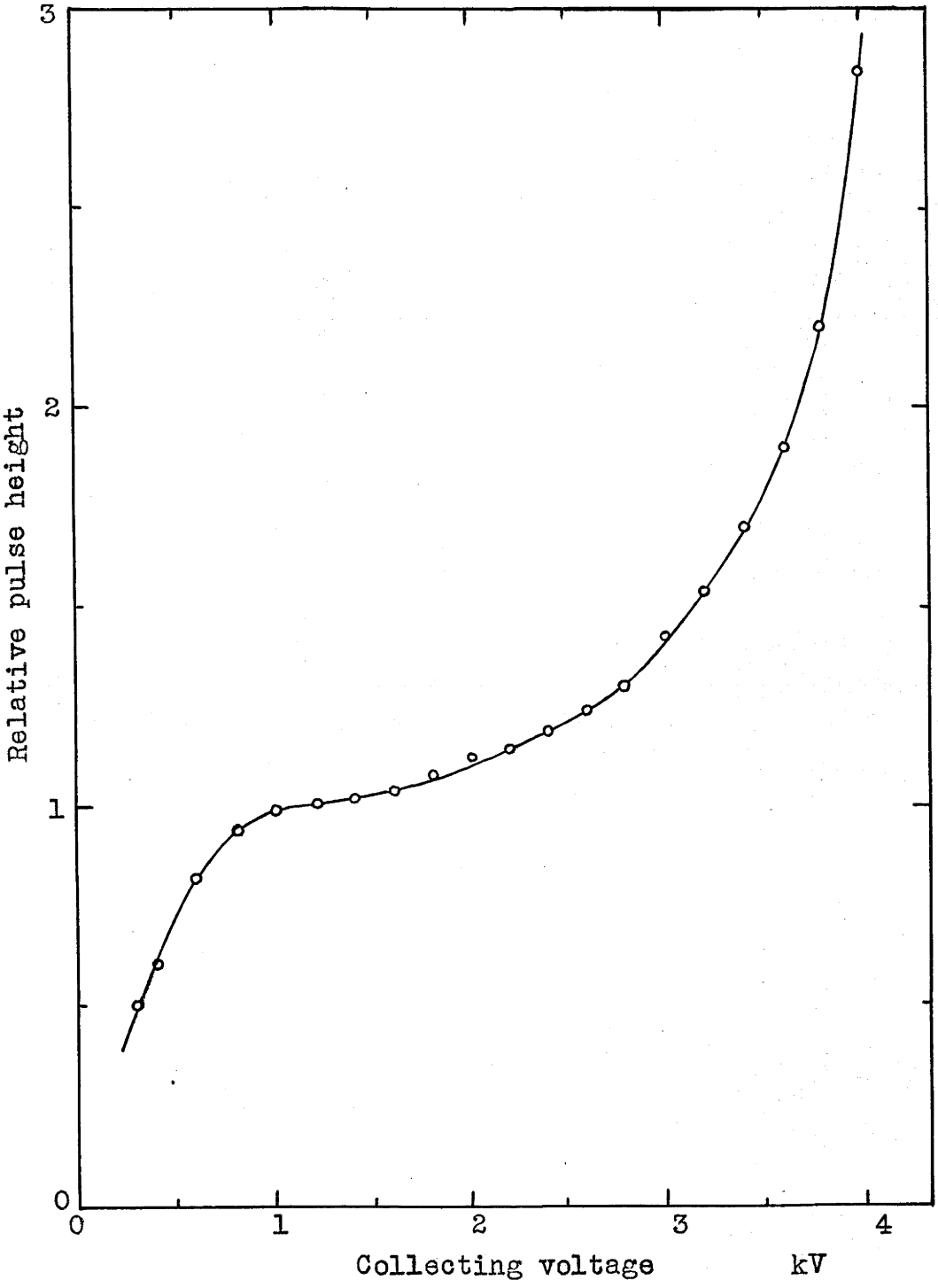

Fig.3.7 Pulse height from the nitrogen counter at 3 atmospheres pressure.

pulse formation in cylindrical chambers given by Wilkinson[52]. The rise of the pulse is expected to take place in two stages: at first a slow rise, then a final rapid rise as the electrons reach the wire. The final rise is not as rapid as that due to a single electron, nor as rapid as that due to the positive ion motion away from the wire when gas gain begins, but is smeared out because of the extended time during which the original electrons from different parts of the track are arriving at the wire. If the radial extension of the initial ionisation is a fraction 'f' of the distance of the furthest point of the track from the wire, then the time for the final rapid rise is roughly 1.6f of the total pulse length. For f values between 0.1 and 0.3 the pulse rises to about 0.2 of its final height during the first slow rise.

The pulses from the counter were fed into an amplifier with integration time constant 0.5μs, and differentiation time constant 50μs, and observed on an oscilloscope. The trigger setting was almost at the noise level, so that all of the pulse traces were superimposed. Since the tracks could be up to 75^{o} from the radial direction in the counter, the pulses had slightly

52. Wilkinson, D.H. 'Ionisation Chambers and Counters', C.U.P. (1950), p.p.77-92.

different shapes corresponding to the range of possible f values, but the 'average pulse' shape could be fairly well measured on the screen. The range of a 5.3 MeV alpha particle in the 9.1 cm. diameter chamber was 1.3 cm, giving a maximum value for f of

$$f_{max} = 1.3/4.55 = 0.29,$$

and, assuming that the directions of the tracks were uniformly distributed throughout a cone of semi-angle 75°, the average f was

$$f_{av} = 0.63 f_{max} = 0.18.$$

The final rise of the pulse would therefore be expected to last for $1.6f = 0.29$ of the total pulse length. This estimate agreed with the experimental observations, as can be seen from Fig.3.8 in which the total time t_2 to reach the peak, and the time t_1 to the start of the final rise, are plotted for different voltages. Between 300 and 4000 volts it is seen that $t_1 \doteq 0.7t_2 = (1-1.6f)t_2$.

The observed values for t_2 can also be used to estimate the electron mobility in nitrogen. In a cylindrical counter the time taken for an electron to reach the wire from a distance $r \gg a$ is

$$t_r = \frac{3}{2K}\left(\frac{p \ln(b/a)}{V}\right)^{\frac{1}{2}} r^{3/2}$$

where the electron mobility K is defined by $v = K(X/p)^{\frac{1}{2}}$ and the symbols have their usual meanings. If we

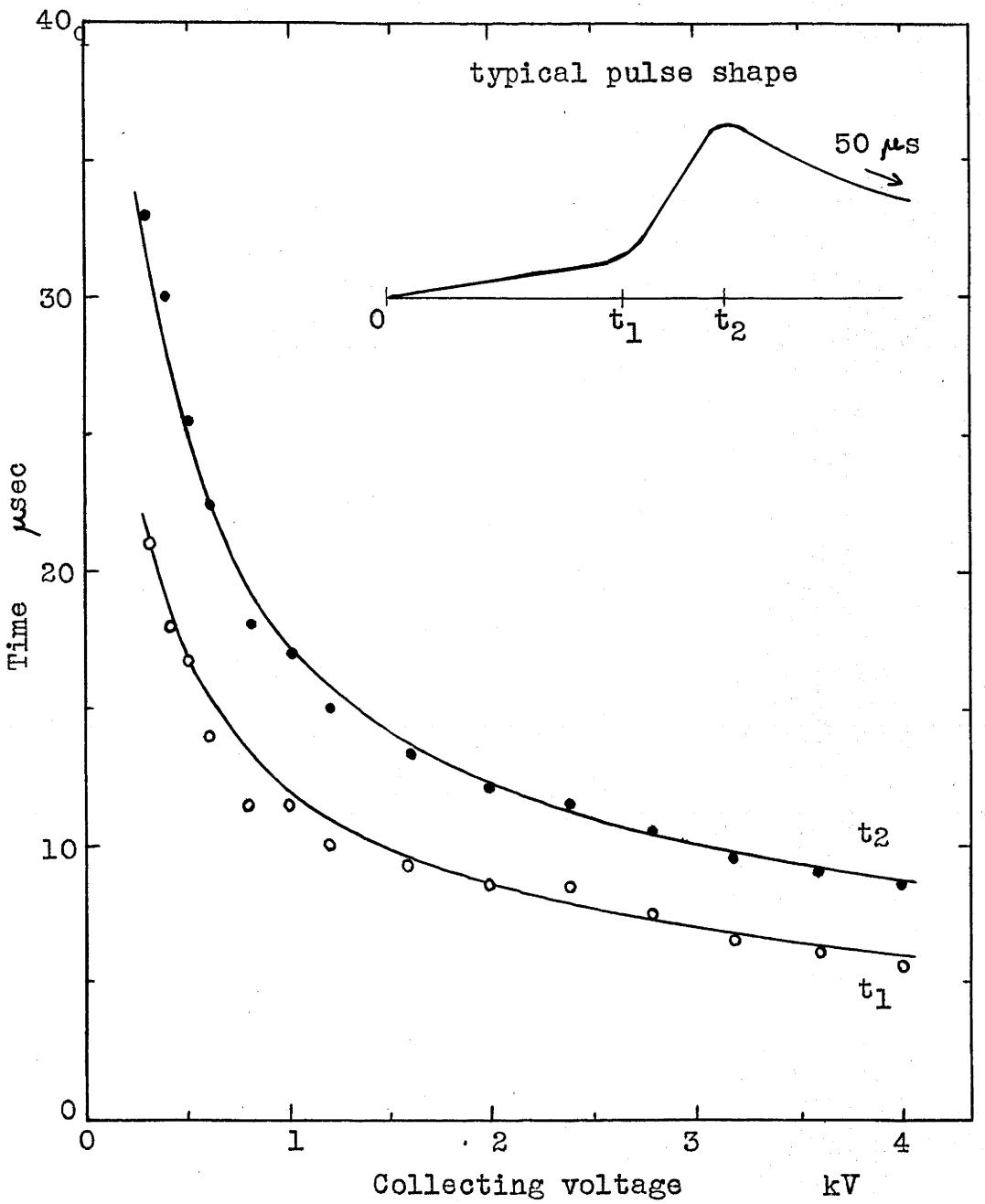

Fig.3.8 Average rise times of 5.30 MeV pulses in the nitrogen chamber. The observed times are plotted, and curves are drawn for t_2 corresponding to $K = 1.3 \times 10^6$ and $t_1 = 0.7 t_2$.

assume the range-energy relation $R \propto E^{3/2}$ for alpha particles, and the energy per ion pair to be constant, it follows that the centre of gravity of a track is 0.6R from its start. Hence the average pulse can be considered to arise from ionisation concentrated at a distance $0.6f_{av}$ = 0.5 cm. from the wall, i.e. 4cm. from the wire. Substituting this value for r, p = 3x760 mm, ln(b/a) = 7.7, and the observed values of t_2 and V, in the above equation leads to an average value for the electron mobility of

$$K = 1.3 \times 10^6$$

in the range 300 to 4000 volts, i.e. for (X/p) values between 0.005 and 1 over most of the counter. This value is only a little larger than the value 1×10^6 deduced from the electron velocities in nitrogen, which are quoted by Wilkinson[53] for X/p values in the range 0.1 to 1. The mobility as defined here is not expected to be constant, and the velocities give increasing values for K as X/p decreases.

The low voltage at which pulses were observed and the low value which was found for K were considered to show that the purification procedure was satisfactory. A high electron velocity would have been desirable

53. Wilkinson, D.H. 'Ionisation Chambers and Counters', C.U.P. (1950), p.33.

so that stronger differentiation of the pulses would have been possible during the photodisintegration experiment, but unfortunately no suitable impurity could be found which would speed up the electron collection without destroying the resolution.

3.5.3. Energy resolution in the presence of radiation.

While the pulse shape measurements were being made, the pulses from the 5.3 MeV alpha particles were recorded on a multichannel amplitude analyser. To give reasonable reproduction of the pulse shapes from the counter, the amplifier time constants were set at 0.5μs rise (fixed) and 50μs for clipping. Under these conditions the width of the pulse group at half maximum height decreased from 10% at 300 volts to 3% at 4000 volts (Fig.3.9). The contributions to the width from various causes have been estimated by means of the analysis given by Wilkinson[52], and are presented in Table 3.2. As the calculated and observed widths for the 5.3 MeV group are in reasonable agreement, the calculations serve as a guide for the resolution which can be expected under working conditions. The maximum alpha particle energy released from $N^{14}(\gamma\alpha)B^{10}$ at 17.6 MeV is 4.3 MeV instead of 5.3 MeV, but as the track orientations can be over all angles instead of only 75° from the radial direction, the largest contribution to the resolution width will be

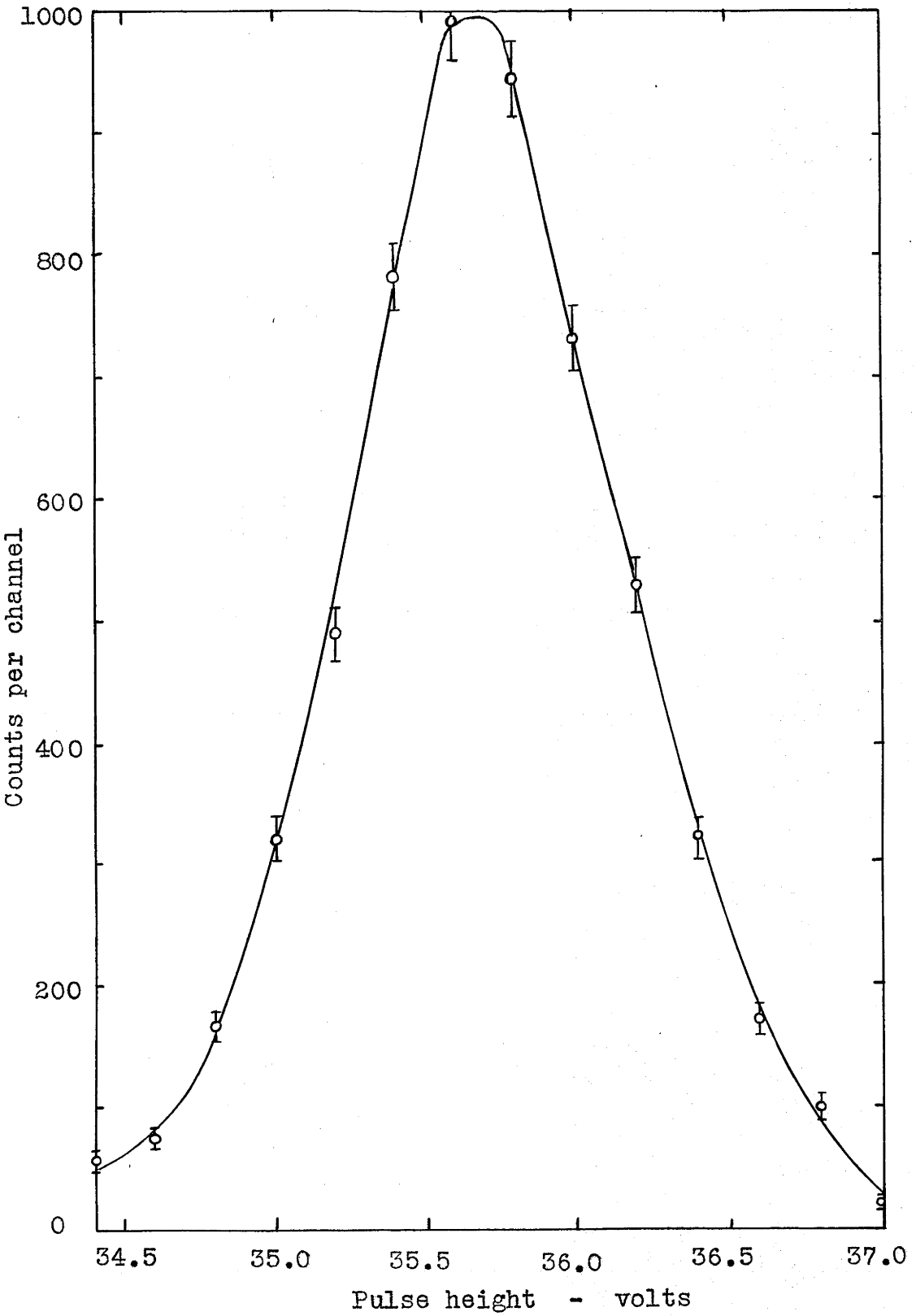

Fig.3.9 5.30 MeV alpha particle group. Width at half maximum height is 3%.

Table 3.2. Contributions to the spread in pulse height.

Collecting voltage	4000	2000	1000	500
Source of spread:	Contribution in %:			
Orientation of 1.3cm alpha tracks	1.5	1.5	1.5	1.5
Clipping time 50μs	1.35	3.4	5.2	8.4
Signal/noise (C.R.O.estimate)	2.3	3.0	3.5	4.5
Total from these sources	3.1	4.8	6.4	9.7
Observed	3.3	4.4	6.5	10
Uniform origin throughout chamber	4.5 at all voltages			

5% for tracks originating uniformly throughout the counter, The other main contribution comes from the effect of the differentiation on pulses having different rise times, and is reduced if the clipping time constant is made greater than the maximum time during which electrons from different parts of a track arrive at the wire. On the other hand, the signal to noise ratio is improved by shortening the clipping time constant.

When the counter is irradiated the noise level is effectively increased by the many electrons which result from photon absorption in the counter walls, and to a small extent, in the gas. The variation in the width of the Po^{210} alpha group was investigated as a function of the clipping time constant and the gamma flux, and the results are contained in Table 3.3 and Fig.3.10. It is seen that no appreciable increase in width occurs when less than an average of 5 photons pass through the

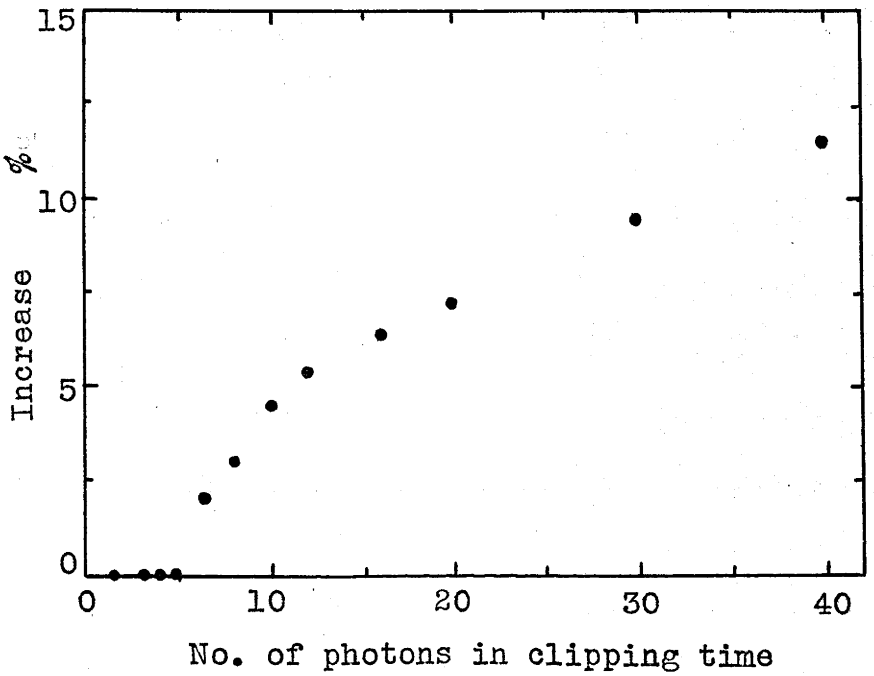

Fig.3.10 Contribution to resolution width from gamma radiation.

Table 3.3. Effect of gamma flux on the resolution.

Beam current μA	0	100	200	300	400
Photons/second through counter sensitive region	0	2×10^5	4×10^5	6×10^5	8×10^5
Mean time between photons: μsec		5	2.5	1.67	1.25
Observed resolution width in % for the given clipping times:					
50 μsec	3.5	5.8	8.0	10	12
20 μsec	5.3	5.3	6.0	7.5	8.3
8 μsec	8.0	8.0	8.0	8.0	8.3

sensitive volume of the counter in a time equal to the clipping time constant. Hence proton beam currents of up to 400 μA could safely be used with an 8 μsec clipping time, which gives a resolution of 8%.

The many small electron pulses can also occasionally 'pile-up' to give a large pulse, and are therefore a source of unwanted background counts. The low energy spectra which were recorded for different clipping times have been plotted in Fig.3.11, from which it is seen that for 8 μsec there will be no pile-up pulses above 2 MeV and probably very few above 1.5 MeV.

3.6. The Neon Counters.

3.6.1. The proportional counter.

With the amount of very pure neon available it was decided to investigate the $(\gamma\alpha)$ reaction using a proportional counter of conventional cylindrical design

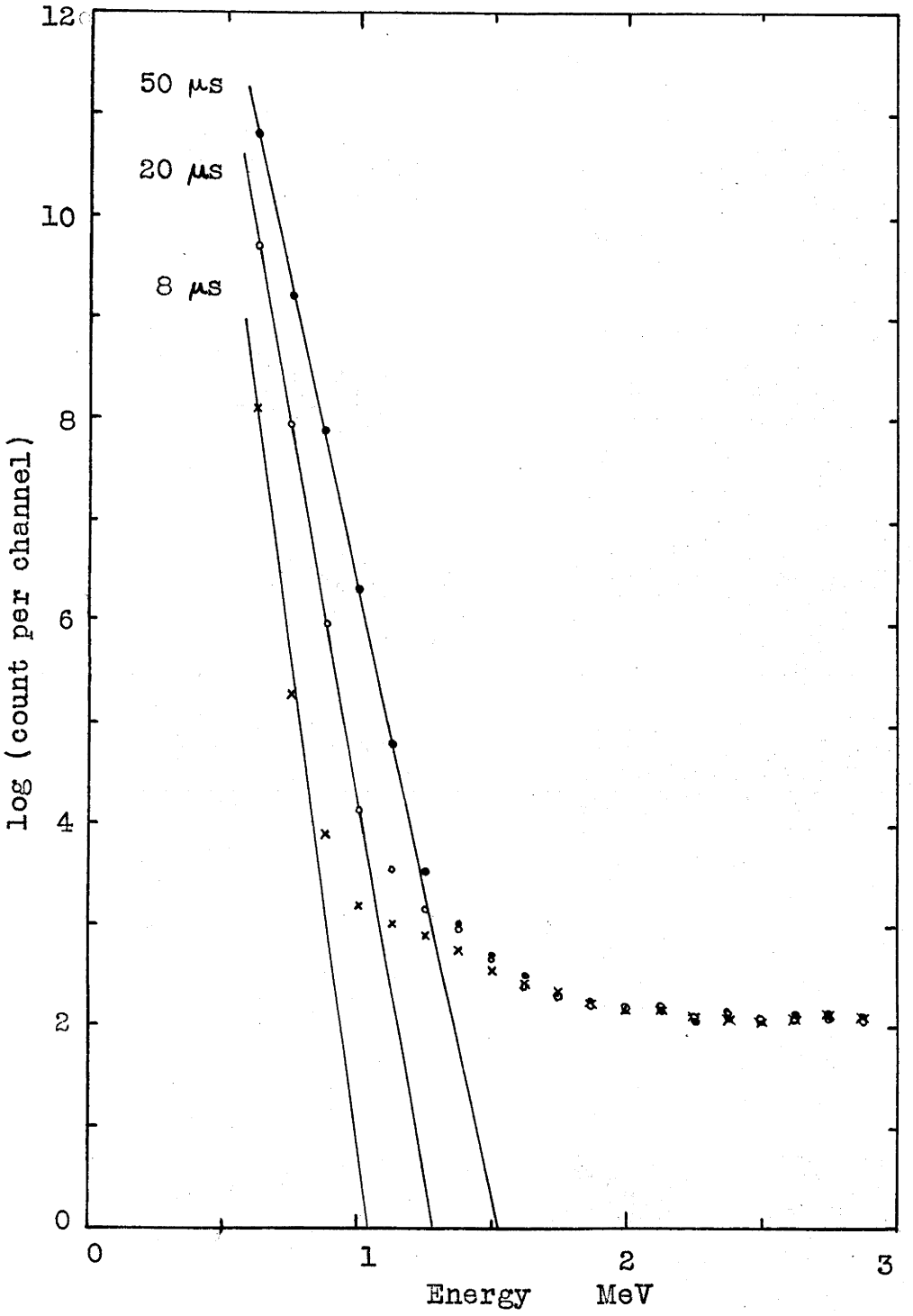

Fig.3.11 Low energy pile-up pulse spectrum for 300 μA. The clipping time constants are marked on the curves.

with a sensitive region 4" in diameter and 9 5/16" long. The central wire, of smooth 0.005" tungsten, was held at high tension and provided with shield and field tubes, the latter extending $2\frac{1}{4}$" inside the walls at each end. The counter wall was of mild steel 3/16" thick and was coated on the inside with graphite to reduce the natural radioactivity. Energy calibration was provided by a plutonium source (5.16 MeV alphas) mounted on a small gravity operated hinge. A calcium purifier was provided through which the circulation was achieved by convection. After pumping and outgassing of the chamber, pure neon was introduced via a liquid air trap until a pressure of 60 lbs/sq.in. was reached.

Saturation of the chamber pulses was attained with an applied potential of 500 volts, the onset of proportional amplification was at about 1200 volts, a gas gain of 8 times was obtained at 1500 volts, and the counter breakdown voltage was around 2200 volts; all of these figures were rather lower at the time of filling when presumably the gas was very clean and a little cool. The counter was operated at 1000 volts and a gas gain of 1, with the amplifier differentiating and integrating time constants set at 8 μsec; under these conditions the plutonium alpha peak had a full width at half maximum of 6%.

3.6.2. The gridded ionisation chamber.

In order to study the $Ne^{20}(\gamma p)F^{19}$ reaction it was necessary to have a much greater stopping power in the counter gas; this could be achieved by using a higher pressure and larger dimensions. Consequently it was decided to construct a cylindrical gridded ionisation chamber. The main advantage of such a chamber over a proportional counter is that the electric field at the walls may be made much larger, so that electron collection from remote regions of the counter is considerably improved. The cylindrical design makes better use of the available gas than does a parallel plate chamber.

The design of the counter is given in Fig.3.12. The body was constructed from mild steel tube 6" in diameter with 1/8" walls and brass end plates 3/4" thick. The sensitive region of the counter was 6.18" in diameter and 8.93" long. The electrode assembly, shown in detail in Fig.3.13, was rigidly attached to one end plate, and supported the 1/4" diameter polished copper anode and the grid, which consisted of 30 wires, 0.007" in diameter, equally spaced on a cylinder of diameter 3/4". Attached to the side of the counter were a purifier tube filled with calcium turnings and a magnetically operated plutonium alpha source.

The neon available in sufficient quantity to fill

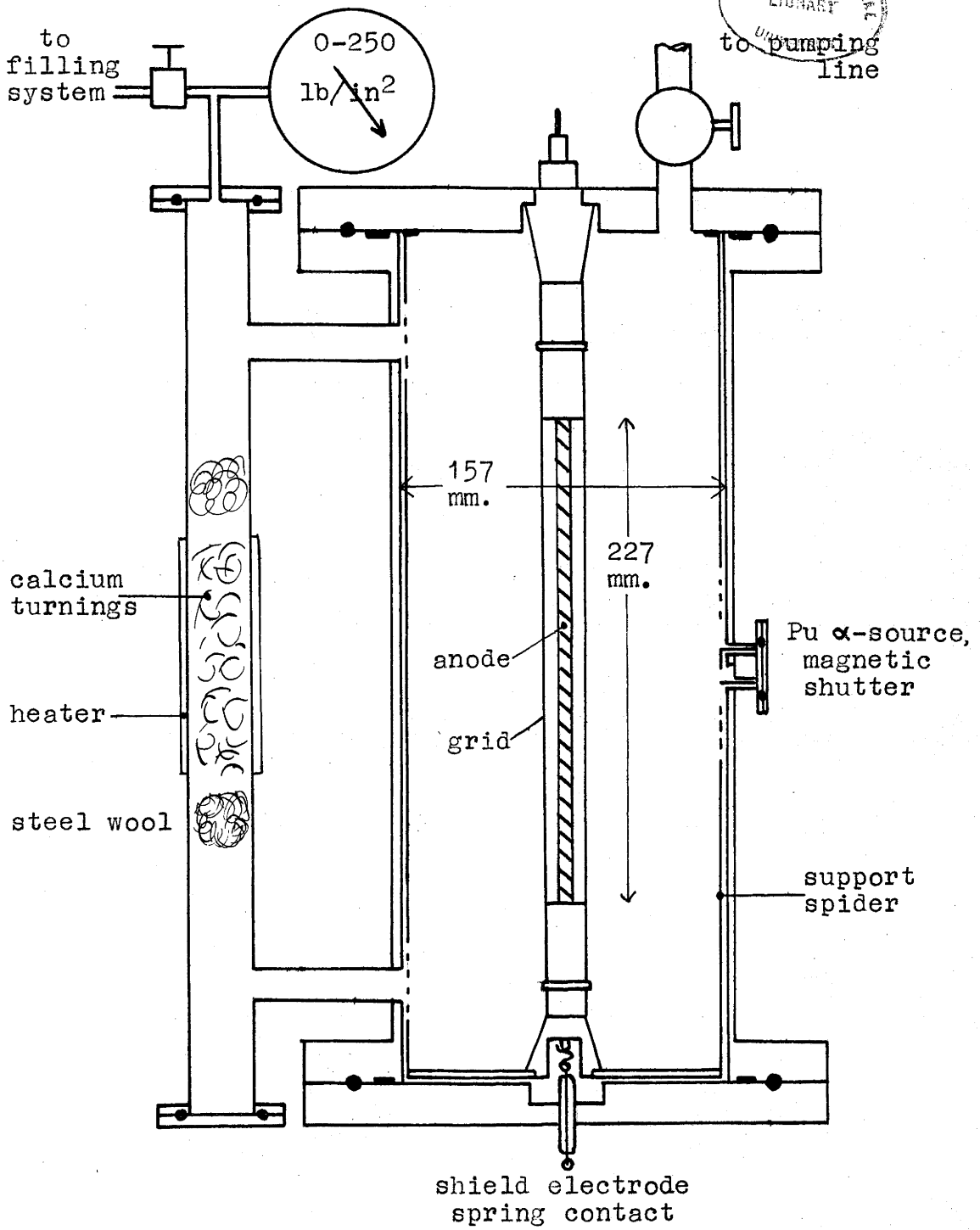

Fig.3.12 Diagram of the Gridded Ionisation Chamber.

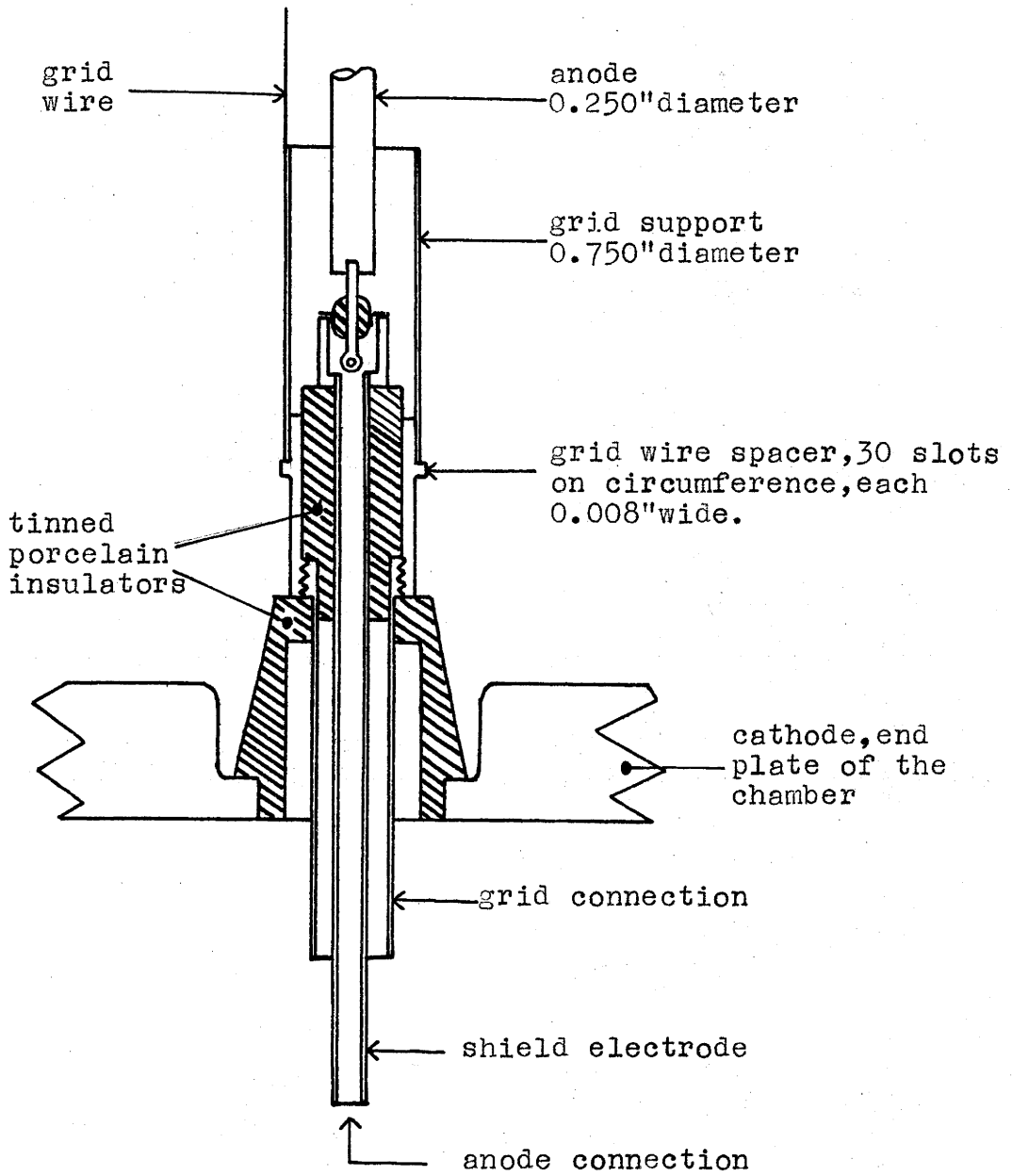

Fig.3.13 Electrode Assembly for the Gridded Chamber.

this chamber was rather impure, containing in particular 25% nitrogen and 15% helium. Consequently, after outgassing and evacuating the chamber, the gas was passed slowly in at about 5 cc./sec. through a system consisting of an activated charcoal in liquid air trap, followed by a hot (350° C.) calcium tube, and a second charcoal trap. Mass spectrographic analysis[54] showed the final gas composition to be Ne^{20} 70.05%, Ne^{22} 7.15%, He 22.80%, the nitrogen having been successfully removed. The presence of the helium appeared to raise the breakdown voltage of the gas and it was possible to operate with 4000 volts between anode and wall at a total pressure of 132 lb/in^2, the limit in voltage being set by the H.T. supply.

The grid potential was chosen to be one half of the anode potential as suggested by theory[55,56], and tests made with various grid voltages indicated that this choice was about optimum, though neither resolution nor pulse height was a very sensitive function of the grid voltage. Calculation showed that under these conditions the grid shielding efficiency was 0.96, while its transparency to electrons was 1. The minimum value of X/p was 0.02 volts/cm/mm Hg compared to 0.005 in the proportional

54. Kindly undertaken by Dr.J.H.Richards of this laboratory.
55. Bunemann,O. N.R.C.Report PD-285. (1946).
56. Whitehouse,W.J.,and Galbraith,W. Phil.Mag.41:429 (1950).

counter, and with this chamber there was much less difficulty with contamination of the gas. The calculated maximum electron collection time for 10 MeV alphas[57], of range $2\frac{1}{2}$ cm. at the working pressure, was 15μs, while for 4.7 MeV protons[57], of range 6 cm, it was 30μs, taking the electron velocity to be $10^6(X/p)^{\frac{1}{2}}$ cm/sec.; experimental results showed these figures were approximately correct.

It was found possible to achieve a width for the plutonium alpha group of less than 5% for [redacted] values of the amplifier integration and differentiation time constants in the range 4 to 50 sec. Although the wall thickness was reduced to 1/8" around the sensitive region to reduce the electron pile up, with the gamma fluxes used the plutonium alpha peak was considerably broadened (~10%) by electron noise, and collimation of the beam made no improvement. The group widths measured in the photodisintegration experiments were wider still (~12%), indicating perhaps a small additional spreading when events are distributed uniformly throughout the sensitive volume. To attain this resolution, an integration time constant of 8μs. and a differentiation time constant of 20μs. or 8μs. were used, the latter being as short as was compatible with the variations in time rises. The

57. See Section 7.3.

limit to the useful duration of an experiment was found to be set by the electron pile up, not by the total gamma flux available. Consequently some improvement in resolution might be achieved by providing a thinner wall and window for the gamma radiation and using higher fluxes corresponding to proton beams above 200μA.

3.7. The Wall Effect in a Cylindrical Counter.

Sometimes, for disintegrations which occur near the boundaries of the counter, the emitted particle will pass out of the sensitive region and the whole of the ionisation along its track will not be collected. It is therefore necessary to correct geometrically for such losses, though usually the gas pressure will be chosen so that the corrections will be small for the reaction which is being studied. Two types of calculation are useful, the first giving the total fraction of events which do not dissipate all their energy in the counter, and the second giving the energy distribution of the incomplete tracks.

For the photodisintegration of medium and heavy weight nuclei at energies below 18 MeV, the assumption of statistical break-up leading to isotropic angular distributions is reasonably good. In the case of light nuclei, however, the angular distribution of a particular group of emitted particles will depend on

the spins and parities of the nuclear levels involved in the reaction. The loss functions for isotropic, $\sin^2\theta$, and $\cos^2\theta$ angular distributions have been calculated[58] and are shown in graphical form in Fig.3.14. The $\sin^2\theta$ loss is less, and the $\cos^2\theta$ loss greater than that for the isotropic case, and the deviations increase as the loss increases. It is found that even for fractional losses as large as 0.5, the corrections for $\sin^2\theta$ and $\cos^2\theta$ distributions are within 10% of the isotropic correction; a similar situation applies for the calculated energy distributions resulting from incomplete tracks[58]. For experiments described in this work the losses were small, so results for isotropic angular distributions have been used to calculate the corrections.

When the range-energy relation for the particles and gas in the counter is known, it can be combined with the functions plotted in Fig.3.14 to give the loss as a function of energy. As an example, Fig.3.15 shows the loss curves for protons and alpha particles in the nitrogen filled counter described in Section 3.5.

The photodisintegration of nitrogen yields protons with up to 9.4 MeV and alpha particles with up to 4.3 MeV. By choosing a suitable gas pressure, the alpha particles can be observed without interference

---

58. See Appendix 1.

from the long range protons. The effectiveness of the discrimination can be judged from Fig.3.16, in which are shown the calculated energy distributions for two groups of photoprotons with maximum energies 9.4 and 3.0 MeV, in the nitrogen counter at 1 and 3 atmospheres pressure. It is found that very few high energy protons can dissipate more than 3 MeV in the counter, while at least 50% of the $N^{14}(\gamma\alpha)B^{10}$ reactions releasing up to 6 MeV are fully recorded at 1 atmosphere, and 90% at 3 atmospheres.

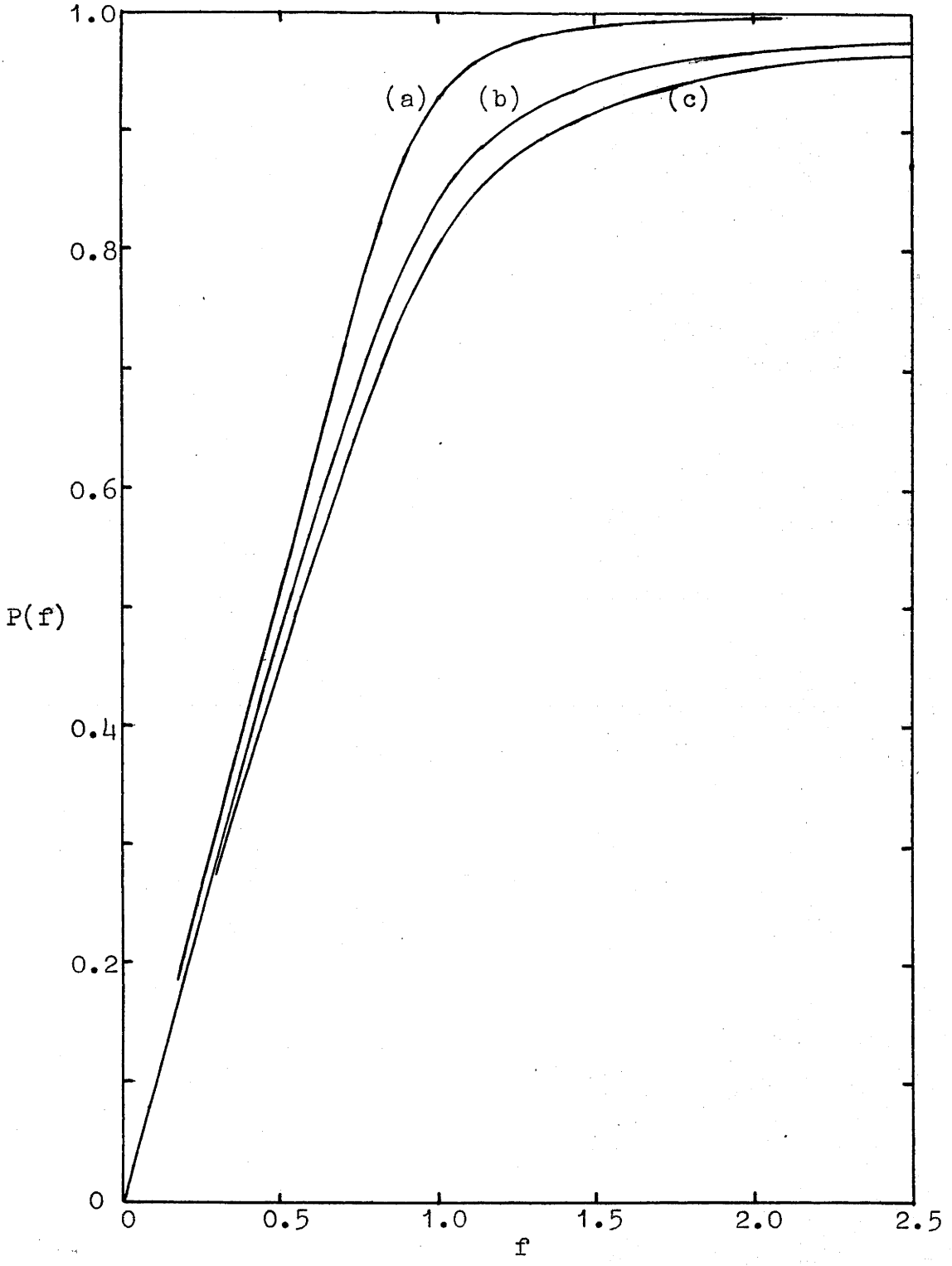

Fig.3.14 Probability of loss for an infinite cylinder.
Angular distribution:
(a) $\cos^2\theta$ (b) isotropic (c) $\sin^2\theta$.

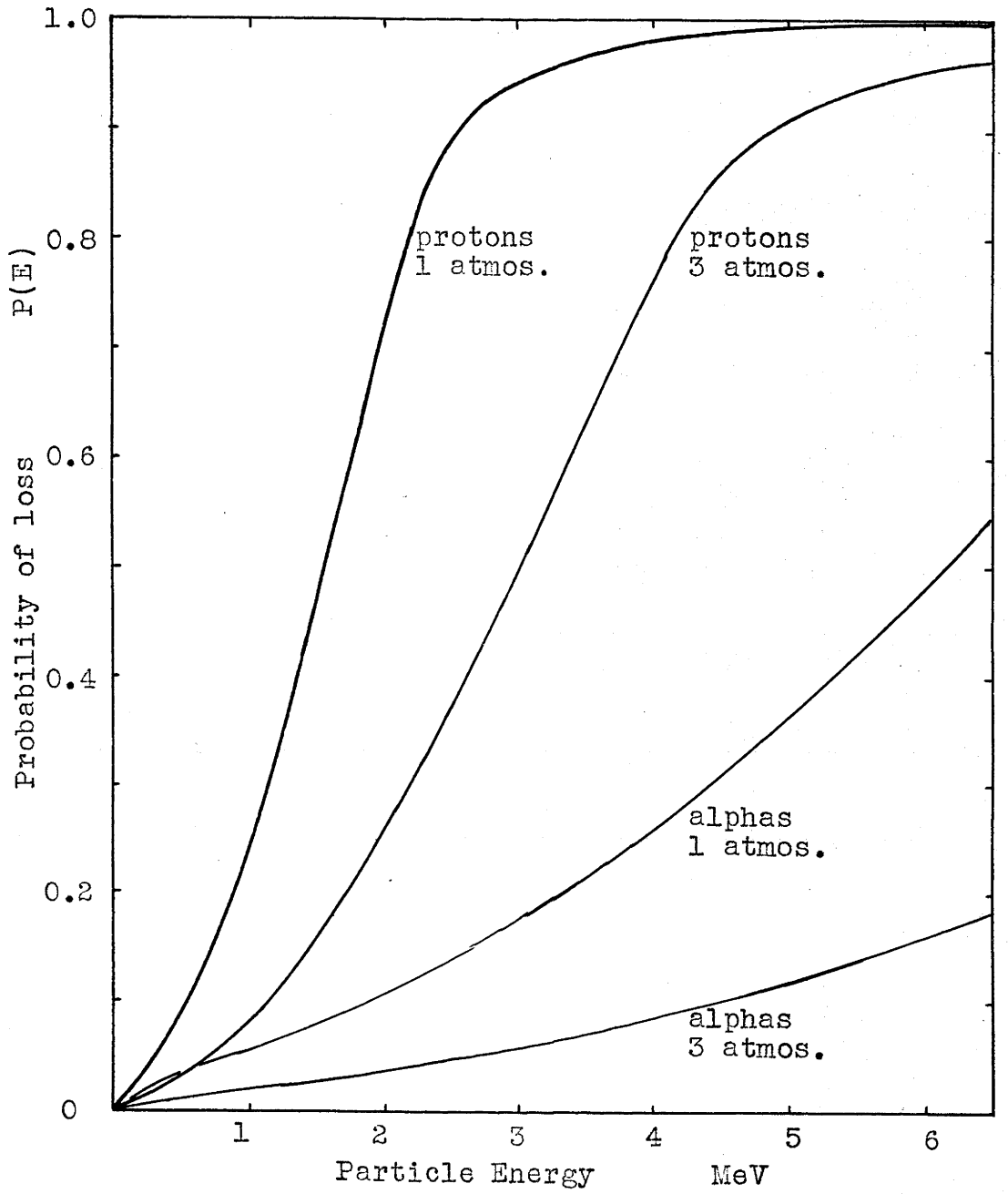

Fig.3.15 The probability for a proton or an alpha particle to strike the wall of an infinite cylinder 9.1 cm in diameter containing nitrogen at 1 or 3 atmospheres pressure.

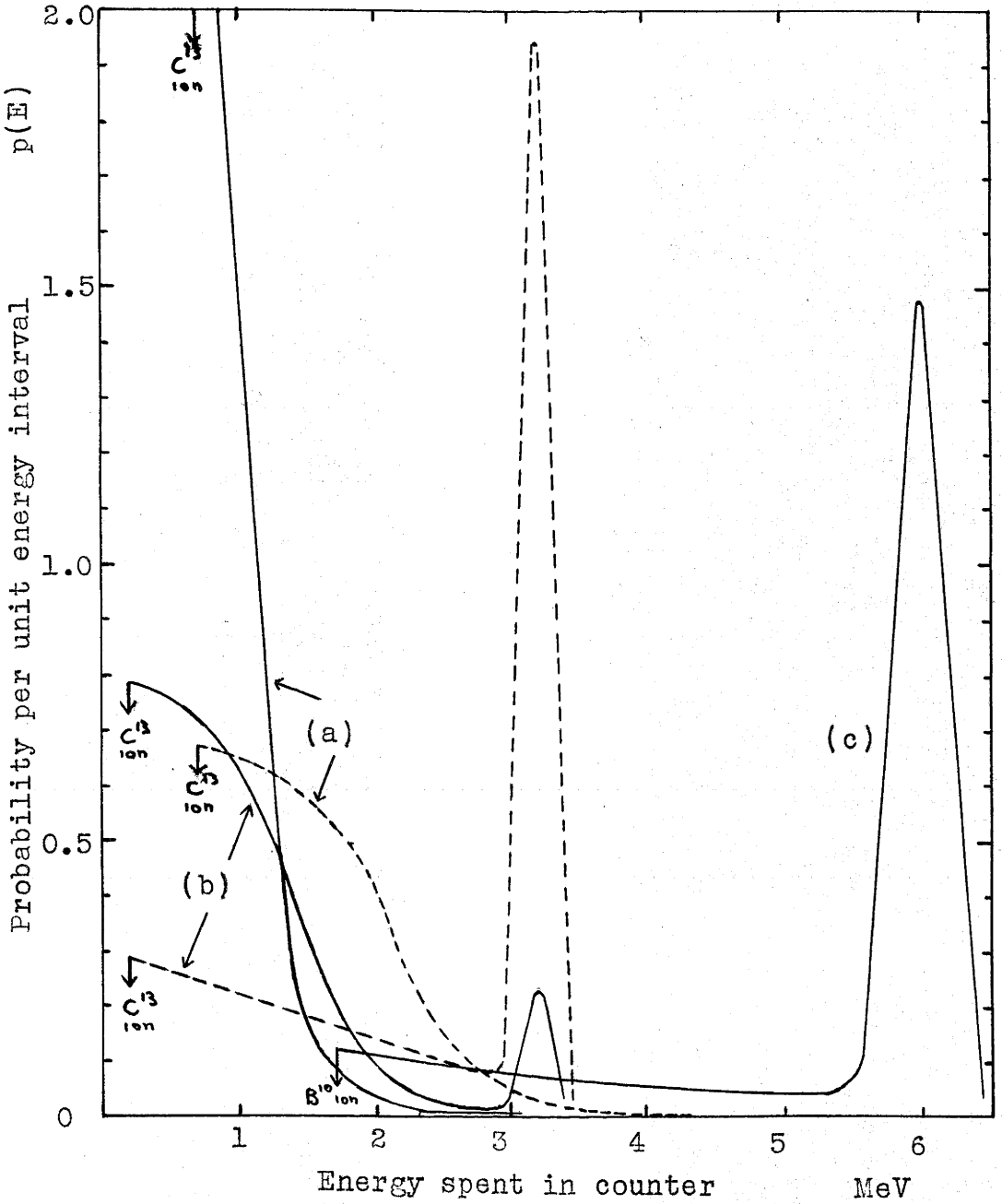

Fig.3.16 Energy distributions calculated for photo-disintegration in the nitrogen counter, 9.1 cm diameter, at pressures of 1 atmosphere (full lines) and 3 atmospheres (broken lines).
(a) $N^{14}(\gamma p)C^{13}$ releasing 10.1 MeV, proton 9.4 MeV.
(b) $N^{14}(\gamma p)C^{13}$ releasing 3.2 MeV, proton 3.0 MeV.
(c) $N^{14}(\gamma \alpha)B^{10}$ releasing 6.0 MeV, alpha 4.3 MeV.

CHAPTER 4.

THE CROSS SECTION FOR $Ta^{181}(\gamma n)Ta^{180}$ AT 17.6 MeV.

4.1. Introduction.

Many photonuclear reactions exhibit the characteristic giant resonance, and of these the (γn) reactions have been the most extensively studied. The decline of the cross section from its peak value may be due to a genuine resonance in the total photon absorption[59], or it may be due to the onset of competing processes such as $(\gamma,2n)$, the total cross section showing little or no resonance at all. The study of competing processes is of interest for other reasons. A comparison of the observed relative cross sections with the statistical theory calculations will give some information about the fractions of photodisintegrations which proceed by compound nucleus formation and by alternative mechanisms such as the direct process.

It is therefore desirable to have some measurements of the cross sections for the various competing reactions. In light nuclei the investigations are complicated since

59. See Sections 2.2 to 2.5.

many processes must be considered, but for the heavy elements the high Coulomb barrier (13 MeV at A = 180) strongly reduces the emission of charged particles. Stearns[60] has shown that the cross sections for (γ,γ) and (γ,γ') processes are small, so that only the $(\gamma,2n)$ process is a possible competitor for (γ,n) at energies just above the giant resonance. For measurements with the $Li^7(p\gamma)$ radiation at energies of 14.8 and 17.6 MeV, tantalum is an eminently suitable element. It consists of only one isotope Ta^{181}, the maximum (γn) cross section is at 14 MeV, decreasing rapidly on the high energy side (see Fig.4.2), the $(\gamma 2n)$ threshold is 14 MeV, and the predicted $(\gamma 2n)$ competition to the (γn) reaction at 17.6 MeV is very large.

The actual magnitude of this competition has been estimated by Carver, Edge and Wilkinson[61,62], from a measurement of the ratio of the cross sections for $Ta^{181}(\gamma 2n)Ta^{179}$ at 17.6 MeV to $Ta^{181}(\gamma n)Ta^{180}$ at 14.6 MeV. The value they obtained for this ratio, 0.29 ± 0.11, was not large enough to destroy the resonance in the total gamma absorption but was too high to be consistent with the concept that a conventional compound nucleus is

61. Carver, J.H., Edge, R.D., and Wilkinson, D.H. Phil.Mag. 44:404 (1953).
62. Carver, J.H., Edge, R.D., and Wilkinson, D.H. Phys.Rev. 89:658 (1952).

always formed. Since the general characteristics of the giant resonances seem to show but little dependence on the specific properties of a particular nucleus (the peak cross sections, positions, and widths are slowly varying and almost monotonic functions of atomic number) Carver et al. suggested their conclusions might be generally applicable to all nuclei. It is therefore important that the experimental data on which their deductions are based should be firmly established.

The principle of the method used by Carver et al. was to measure the total neutron yield from the photodisintegration of Ta^{181} at 14.6 MeV and 17.6 MeV, then, knowing the variations of the (γn) cross section between these energies, the $(\gamma 2n)$ cross section could be deduced. The total photoneutron yield was measured at these two energies by varying the energy of protons incident on lithium, thereby altering the composition of the $Li^7(p\gamma)$ radiation. The (γn) cross section data used by Carver et al. was that which had been measured previously by Haslam, Smith and Taylor[63] using a bremsstrahlung spectrum. Because of the very different conditions in the experiments and the methods of analysis of the results, it was considered worthwhile to remeasure the

63. Haslam, R.N.H., Smith, L.A., and Taylor, J.G.V. Phys.Rev. 84:840 (1951).

ratio of the (γn) cross sections at 17.6 and 14.8 MeV, a ratio fundamental to the $\sigma(\gamma 2n)/\sigma(\gamma n)$ ratio determined by Carver et al. Only a relative measurement of the cross sections is necessary, and by using the same radiation source and method of analysis as used by Carver et al., it was hoped that any small systematic errors in the forms of the cross sections might then be of little importance. Carver et al. measured the total neutron yield by means of a Szilard-Chalmers reaction in manganese; in the experiments to be described the residual Ta^{180} activity was measured after irradiation of a Geiger counter constructed from tantalum. The operating characteristics of the counter have been described in section 3.3.

4.2. Irradiation of the Tantalum.

The tantalum counter, with no voltage on the wire, was placed with its centre 3.75 inches from the lithium target, and its axis at 75° to the proton beam, since at this angle Stearns and McDaniel observed the greatest change in the proportions of the two high energy proton capture gamma lines when the bombarding energy was changed from 500 kV to 1150 kV[64].

Throughout the irradiations, which were for periods

64. See Section 3.1 for a full description of the radiation.

of about 8 hours, the high energy gamma yield was monitored continuously by a 1" x 1" NaI crystal counter and corrections were made for fluctuations in the yield, assuming the half-life of Ta^{180} to be 8.15 hours. The scintillation detector was biassed at 7.5 MeV to exclude the low energy radiation due to inelastic scattering of protons from the 477 kV level in Li^{7}. Because the hard gamma ray energy changes as the proton energy is altered, the relative efficiency of the biassed counter for the two gamma ray mixtures was evaluated by comparing the shapes of the total pulse distributions at each proton energy and calculating the intrinsic efficiencies of detection of the two gamma ray lines in the crystal; this provided a correction of 0.6% to the measured ratio of the induced activity per quantum. At the higher proton energy an additional 2% correction to the untreated gamma yield was necessary, owing to radiation which originated from the beam tube at the analysing magnet; this correction was estimated by using a blank copper target instead of the lithium coated one.

Following each irradiation, the tantalum Geiger counting rate was recorded for about 20 hours, and after subtraction of the counter background, both time independent and that due to previous runs, the initial activity was deduced, again assuming a half-life of

8.15 hours. Altogether 11 irradiations were carried out, 6 at 500 kV and 5 at 1150 kV proton energy. Between these energies the ratio of the 17.6 to 14.8 MeV gamma intensities decreases fourfold and the corresponding change in the Ta^{180} activity can be seen from the data presented in Table 4.1.

Table 4.1. Relative yields of the reaction $Ta^{181}(\gamma n)Ta^{180}$.

E_p kV	Induced activity counts/hour	Corrected γ yield	Relative activity per photon	Mean
500	918 ± 22	663×10^3	1.385	
	1523 ± 11	1108	1.379	
	1721 ± 14	1095	1.571	1.464
	1689 ± 16	1165	1.449	± .046
	3007 ± 13	1991	1.510	
	2125 ± 16	1429	1.490	
1150	1197 ± 19	695×10^3	1.720	
	2082 ± 17	1138	1.831	
	1706 ± 18	879	1.940	1.803
	750 ± 16	417	1.800	± .054
	1154 ± 12	670	1.722	
	1463	Background		

Decay curves for each of the two bombardment conditions are plotted as a function of time in Fig.4.1. At 500 kV proton energy the points fit an 8.15 hour half-life very well, but the agreement is not quite so good at 1150 kV. In the latter case it would be improved if the background correction was increased slightly, (not more than 5%, which would alter the yield ratio by less than 1%), but as the two types of run were

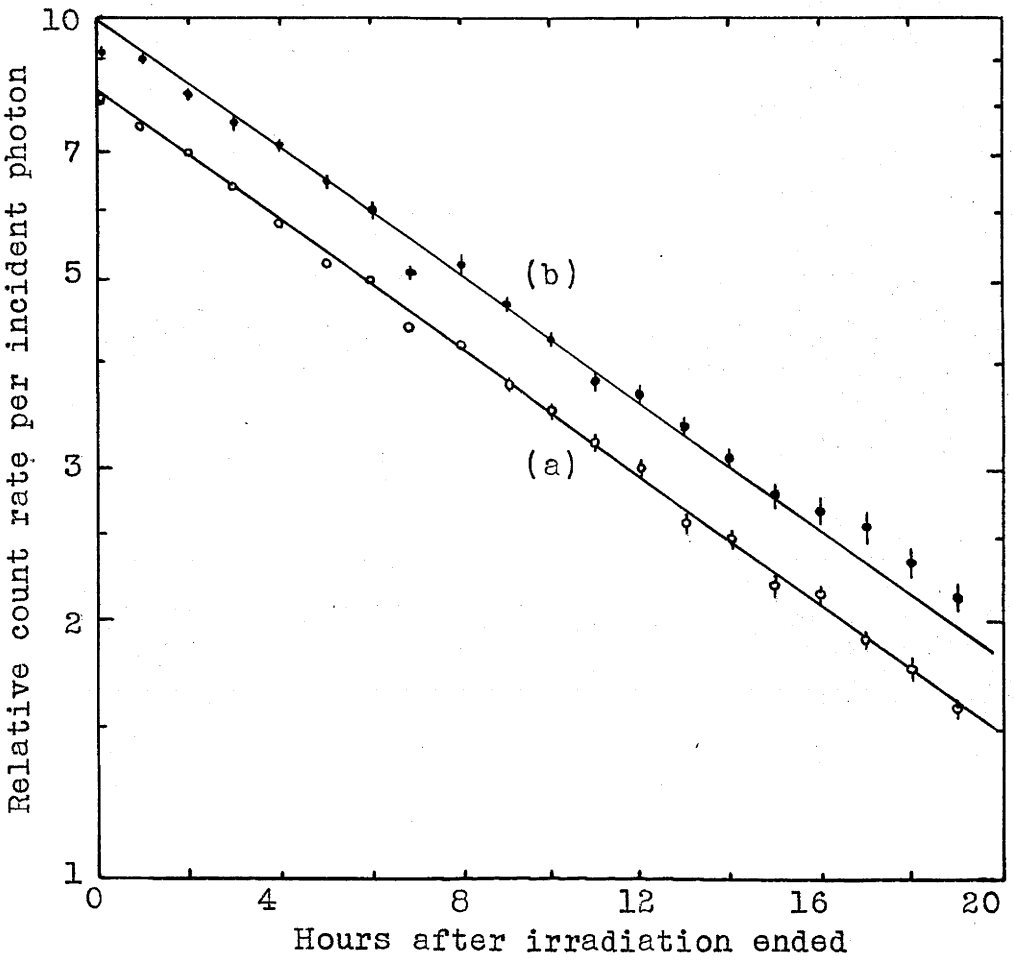

Fig.4.1 Decay curves for Ta^{180}:

(a) Sum of all runs at E_p = 500 kV.
(b) Sum of all runs at E_p =1150 kV.

carried out alternately there appeared to be no reason for supposing the background should have altered, and no change was made to the correction.

The final value obtained for the ratio of the (γn) yield per quantum at E_p = 500 kV to that at E_p = 1150 kV was

$$R = \frac{1.464}{1.803} = 0.811 \pm 0.035$$

4.3. Analysis of the Results.

The object of the following analysis is to deduce, from the measured yield ratio, the ratio of the $Ta^{181}(\gamma n)Ta^{180}$ cross section at 17.6 MeV to that at 14.8 MeV. At the lower proton energy the gamma energies are 17.6 and 14.8 MeV; at the higher energy they are both increased by 0.5 MeV, taking account of the target thickness. It is therefore necessary to allow for the change in the (γn) cross section between 17.6 and 18.1 MeV and over the 2 MeV width of the lower energy gamma line. This has been done by assuming that near 18 MeV and near 15 MeV the form of the (γn) cross section is the same as that given by Haslam et al.[63], but no assumption as to the relative magnitudes of the 17.6 and 14.8 MeV cross sections has been made. The curve obtained by Haslam et al. is reproduced in Fig.4.2; from it are derived the following cross section ratios:

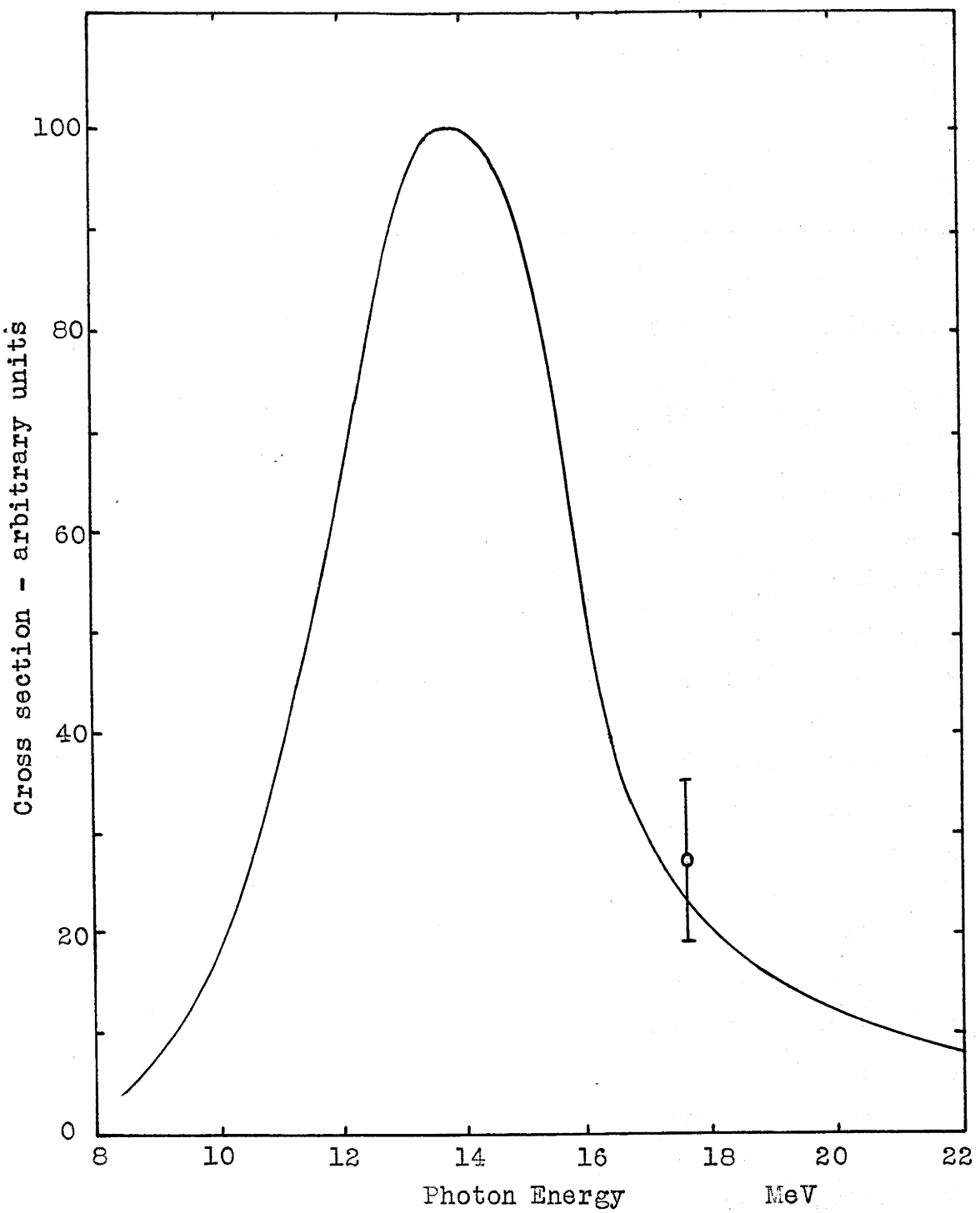

Fig.4.2 The cross section for $Ta^{181}(\gamma n)Ta^{180}$ at 17.6MeV compared with the curve obtained by Haslam, Smith and Taylor.

$$\frac{\sigma(18.1)}{\sigma(17.6)} = 0.84 \qquad \frac{\sigma'(14.8)}{\sigma(14.8)} = 0.93 \qquad \frac{\sigma'(15.3)}{\sigma'(14.8)} = 0.91$$

where $\sigma'(E) = \int\sigma(E)I(E)dE \div \int I(E)dE$, is the effective cross section for the broad gamma ray line of intensity $I(E)$. The values obtained for the last two ratios are relatively insensitive to the shapes and widths assumed for the gamma ray line; the second ratio changes by only 2% if the width is halved, while the third changes imperceptibly (cf. remarks in Section 4.1 re possible systematic errors).

With the above notation the yield ratio which was measured is

$$R = \frac{I_{14.8}\sigma'_{14.8} + I_{17.6}\sigma_{17.6}}{I_{14.8} + I_{17.6}} \div \frac{I_{15.3}\sigma'_{15.3} + I_{18.1}\sigma_{18.1}}{I_{15.3} + I_{18.1}}$$

$$\therefore \quad R\left(\frac{1 + \frac{I_{17.6}}{I_{14.8}}}{1 + \frac{I_{18.1}}{I_{15.3}}}\right) = \frac{1 + \frac{I_{17.6}}{I_{14.8}}\frac{\sigma_{17.6}}{\sigma'_{14.8}}}{\frac{\sigma'_{15.3}}{\sigma'_{14.8}} + \frac{I_{18.1}}{I_{15.3}}\frac{\sigma_{18.1}}{\sigma_{17.6}}\frac{\sigma_{17.6}}{\sigma'_{14.8}}}$$

Substitution of the effective cross section ratios and the gamma ray intensities measured by Stearns and McDaniel, viz. $I_{17.6} = 1.70I_{14.8}$ and $I_{18.1} = 0.45I_{15.3}$ finally gives

$$\frac{\sigma_{17.6}(Ta^{181}(\gamma n)Ta^{180})}{\sigma_{14.8}(Ta^{181}(\gamma n)Ta^{180})} = 0.30 \pm 0.09 .$$

The 5% probable error in R becomes 20% in the final cross section ratio, and an equal contribution to the final error comes from the errors in the gamma intensity ratios.

This result is compared in Fig.4.2 with the curve given by Haslam et al.

4.4. Conclusion.

The cross section for $Ta^{181}(\gamma n)Ta^{180}$ measured with the $Li^{7}(p\gamma)$ radiation agrees with the bremsstrahlung results, and therefore confirms the (γn) data used by Carver et al. to obtain the value 0.29 ± 0.11 for the $Ta^{181}(\gamma 2n)Ta^{179}$ cross section at 17.6 MeV relative to the $Ta^{181}(\gamma n)Ta^{180}$ cross section at 14.6 MeV. Their result agrees with the indirect estimate, 0.41, made by Eyges[17], and is consistent with the total neutron yield measurements made by Halpern, Nathans and Mann[65], and Whalin and Hanson[66] using betatron bremsstrahlung.

The measurements show that the cross sections for $(\gamma 2n)$ and (γn) in tantalum at 17.6 MeV are nearly equal, whereas calculations based on the statistical theory[67,68]

---

65. Halpern,J.,Nathans,R.,and Mann,A.K. Phys.Rev.88:679 (1952).
66. Whalin,E.A.,and Hanson,A.O. Phys.Rev.89:324 (1953).
67. Blatt,J.M.,and Weisskopf,V.F.'Theoretical Nuclear Physics', Wiley (1952). p.p.365-374.
68. Heidmann,J.,and Bethe,H.A. Phys.Rev.84:274 (1951).

predict that at this energy the $(\gamma 2n)$ cross section should be some 16 times larger. Hence the $(\gamma 2n)$ cross section must be virtually the cross section for compound nucleus formation, while most of the (γn) cross section must correspond to a direct photo-ejection mechanism. Using the statistical theory prediction and the measured cross section ratios, it is found that the cross section for the direct process is 0.85 ± 0.07 of the cross section for compound nucleus formation.

The high (γn) cross section makes it likely that the (γp) cross section will not be negligible even at 18 MeV, as the Coulomb barrier is 13 MeV and the proton binding energy is only 5.8 MeV. This raises doubts as to whether all important competing processes have been measured. The $Ta(\gamma p)$ reaction would not have been observed by Haslam et al. since Hf^{180} is stable. Levinger and Bethe[34] assumed that competing processes occurred with the frequencies given by the statistical theory in order to obtain agreement between the results calculated from dipole sum rules and the measured neutron yield data. For tantalum the experimental value was at the extreme upper limit of the theoretical one, and since the $(\gamma 2n)$ competition is in fact less than they assumed, the disagreement is increased. The idea of purely statistical competition must therefore be modified

when neutron yields from heavy elements are to be used to calculate the integrated absorption cross section for comparison with the dipole sum rules.

Since this work was completed, information has been published showing that naturally occurring Ta^{180} is stable ($T_{\frac{1}{2}} > 4 \times 10^9$ years)[69], and the question arises whether the results are affected by (γn) transitions which go to the ground state of Ta^{180} instead of the 8.15 hour metastable state. Since all of the calculations have been made from comparisons of shapes rather than absolute values of cross section vs. energy curves, the deduced ratio for $\sigma(\gamma 2n)$ to $\sigma(\gamma n)$ is unaffected so long as the fraction of (γn) transitions to the 8.15 hour state is constant over the energy range considered. It is reasonable to assume that this is so, since the ratio for the production of two isomeric states in Mo^{91} by (γn) reactions remains constant from 15 to 67 MeV[70].

69. Zweifel, P.F. Phys.Rev.98:1174 (1955).
70. Sagane, R. Phys.Rev.85:926 (1952).

CHAPTER 5.

CROSS SECTIONS FOR THE REACTION $C^{12}(\gamma 3\alpha)$ IN THE ENERGY RANGE 12-18 MeV.

5.1. Introduction.

Considerable attention has been given to the reaction $C^{12}(\gamma 3\alpha)$ and the position has been reviewed recently by Titterton[71]. The photographic plate method has been used by many observers to determine the cross section for the $Li^7(p\gamma)$ resonance radiation, a knowledge of this being important since it is often convenient to use it for the determination of cross sections for other less intense reactions occurring in the emulsion. The wide spread of values which have been reported (Table 5.1 and Fig.5.5) is unsatisfactory and makes a redetermination of the cross section at 17.6 MeV desirable; at the same time it was hoped that by using other lines in the $Li^7(p\gamma)$ spectrum, particularly the broad one at 14.8 MeV, information could be obtained on the resonance absorption of radiation by states of C^{12}, evidence for which had been presented by Goward and Wilkins[72].

---

71. Titterton, E.W. Prog. Nuc. Phys. 4:1 (1955).
72. Goward, F.K., and Wilkins, J.J. Proc. Roy. Soc. A217:357 (1953).

To determine the cross section at 17.6 MeV a methane filled proportional counter was used, since this enables data to be collected more quickly and with better energy resolution than is possible by the emulsion method. However, the information obtained is less definite; only the total disintegration energy is measured and it is impossible to distinguish experimentally between events where one particle strikes the counter wall and events due to gamma rays of energy lower than the main line, although the number of events in the former class can be estimated by calculation. For this reason the proportional counter was used to obtain the absolute cross section at 17.6 MeV, while the results of photographic plate studies were employed to investigate the reaction at lower energies and to determine the cross section values at 14.8 and 12.3 MeV relative to the 17.6 MeV measurement.

5.2. The Counter Experiment.

Resonance radiation from the $Li^7(p\gamma)$ reaction was excited by bombarding a thick lithium metal target with 500 kV protons, the counter[73] being situated with its axis perpendicular to the proton beam and its centre 10.8 cm. from the target at 0°. Irradiation was carried

73. A description of the counter is given in Section 3.4.

out in 8 hour runs, alternating with background runs of similar duration. The $C^{12}(\gamma 3\alpha)$ counting rate was small (~140 per hour) necessitating accurate knowledge of the counter background (~180 per hour). Actually the $C^{12}(\gamma 3\alpha)$ peak produced by the 17.6 MeV gamma rays yields alpha particles with a total energy of 10.3 MeV, well above the background due to the radioactive contamination, and in 44 hours no background pulses over 9.2 MeV were observed. However, a knowledge of the background was important for an analysis of the tail of the 17.6 MeV peak and of peaks due to lower energy gamma rays.

The radiation was monitored as described in Section 3.2 using the thick walled brass Geiger counter. Readings of pulse counts were recorded at one hour intervals during each run. The relative photodisintegration yield per quantum (which is proportional to total photodisintegration counts/total gamma flux) in the four runs was 1.00 : 1.00 : 1.06 : 0.96.

5.3. The Cross Section at 17.6 MeV.

The pulse spectrum resulting from 31 hours irradiation is shown in Fig.5.1(a) which, after subtraction of the background given in Fig.5.1(b), leads to the curve of Fig.5.1(c). The high energy peak

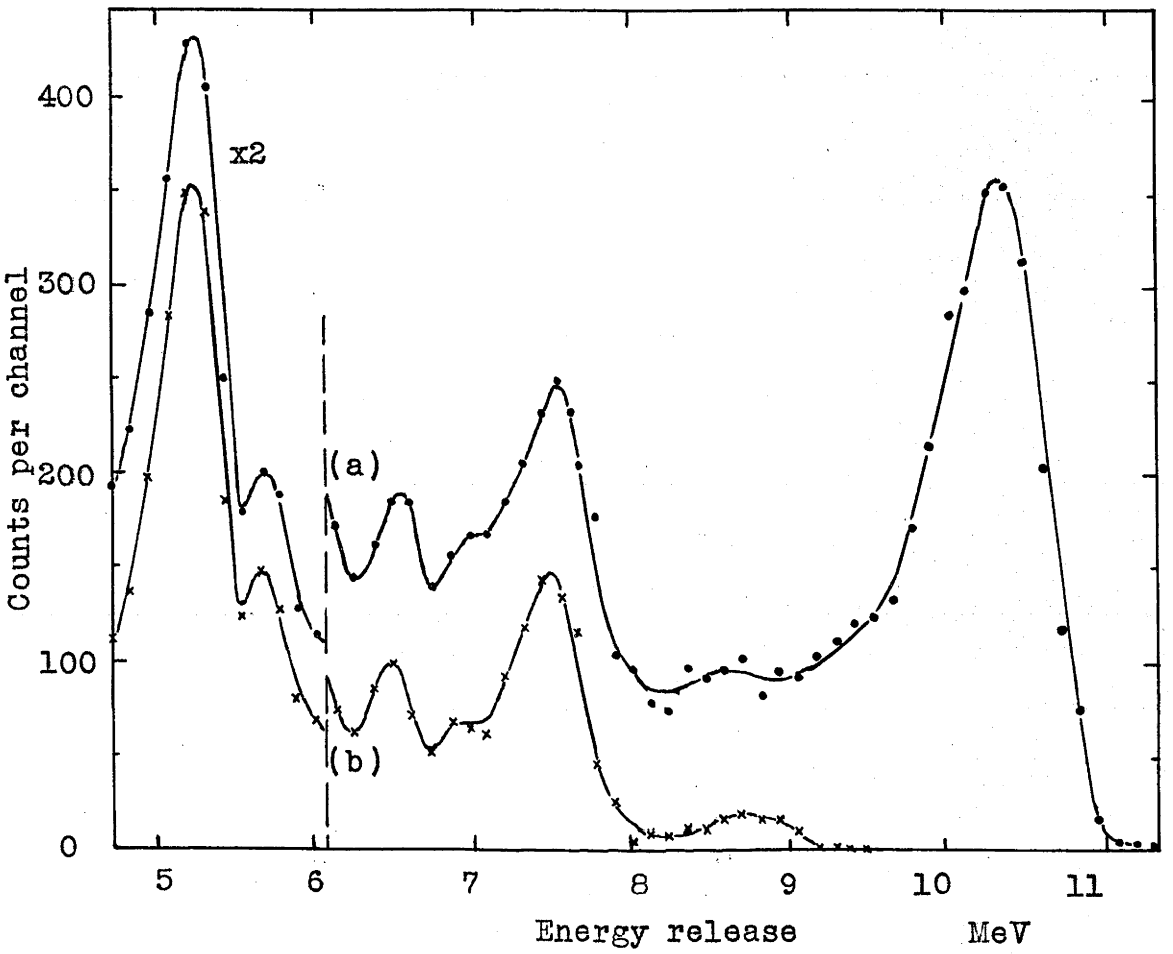

Fig.5.1 (a) Pulse spectrum obtained in 31 hours irradiation of the methane counter.
(b) Counter background spectrum normalised to 31 hours running time.

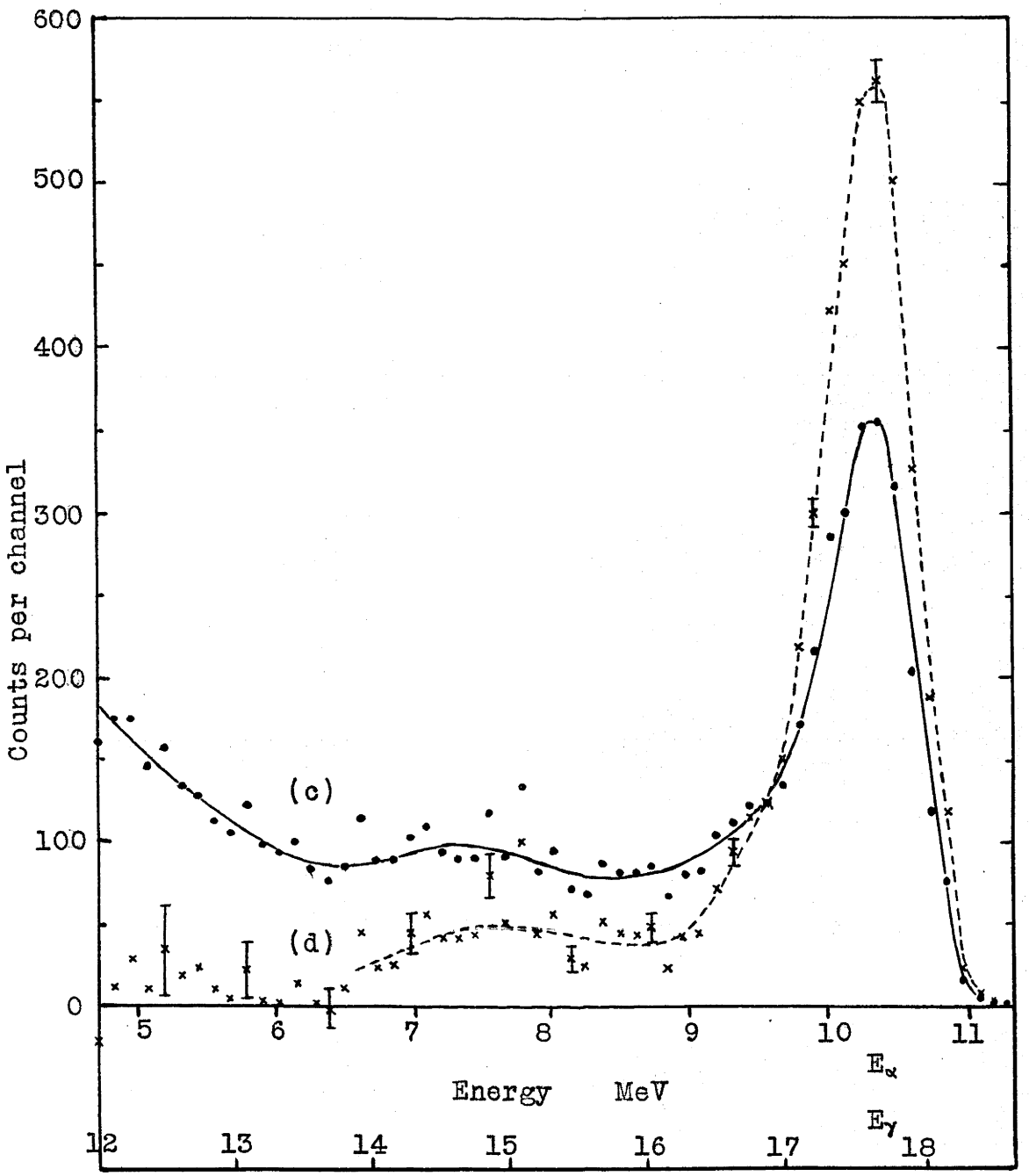

Fig.5.1 (c) Pulse spectrum resulting from the photo-disintegration of C^{12} (difference of (a) and (b)).

(d) Corrected distribution.

contains approximately 2900 counts, has a half-width of 0.8 MeV, and centres at 10.30 ± 0.06 MeV as expected from the mass data which gives the reaction threshold as 7.28 MeV. Contributions to the spectrum below the main peak come from gamma ray pile up pulses, alpha particles from 17.6 MeV events which are not contained entirely within the counting region, and $C^{12}(\gamma 3\alpha)$ events induced by gamma rays of energies less than 17.6 MeV. The pile up pulse contribution, although small, was significant, amounting to 130 counts per channel at 5 MeV, decreasing nearly exponentially to 10 counts per channel at 8 MeV, for a 31 hour period.

To allow for losses to the walls a knowledge of the ranges and directions of the alpha particles is necessary. The correction applied assumes the disintegration to be two-stage:

$$C^{12} \rightarrow \alpha + Be^{8} \quad : \quad Be^{8} \rightarrow 2\alpha$$

and to be isotropic, with 93% of the transitions through the 2.8 MeV level of Be^{8} and the remaining 7% through the ground state[72,74]. A range energy relation for alpha particles in methane was deduced from the curves of Livingston and Bethe[75], and correction factors were

---

74. Titterton, E.W. Present work, Section 5.4.
75. Livingston, M.S., and Bethe, H.A. Rev. Mod. Phys. 9:245 (1937).

derived fron those for single alpha particles to give the fraction of events in which one or two alpha particles of a star intercept the boundaries of the counter. The energy distribution of the resulting degraded pulses is shown in Fig.5.2; it was calculated by a method similar to that of Section 3.7 for single alpha particle tracks. The shape of the distribution has little effect on the magnitude of the peak at 17.6 MeV, but makes the yield at lower energies uncertain, and it is for this reason that the cross section at 17.6 MeV only has been calculated from the counter data.

The final distribution, Fig.5.1(d), was derived from Fig.5.1(c) by subtracting the pulse distributions arising from pile up and wall losses, and then adding the loss corrections, at the appropriate energy, to the 17.6 MeV peak. The peak is asymmetrical, probably because the amplifier time constants were shorter than the rise-times of some of the pulses[76].

A small correction (5%) for absorption of radiation in the counter walls was calculated from the data given by Heitler[77] and confirmed by direct measurement with the gamma ray counter. The intensities of the gamma

---

76. See Section 3.4.
77. Heitler, W. 'The Quantum Theory of Radiation', 2nd.ed., O.U.P. (1949).

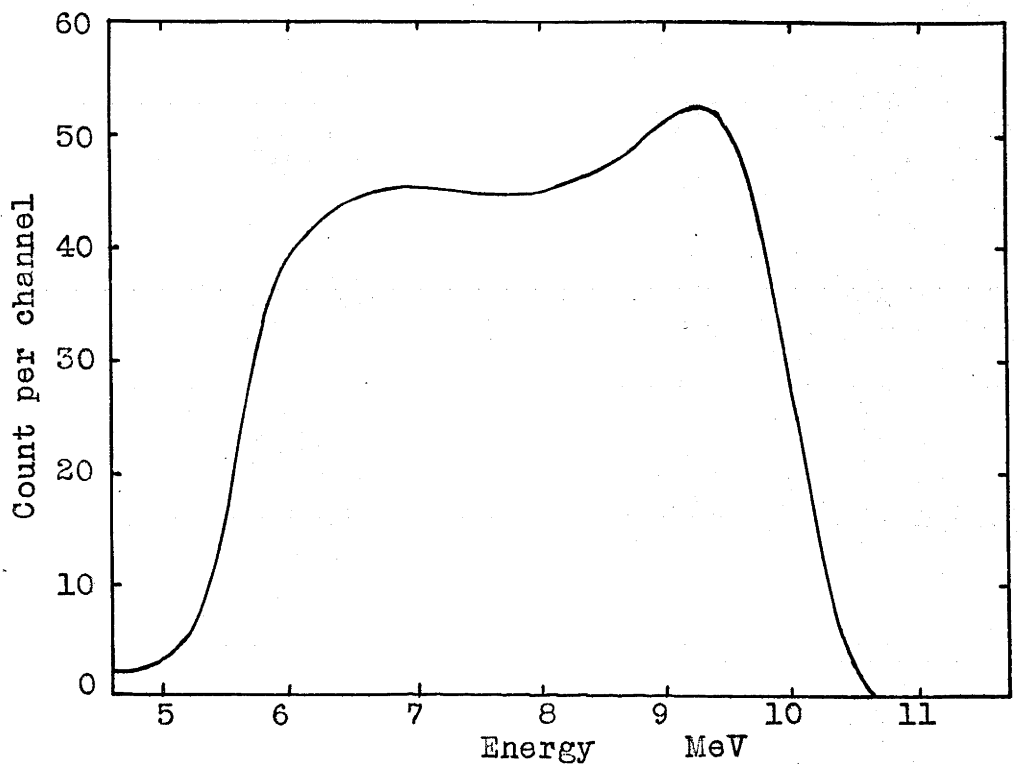

Fig.5.2 Energy distribution of pulses from $C^{12}(\gamma,3\alpha)$ events at 17.6 MeV in which 1 or 2 of the particles strike the walls of the counter, for the 31 hour run.

lines were assumed to be in the ratios

$$I_{17.6} : I_{14.8} : I_{12.3} = 0.62\pm5\% : 0.36\pm12\% : 0.02\pm50\%,$$

the first two values being based on the data of Stearns and McDaniel[46] and the last figure being based on the results given by Inall[42] and Titterton[78].

The final value for the cross section at 17.6 MeV is

$$\sigma_{17.6}(C^{12}\gamma 3\alpha) = (1.70 \pm 0.24)10^{-28} \text{ cm}^2.$$

A summary of cross section measurements at 17.6 MeV is given in Table 5.1. The agreement between the last three values listed may be fortuitous; the value for $\sigma_{17.6}$ obtained with the lithium radiation will depend on the relative intensity assumed for the narrow

Table 5.1. Absolute measurements of the cross section for $C^{12}(\gamma 3\alpha)$.

	$\sigma_{17.6}$ in 10^{-28} cm^2	σ_{mean}
Waffler & Younis(1949)[79]		0.8 ±0.3
Glattli,Seippel & Stoll(1952)[80]	2.4	1.75±0.25
Goward & Wilkins(1953)[72]	1.70±0.34*	1.40±0.26
Greenberg,Taylor & Haslam(1954)[81]	1.7†	
Present work	1.70±0.24	1.19±0.20

*Combination of lithium radiation and bremsstrahlung measurements.
†Bremsstrahlung measurement.

78. Titterton,E.W. Aust.J.Sci.15:174 (1953).
79. Waffler,H.and Younis,S. Helv.Phys.Acta 22:614 (1949).
80. Glattli,H.,Seippel,O.,and Stoll,P. Helv.Phys.Acta 25:491 (1952).
81. Greenberg,L.H.,Taylor,J.G.V.,and Haslam,R.N.H. Phys.Rev. 95:1540 (1954).

17.6 MeV line, which was not the same in the experiments listed, while the value from bremsstrahlung experiments will be an average over a much wider energy range.

5.4. Photographic Plate Measurements.

Incidental to another investigation some 1000 $C^{12}(\gamma 3\alpha)$ 'stars' were measured in Ilford 200μ type E1 boron-loaded emulsions which had been exposed to the $Li^{7}(p\gamma)$ resonance radiation. The stars were identified by the usual method of momentum balance and the number-energy histogram is given in Fig.5.3. Three peaks are resolved, the main one at 17.6 MeV contains 742 events, the broad 14.8 MeV group has 86 events, and the group centring on 12.5 MeV has 17 events. These numbers may be compared with 2160, 300, 35 observed by Nabholz, Stoll and Waffler[82], and 390, 50, 12 observed by Goward and Wilkins[72].

Loss corrections were made by the geometric method of Goward and Wilkins and the smooth distribution, full line of Fig.5.3, obtained. The final result is compared with the methane chamber data in Fig.5.4, the curves being normalised by the area of the 17.6 MeV peak.

82. Nabholz,H.,Stoll,P.,and Waffler,H. Helv.Phys.Acta 25: 153 (1952).

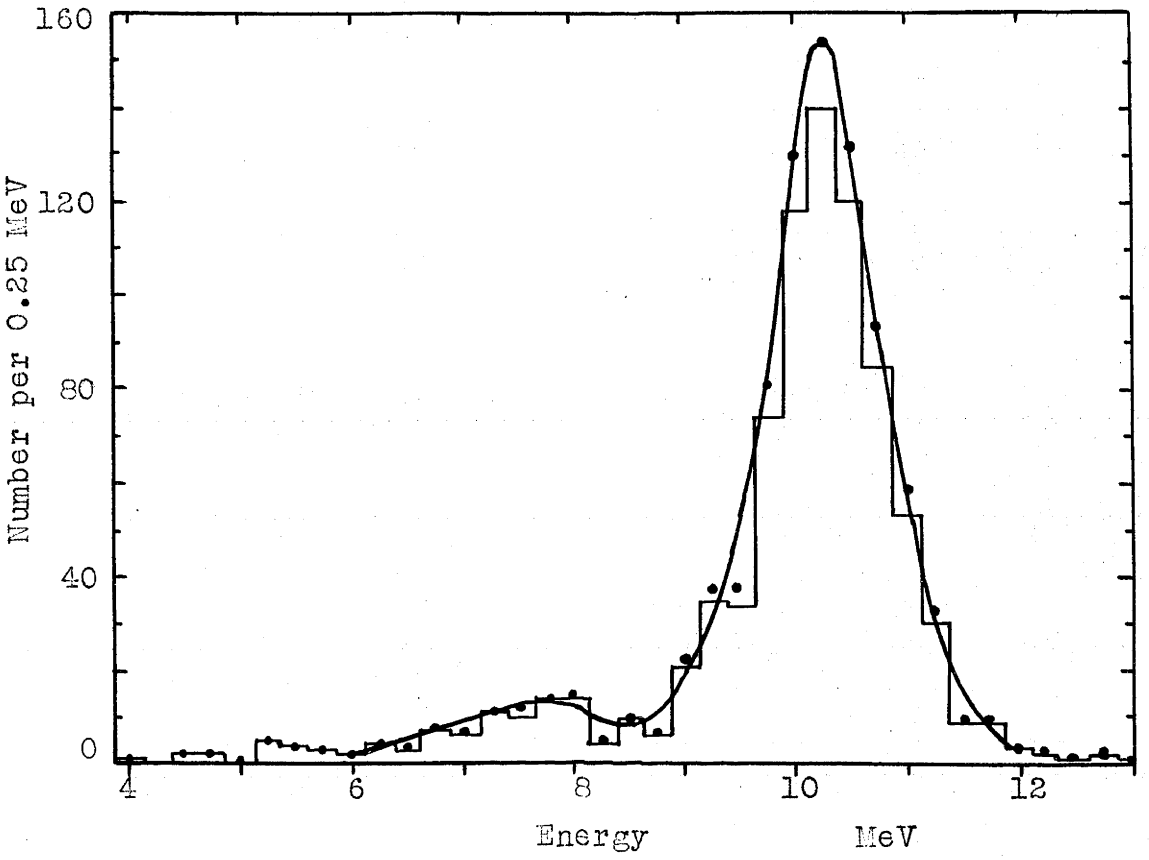

Fig.5.3 Histogram of energy released in 845 $C^{12}(\gamma,3\alpha)$ 'stars', with the corrected curve superimposed.

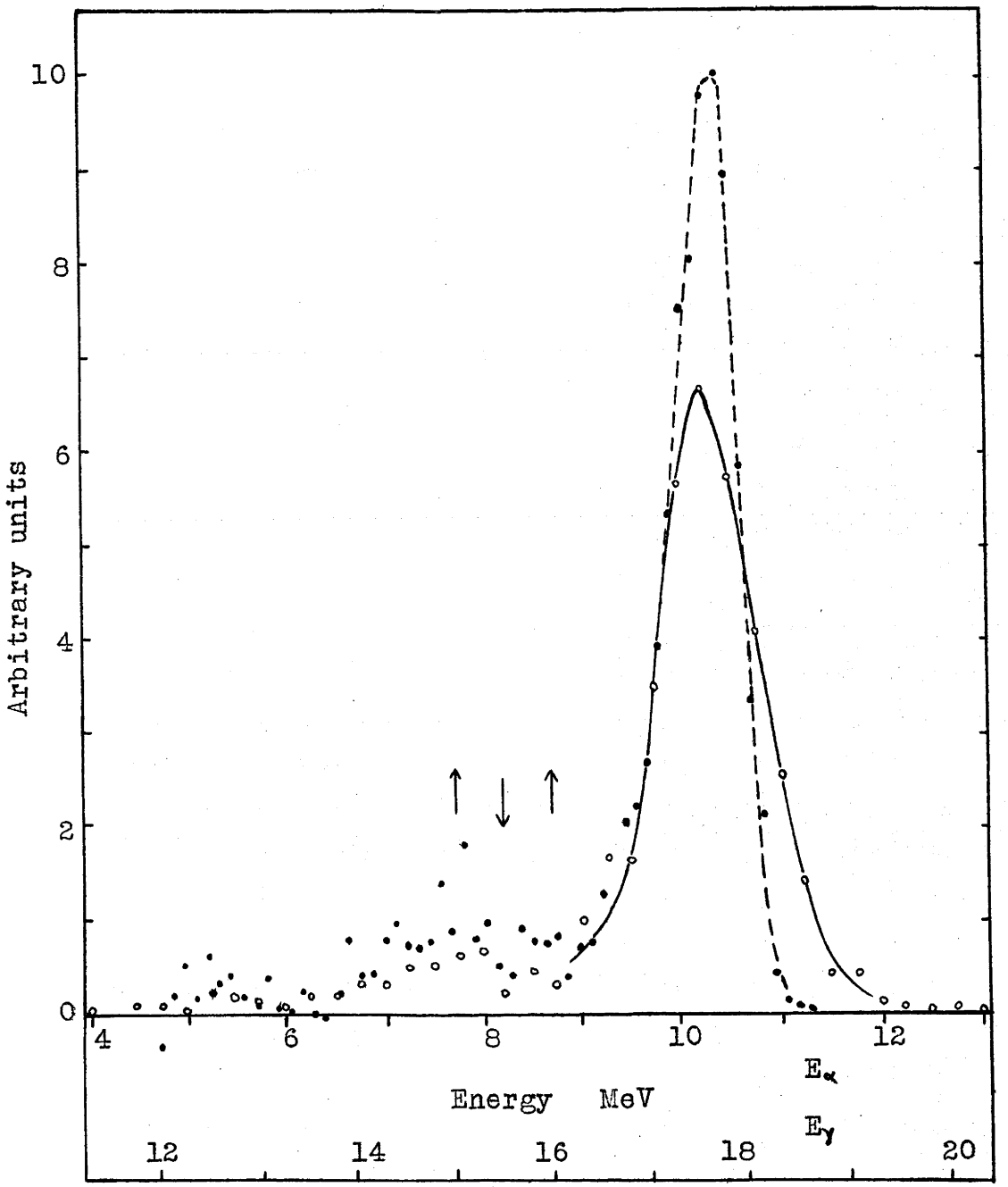

Fig.5.4 Comparison of results from methane counter and photographic plate, normalised by areas of the high energy peak.

• counter ○ plate

5.5. Cross Sections at 14.8 and 12.3 MeV.

Taking the cross section at 17.6 MeV to be 1.70×10^{-28} cm^2, and the relative intensities of the 17.6 and 14.8 MeV lines to be as given in Section 5.3, the photographic plate data gives

$$\sigma_{14.8}(C^{12}\gamma 3\alpha) = (0.33 \pm 0.07)10^{-28} \text{cm}^2.$$

The group centring on 12.5 MeV in Fig.5.4 could be due to a reaction of the type $C^{12}(\gamma\gamma')3\alpha$, if a level in C^{12} is available at the appropriate energy. However, strong evidence from experiments in this laboratory has been presented by Titterton[78], Inall and Boyle[83], and Inall[42] to show that there is a weak line in the lithium gamma spectrum at 12.3 MeV, corresponding to a transition to a state in Be^8 at 5.3 MeV. Discarding the possibility that the group may be due to inelastic scattering, the cross section for the reaction $C^{12}(\gamma 3\alpha)$ at 12.3 MeV has been calculated, taking the intensity of this gamma ray to be 2 ± 1% of the total radiation. The figure obtained is

$$\sigma_{12.3}(C^{12}\gamma 3\alpha) = (1.15 \pm 0.6)10^{-28} \text{cm}^2.$$

Using the same set of conditions and normalising all cross sections to the present 17.6 MeV figure, cross sections at 14.8 and 12.3 MeV have been calculated from the histograms published by Nabholz et al.[82] and

83. Inall, E.K., and Boyle, A.J.F. Phil.Mag.Ser.7 44:1081 (1953).

Goward and Wilkins[72], and are presented in Table 5.2. It will be seen that there is reasonable agreement among the three experiments for the cross section at 14.8 MeV, but considerable relative differences at 12.3 MeV. In each case the extreme values in columns 3 and 4 differ by twice the sum of the errors calculated from the total numbers of counts.

Table 5.2. Cross sections for $C^{12}(\gamma 3\alpha)$ at 14.8 and 12.3MeV

Normalised to $\sigma_{17.6} = 1.70 \times 10^{-28}$ cm^2. The lower two sets of results were calculated from the published histograms. The relative gamma ray intensities used were:
$I_{17.6} = 0.62 \pm 5\%$ $I_{14.8} = 0.36 \pm 12\%$ $I_{12.3} = 0.02 \pm 50\%$

Source	Cross section x gamma intensity			Cross section in 10^{-28}cm^2			
	17.6	14.8	12.3	17.6	14.8	12.3	mean
a	1.05			1.70 ±.24			
b	1.05 ±.024	0.118 ±.007	0.023 ±.004		0.33 ±.07	1.15 ±0.6	1.19 ±.020
c	1.05 ±.015	0.144 ±.005	0.015 ±.002		0.40 ±.08	0.75 ±0.4	1.21 ±.020
d	1.05 ±.033	0.130 ±.012	0.032 ±.006		0.36 ±.07	1.6 ±0.9	1.21 ±.020

a Present work, methane counter
b Present work, photoplate
c Nabholz et al.
d Goward and Wilkins.

The high cross section at 12.3 MeV implies the presence of a C^{12} level in this region and the resonance absorption of radiation of this energy. Such an

interpretation is supported by some of the bremsstrahlung data and by results obtained in a study of the reaction $C^{12}(nn')3\alpha$ by Livesy and Smith[84]. Excitation functions over the region 12 - 18 MeV have been measured with poor agreement by five groups, and are presented in Fig.5.5; the present three points have been plotted for comparison.

Inspection of both the methane chamber and the photoplate data over the width of the 14.8 MeV line, Fig.5.4, shows elevation of the points near 15 and 16 MeV and a trough at $15\frac{1}{2}$ MeV as indicated by the arrows. Taken separately, little weight could be placed on either result, but the two sets of data support each other. Moreover, examination of the photoplate results of Goward and Wilkins, and Nabholz et al. show the same features to be present in each of these experiments. Taken together, all the results lend support to the presence of peaks in the cross section at 15 and 16 MeV as observed by Goward and Wilkins (Fig.5.5), but suggest that the resonances are more marked than their excitation function indicates.

84. Livesy, D.L., and Smith, C.L. Proc. Phys. Soc. A66:689 (1953).

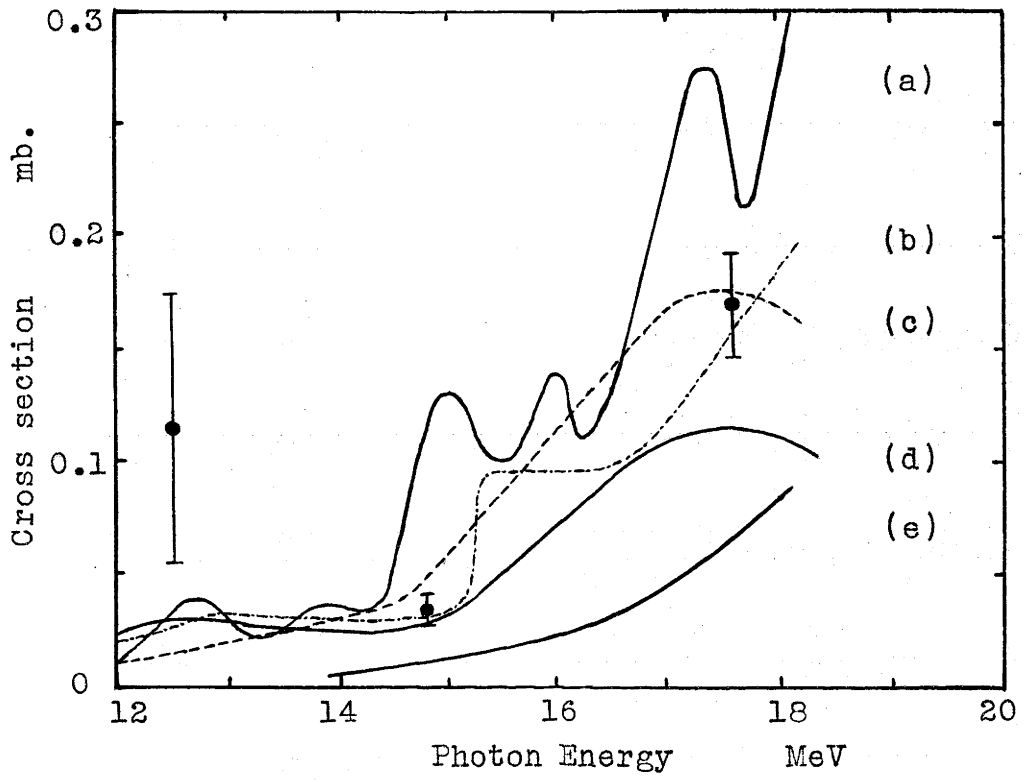

Fig.5.5 Cross sections for $C^{12}(\gamma,3\alpha)$ in the range 12 - 18 MeV.

(a)Goward and Wilkins (1953) Proc.Roy.Soc. A,217,357.
(b)Dawson and Bigham (1953) Can.J.Phys.,31,167.
(c)Millar and Cameron (1953)Can.J.Phys.,31,723.
(d)Eder and Telegdi (1952) Helv.Phys.Acta., 25,55.
(e)Telegdi and Zunti (1950) Helv.Phys.Acta., 23,745.

I Present results plotted.

CHAPTER 6.

THE REACTION $N^{14}(\gamma\alpha)B^{10}$ AT 17.6 MeV.

6.1. Introduction.

The photodisintegration of nitrogen has been observed in photographic plates by several groups of workers, including Goward and Wilkins[85], Dawson and Bigham[86], and Millar and Cameron[87]. Most of the reactions observed in the emulsions were ones in which several particles were emitted from the nitrogen nucleus, but apart from an estimate by Goward and Wilkins of about $10^{-28}cm^2$ for the $N^{14}(\gamma,d3\alpha)$ cross section at 23 MeV, no detailed results have been published. Wright, Morrison, Reid and Atkinson[88] used a cloud chamber to study the (γp) reaction in nitrogen from threshold to 23 MeV, and showed that the cross section exhibits the same sharp rise near 20 MeV as was seen in the (γn) cross section by Horsley, Haslam and Johns[89].

85. Goward,F.K.,and Wilkins,J.J. Proc.Phys.Soc.A64:312(1951).
86. Dawson,W.K.,and Bigham,C.B. Can.J.Phys.31:167 (1953).
87. Millar,C.H.,and Cameron,A.G.W.Can.J.Phys.31:723 (1953).
88. Wright,I.F.,Morrison,D.R.O.,Reid,J.M.,and Atkinson,J.R. Proc.Phys.Soc.A69:77 (1956).
89. Horsley,R.J.,Haslam,R.N.H.,and Johns,H.E. Can.J.Phys. 30:159 (1952).

The present investigation is by means of the $(\gamma\alpha)$ reaction, for which the isotopic spin selection rules inhibit electric dipole absorption in most cases, the only exception being for transitions to the 1.74 MeV level in B^{10} for which electric dipole is allowed (see Table 6.2). Transitions to other levels which can be excited must follow from magnetic dipole or electric quadrupole absorption. The experiment was performed in a nitrogen filled proportional counter, so that a suitable choice of counter pressure made it possible to study the high energy alpha spectrum without any background due to protons.

6.2. Experimental Method.

Details of the nitrogen filled counter and its operating characteristics are given in Section 3.5. The source of radiation, flux determination and geometry of the experiment were the same as for the methane counter experiment, and are described in Sections 3.1, 3.2 and 5.2. In this experiment, counts were recorded for half hour periods, alternating between irradiation and background runs.

The photodisintegration of nitrogen at 17.6 MeV can release protons with energies up to 9.3 MeV (reaction energy release 10.1 MeV), and alpha particles with up to 4.3 MeV (reaction energy release 6.0 MeV), which

have ranges of 100 cm. and 2.7 cm. respectively in 1 atmosphere of nitrogen. The 9.1cm. diameter counter was not strong enough to withstand the pressure of over ten atmospheres which would have been necessary to stop most of the high energy protons, so a pressure of 3 atmospheres was used, thus making it possible to observe the alpha particle spectrum without any proton background. The maximum possible energy release by a proton crossing a diagonal of the 18 cm. long counter would be 7.3 MeV, but less than $\frac{1}{2}\%$ of the (γp) reactions releasing 10.1 MeV would release more than 4 MeV in the counting region, as can be seen by a simple extension from Figs.3.15 and 3.16, which are for an infinitely long cylinder. Pulse spectra were also obtained for a counter pressure of 1 atmosphere, when the maximum proton energy release could be 3.9 MeV, in order to confirm that the number of proton counts above 4 MeV was negligible in the spectra taken at 3 atmospheres.

Since transitions may go to excited states in the product nuclei, there are numerous possibilities for the values of the energy released in the counter by charged particles. The energy release from the reactions most likely to be observed in this experiment is included in the information given in Table 6.1.

Table 6.1. Reactions in Nitrogen.

Reaction	Level in residual nucleus*	E_γ = 17.6 MeV					E_γ = 14.8 MeV	
		Energy release	Loss at 3 atmos. pressure†	Group in fig. 6.2	No. of events	Cross section	Energy release	Cross section
	MeV	MeV	%			mb.	MeV	mb.
$N^{14}(\gamma\alpha)B^{10}$ Q=−11.61	0	6.0	10	α_0	245	0.25	3.2	~1
	0.72	5.3	9	α_1	96	0.10	2.5	
	1.74	4.3	6	α_2	300	0.29	1.5	
	2.15	3.9	5	α_3	~125	~0.12	1.1	
	3.58	2.4	4	α_4				
	4.77	1.2						
$N^{14}(\gamma p)C^{13}$ Q=−7.54	0	10.1	100	Change in spectrum with pressure			7.3	
	3.09	7.0	more				4.2	
	3.68	6.4	than				3.6	
	3.86	6.2	99%				3.4	
	6.87	3.2	55	p_4	<50	<0.1	0.4	
	7.75	2.3	33	p_5				
	8.4	1.7	20	p_6	<50	<0.1		
$N^{14}(\gamma d)C^{12}$ Q=−10.3	0	7.3						
	4.43	2.9	25		<70?	<0.1?		
$N^{14}(\gamma, np)C^{12}$ Q=−12.5	Can not give protons with more than 5.1 MeV.							
$N^{15}(\gamma\alpha)B^{11}$ Q=−11.0	0	6.6					3.8	
	2.14	4.5	7½%					
	4.46	2.2						
	5.03	1.6						
$N^{15}(\gamma p)C^{14}$ Q=−12.2	0	7.4						
	6.09	1.3						

*Ajzenberg and Lauritsen (1955)[90]
†Recoil range neglected.

6.3. Results.

The pulse height distribution resulting from 2 hours irradiation is plotted in Fig.6.1(a), and after subtraction of the background in Fig.6.1(b), leads to the points plotted in Fig.6.2(a). The background rate for this run was rather high; it appeared to be due to contamination arising from the ThC calibration source, because it eventually decayed with a half-life of about 12 hours to less than one tenth of the rate of Fig.6.1(b). The curve drawn in Fig.6.2(b) shows the shape of the spectrum resulting from another 5 hours irradiation. It is a composite curve, made up from several runs performed with reduced gamma flux, longer clipping time constants and different amplifier gain, and has been adjusted to the same ordinate and energy scales as Fig.6.2(a) by normalising to the same gamma flux. The points and the curve have the same general shape, and peaks can be distinguished at 6.0, 5.3, 4.75, 4.2, 3.8 and 1.8 MeV, and possibly at 3.2, 2.9 and 2.5 MeV. Except for that at 4.75 MeV, they can be identified with one or other of the reactions listed in Table 6.1. Unfortunately the counter was damaged before further observations could be made with the low background, when the peaks would have shown up rather better than they do in Fig.6.1(a). However, spectra had already been obtained for which

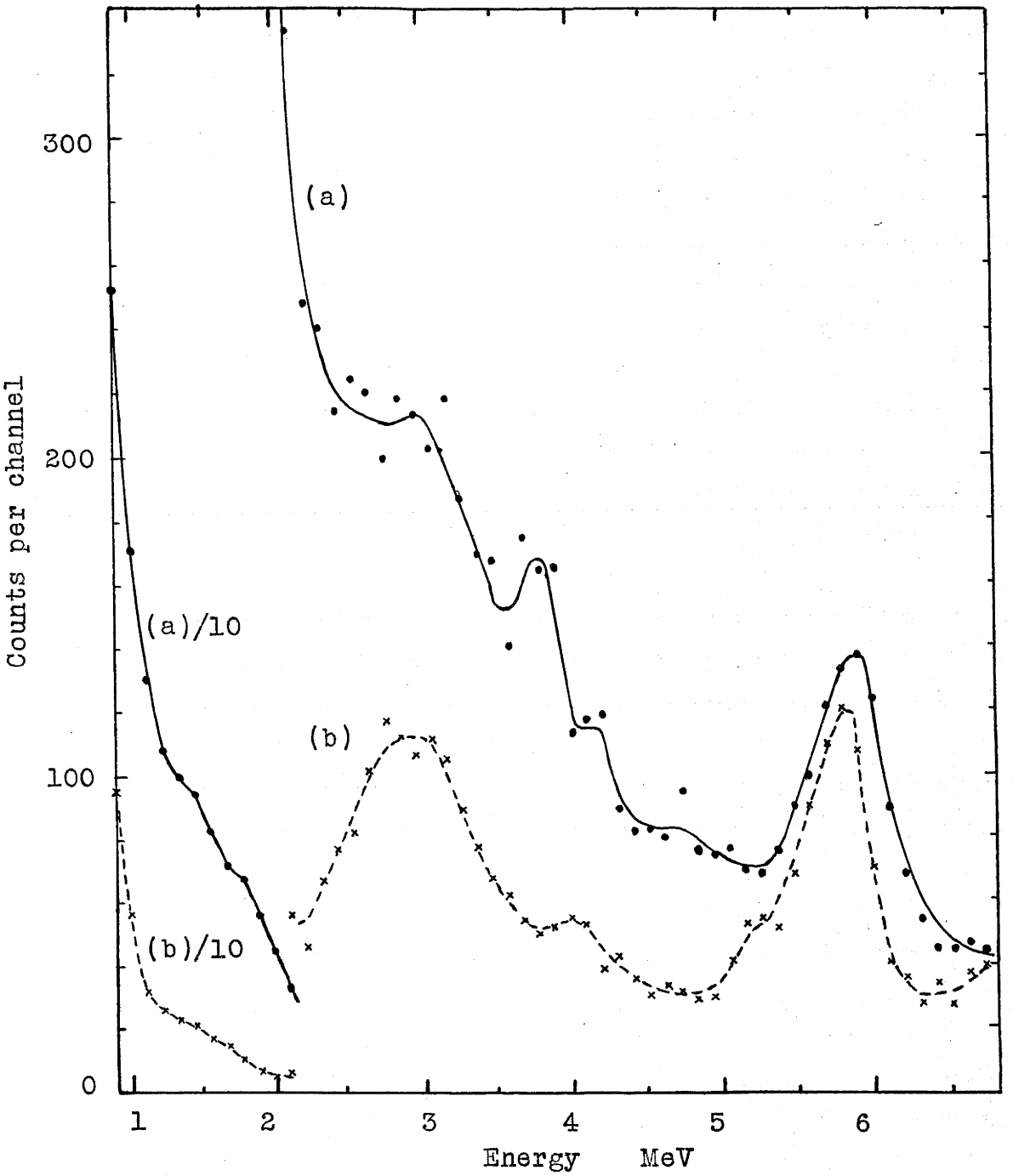

Fig.6.1 (a) Pulse spectrum obtained in 2 hours irradiation of the nitrogen counter at 3 atmos. pressure.
(b) Counter background normalised to 2 hours.

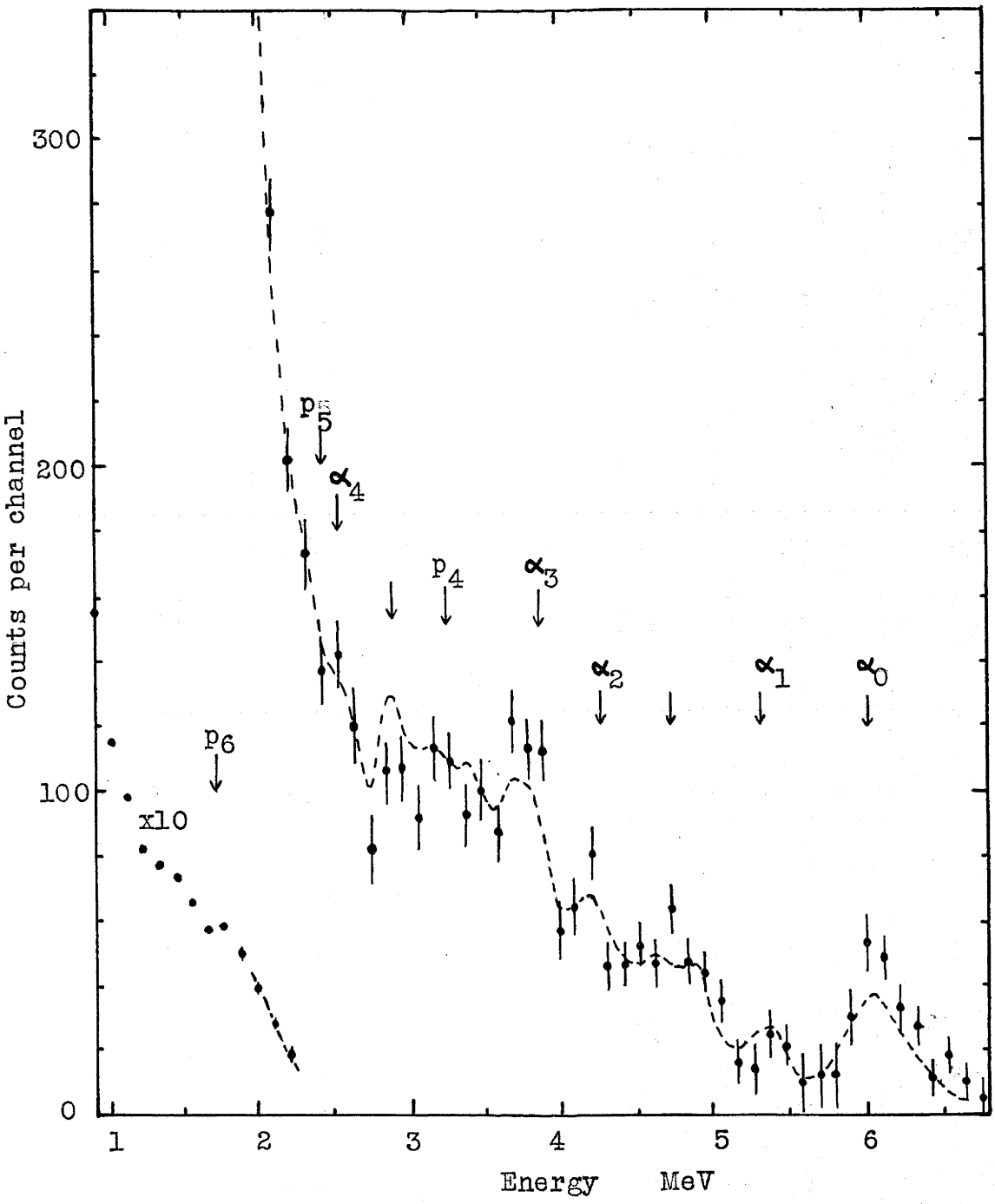

Fig.6.2 Pulse spectrum resulting from photodisintegration of nitrogen.
(a) plotted points. Difference of Fig.6.1(a) &(b).
(b) curve. Composite spectrum for 5 hours irradiation under different conditions.

changes had been made in some or all of the following conditions: nitrogen pressure (to 1 atmosphere), anode voltage, amplifier time constants, gain, and kicksorter bias. These spectra showed the same peaks as Fig 6.2, and in particular the low pressure runs showed that the 4.75 MeV group was due to particles heavier than deuterons which were emitted from the nitrogen when it was irradiated, and it has been assumed that these were alpha particles.

The radiation yield was monitored by the standard Geiger counter, and after corrections had been made for the distances of the monitor and nitrogen counters from the source, and absorption of radiation in the walls, the total flux through the counter was found to be 7.85×10^6 photons/cm^2. Using the data given in Section 3.1 for the composition of the $Li^7(p\gamma)$ resonance radiation, the flux at 17.6 MeV was

$$F_{17.6} = (4.95 \pm 0.7)10^6 \text{ photons/cm}^2.$$

The 14% probable error in the flux comes from the following sources:

absolute calibration of the Geiger counter	12%
short term variation in Geiger sensitivity	3%
corrections made by inverse square law	2%
17.6 MeV fraction of the total radiation	5%.

The number of atoms of nitrogen contained in the sensitive

volume of the counter, 9.1 cm. in diameter and 20 cm. long, at 3 atmospheres pressure was

$$N = (2.1 \pm 0.1)10^{23}$$

where the main contribution to the error arises from uncertainty about the electric field distribution near the ends of the wire. Cross sections for the photo-disintegration reactions were calculated from the observed number of disintegrations 'D' by means of the relation $\sigma = D/NF$

$$= (0.96 \pm 0.12)10^{-30}D.$$

The analysis of the spectrum falls conveniently into two divisions: (i) above 4 MeV, where only $(\gamma\alpha)$ reactions at 17.6 MeV can contribute, and (ii) below 4 MeV, where the spectrum is confused by contributions from other $(\gamma\alpha)$ and (γp) reactions at both 17.6 and 14.8 MeV.

(i) Above 4 MeV only alpha particles from the reactions at 17.6 MeV are counted. The total number of counts is 924 ± 60, which, after correction for loss to the walls varying from 6% at 4 MeV to 10% at 6 MeV, gives the cross section for these $(\gamma\alpha)$ reactions:

$$\sigma_{17.6}(N^{14}(\gamma\alpha)B^{10}) = 0.93 \pm 0.14 \text{ millibarns.}$$

The spectrum can be divided into groups about 8% wide, and the partial cross sections so obtained are 0.25, 0.1, 0.3, and 0,3 mb for the 6.0, 5.3, 4.75, and 4.3 MeV groups respectively.

The total cross section includes electric dipole as well as magnetic dipole and electric quadrupole components. As the spins and parities of the levels in the initial and final nuclei are known[90], it is possible to calculate the relative probabilities for emission of alpha particles from the compound nucleus to the different levels in B^{10}; the barrier penetrabilities, $(F^2 + G^2)^{-1}$,[91] for the cases arising from electric dipole, magnetic dipole, and electric quadrupole absorption are given in Table 6.2. Also, since the N^{14} nucleus contains equal numbers of neutrons and protons, the isotopic spin selection rules for electric dipole absorption, viz.

Table 6.2. Coulomb barrier penetrabilities for emission of alpha particles from N^{14}.

(f means forbidden by spin and parity selection rules.)

Nucleus	N^{14}	N^{14*}	B^{10}				
Level	0	17.6	0	.72	1.74	2.15	3.58
J	1^+		3^+	1^+	0^+	1^+	2^+
T	0		0	0	1	0	0
E1		0^-	.09	.40	f	.24	f
		1^-	.09	.40	.29	.24	.06
		2^-	.48	.40	f	.24	.06
M1		0^+	f	f	.42	f	.03
		1^+	.27	.54	f	.36	.03
E2		2^+	.27	.21	.11	.09	.13
		3^+	.60	.21	f	.09	.03
Energy release MeV			6.0	5.3	4.3	3.9	2.4
observed mb.			.25	.10	.30	.1	

90. Ajzenberg, F., and Lauritsen, T. Rev. Mod. Phys. 27:77 (1955).
91. Sharp, W. T., Gove, H. E., and Paul, E. B. AECL Rep. TPI-70 (1953).

$\Delta T = \pm 1$ when $T_z = 0$, will apply and alpha particle emission to T = 0 levels in B^{10} will be suppressed. Hence the transition to the 1.74 MeV T = 1 level will be the only important one if the absorption process is electric dipole to a 1^- level in N^{14}. The observed cross sections show immediately that this is not the case, but even if it is assumed that all of the 4.3 MeV group results from electric dipole absorption, then it is seen that it accounts for only a third of the observed cross section. The other transitions result from magnetic dipole or electric quadrupole interactions, and inspection of Table 6.2 indicates that the most reasonable agreement with the observed cross sections is for emission from a 2^+ or 3^+ state in N^{14}. The 17.6 MeV line is so sharp that until further information is obtained, e.g. from angular distribution measurements, no definite conclusion is possible regarding the weakness of the electric dipole transitions in the neighbourhood of 18 MeV.

The peak which was observed at 4.75 MeV has not yet been assigned to any of the reactions listed in Table 6.1. Possibly parts of the group could be included in the 4.3 and 5.3 MeV groups, but this would still leave many counts unexplained. The peak was present with the same intensity as the alpha particle peaks for both 3 and 1

atmospheres pressure in the counter, so it could not have been due to protons or deuterons. It is unlikely that it was due to particles heavier than alphas because the thresholds for such reactions are too high, therefore the group must be due to an alpha emitting reaction. If it is assumed that the gas contained the normal 0.3% of N^{15}, and the 4.75 MeV peak is assigned to the $N^{15}(\gamma\alpha)B^{11}$ reaction which releases 4.5 MeV, then it implies a cross section of about 100 mb. This possibility is rejected on account of the exceedingly large cross section and the incorrect energy release. The correct energy would be released from an alpha particle transition to a new level in B^{10} at 1.25 MeV. However, the low lying levels of this nucleus, both of T = 0 and T = 1, have been extensively studied[92] and there have been no suggestions that a 1.25 MeV level could be expected. Alternatively, the alpha particle could be emitted following inelastic scattering of the photons leaving the N^{14} nucleus at 16.4 MeV excitation, but this implies rather a large cross section for $(\gamma\gamma')$, and is unlikely. The peak remains unexplained.

(ii) Below 4 MeV the curve can not be analysed with confidence because of the contributions from reactions

92. Shafroth, S.M., and Hanna, S.S. Phys. Rev. 95:86 (1954).

due to the 2 MeV wide gamma line at 14.8 MeV, and from high energy photoprotons which dissipate only part of their energy in the counter. The distribution of track lengths within the counter was calculated and combined with the range-energy relation for protons to give the shape of the spectrum expected from each proton-yielding reaction. The general shape of these spectra indicated that changing the counter pressure from 3 to 1 atmospheres would reduce the proton counts between 2 and 3 MeV by a factor six, and the height of the proton peak at 3.2 MeV by a factor nine, relative to the high energy alpha peaks. The observed spectra for 1 atmosphere were 30% lower in the range 2 - 3 MeV, but the peak at 3.2 MeV did not alter perceptibly; these changes correspond to a little over 1 mb. for the cross section for $N^{14}(\gamma p)C^{13}$ by both of the lithium gamma rays, and considerably less than 0.1 mb. for the 3.2 MeV reaction from the 17.6 MeV gamma ray.

The possible peak at 2.9 MeV could be due to the reaction $N^{14}(\gamma d)C^{12}$, and if so the cross section is about 0.1 mb. which is approximately the same as Goward and Wilkins[85] report for $N^{14}(\gamma, d3\alpha)$ at 23 MeV. A more likely explanation of this peak, and of the one at 3.2 MeV, is that there are considerable fluctuations in the photon absorption cross section over the width of the 14.8 MeV line; such variations are indicated in the broad peak

from this gamma ray in the reactions $C^{12}(\gamma 3\alpha)$ and $Ne^{20}(\gamma\alpha)O^{16}$,[93] and could be expected in nitrogen since the absorption shows well defined resonances at only 4 MeV lower energy (Wright et al.). If this explanation is accepted then the remaining counts between 2.5 and 4 MeV give 1.5 mb. for the $(\gamma p)+(\gamma\alpha)$ cross sections for the broad 14.8 MeV line.

6.4. Discussion of Results.

The value found for the $N^{14}(\gamma\alpha)$ cross section at 17.6 MeV, 0.9 mb, is approximately equal to the (γn) cross section at this energy, 0.6 mb, found by Horsley et al. In contrast to this, Wright et al. find that for energies up to 23 MeV the average $(\gamma\alpha)$ cross section is only about one tenth of the average (γn) cross section. Hence the photonuclear process in N^{14} is markedly energy dependent, a result that is naturally explained if the photon absorption at energies up to the giant resonance involves essentially discrete levels of a compound nucleus. A strong energy dependence may also be in accord with the conclusion that the $(\gamma\alpha)$ reaction at 17.6 MeV involves magnetic dipole and electric quadrupole absorption, since it is known that between 20 and 24 MeV, the giant resonance region, the greater part of the absorption must be electric dipole. In a detailed study

93. Shown in Figs. 5.4 and 7.2.

of the (γp) reaction below 10.5 MeV, Wright et al. found that the cross section consists of a series of sharp resonances at the energies of known levels in N^{14}, and the spins and parities of these levels imply that a large proportion of the absorption is electric dipole. They therefore suggested that the giant resonance is due to an increase in the probability of absorption rather than a change in the multipolarity of the predominant absorption process (see Sections 2.2 and 2.4). However, a general conclusion of this nature is not supported by the observations of Spicer[94] on the (γp) and (γn) reactions in a nearby nucleus, O^{16}. The angular distribution of the photoprotons and the fine structure in the (γn) cross section indicate that magnetic dipole and electric quadrupole absorption is predominant below 19 MeV, even though electric dipole is allowed by the isotopic spin rules. While the present results appear to agree with those of Spicer, they do not necessarily invalidate the conclusion of Wright et al. The relatively low intensity ($\gamma\alpha$) transition to the 1.74 MeV state of B^{10} may come about merely because the electric dipole absorption is masked by a resonance in the magnetic dipole or electric quadrupole absorption, owing to the level properties of N^{14} near 17.6 MeV.

94. Spicer, B.M. Phys. Rev. 99:33 (1955).

CHAPTER 7.

THE PHOTODISINTEGRATION OF NEON.

7.1. Introduction.

A study of the charged particles produced by the photodisintegration of Ne^{20} provides an opportunity for examining several features concerning the photodisintegration process. An investigation of the alpha particles proceeding to different levels of O^{16} should provide a further example of the isotopic spin selection rules. A more detailed account of the reactions may perhaps be given by an alpha particle model. The nucleus may be regarded as a bipyramid of alpha particle groupings, and for photon energies not great enough to disrupt these structures such a system will not oscillate under the influence of electric dipole radiation. The absorption process, therefore, would be expected to arise from magnetic dipole or electric quadrupole interactions, and if the binding between alpha particle configurations is relatively small, the ejection of an alpha particle should be quite a probable process. The reaction $Ne^{20}(\gamma\alpha)O^{16}$ was in fact the first observed photodisintegration process in neon. Erdman and Barnes[95], and, in greater detail

95. Erdman, K.L., and Barnes, C.A. Proc. Roy. Soc. Can. 47:131 (1953).

Erdman[96], studied this reaction using the radiation from lithium bombarded by protons and observed the disintegrations produced in neon contained in a parallel plate ionisation chamber. They found a surprisingly small cross section for the disintegration proceeding to the ground state of O^{16}, and noticed that considerably more transitions occurred to the 6 and 7 MeV excited states in O^{16}. Moreover, observation of the alpha particle energies provides an opportunity to search for low lying states in O^{16}; no state has been observed below 6 MeV, and such states would not be expected on an alpha particle model.

A second process of interest is the photoproton disintegration, $Ne^{20}(\gamma p)F^{19}$. From a study of the gamma ray yield from proton bombardment of fluorine[97], the levels of the compound nucleus appear to be reasonably well separated at excitations near 17 MeV. Consequently, by the principle of reciprocity, the cross section $\sigma(\gamma p)$ could show resonant behaviour as the energy of the $Li^7(p\gamma)$ radiation is varied from 17.6 MeV.

Neon is an excellent counter gas, except for its low breakdown voltage. The photodisintegration processes leading to charged particle emission may be conveniently

96. Erdman, K.L. Thesis, University of British Columbia, (1953).
97. Willard, H.B., Bair, J.K., Kington, J.D., Hahn, T.M., Snyder, C.W. and Green, F.P. Phys.Rev. 85:849 (1952).

studied by means of a proportional counter or ionisation chamber technique, pulse amplitude analysis giving the energy released in the counter from the disintegrations. The range of alpha particles is very much less than that of protons of similar energy, so changing the gas pressure will permit a clear distinction between groups in the pulse height distribution arising from $(\gamma\alpha)$ reactions and those from (γp) reactions. This method was used in the present study of the photodisintegration of neon by the $Li^7(p\gamma)Be^8$ radiation.

A small proportional counter was used for the $(\gamma\alpha)$ reactions produced by the 17.6 MeV radiation, and a larger gridded ionisation chamber was used for the $(\gamma\alpha)$ and (γp) reactions at both photon energies. Descriptions of the counters have been given in Section 3.6.

7.2. Possible Reactions in Neon.

Because natural neon contains the isotopes Ne^{20}, Ne^{21} and Ne^{22} in the proportions 90.51 : 0.28 : 9.21, and since the induced transitions may go to excited levels in the product nuclei, from the energetic viewpoint there are numerous possibilities for the amounts of energy which may be released in the chamber as kinetic energy of charged particles. If it is assumed that the energy lost by a recoil fragment per ion pair produced is not very different from the same quantity for protons or alphas,

then the pulse amplitude produced by a disintegration in the chamber is directly proportional to the kinetic energy released, provided that the energy per ion pair is constant, independent of particle energy, within the accuracy of the chamber resolution. In Table 7.1 are listed those reactions resulting in charged particles which are most likely to be observed when neon is irradiated with the $Li^7(p\gamma)Be^8$ radiation, according to present energy level diagrams (Ajzenberg and Lauritsen[90]), together with some other data which applies to the gridded chamber results.

7.3. Experimental Results.

7.3.1. For the 440 kV resonance radiation.

After preliminary runs had established the general form of the pulse height distributions and the counting rates to be expected, the pulse spectrum was examined in detail in three sections. Fig.7.1 shows the spectrum above 3 MeV and the corresponding background taken with the gridded ionisation chamber and low kicksorter resolution. Fig. 7.2 shows the pulse distribution after background subtraction, due allowance being made for the extra spreading of the two contamination peaks when the gamma flux passes through the counter. The assigment of the groups fits well with a linear energy scale based on the position of the plutonium alpha peak at 5.16 MeV.

Table 7.1 Possible reactions in Neon.

Reaction	Level in residual nucleus	Energy release MeV	Light particle range^{x} cm	Number of events	Loss %	Cross section 10^{-28} cm^2
A Type $Ne^{20}(\gamma,\alpha)O^{16}$ Q = -4.75 MeV						
$Ne^{20}(17.6,\alpha)O^{16}$						
1	ground	12.88	2.34	200	20	0.47
2	6.06,6.14	6.8	0.80	3130	6.7	6.3
3	6.91,7.12	5.9	0.64	8550	5.6	17
4	9.58(wide)	3.3	0.28			
5	9.84	3.0	0.25			
6	10.36	2.5	0.21			
7	11.25(wide)	1.6	0.14			
$Ne^{20}(14.8,\alpha)O^{16}$						
11	ground	10.0	1.55	230	13	0.81
12	6.06,6.14	3.9	0.37	~800	3	~3
13	6.91,7.12	2.9	0.25			
B Type $Ne^{22}(\gamma,\alpha)O^{18}$ Q = -9.66 MeV						
$Ne^{22}(17.6,\alpha)O^{18}$						
1	ground	8.0	1.08	360	8.9	7.2
2	1.98	6.0	0.69			
	perhaps others					
$Ne^{22}(14.8,\alpha)O^{18}$						
11	ground	5.1	0.55			
12	1.98	3.1	0.28			

(Table 7.1 contd.)

Reaction	Level in residual nucleus	Energy release MeV	Light particle range[x] cm	Number of events	Loss %	Cross section 10^{-28} cm^2
C Type $Ne^{20}(\gamma,p)F^{19}$ Q = -12.87						
$Ne^{20}(17.6,p)F^{19}$						
1	ground 0.110 0.197	4.76 to 4.56	5.93	61300	43	200
2	1.35	3.4	3.28	~20000	24	~50
3	1.57	3.2	2.94			
4	2.82	1.9	1.25			
$Ne^{20}(14.8,p)F^{19}$						
11	ground 0.110 0.197	1.9	1.25			
D Type $Ne^{20}(\gamma,2\alpha)C^{12}$ Q = -11.9 MeV						
$Ne^{20}(17.6,2\alpha)C^{12}$						
1	ground	5.7				
$Ne^{20}(14.8,2\alpha)C^{12}$						
11	ground	2.9				
E Type $Ne^{20}(\gamma,\alpha p)N^{15}$ Q = -16.9						
Insufficient energy						

x In 9 atmospheres of neon + helium

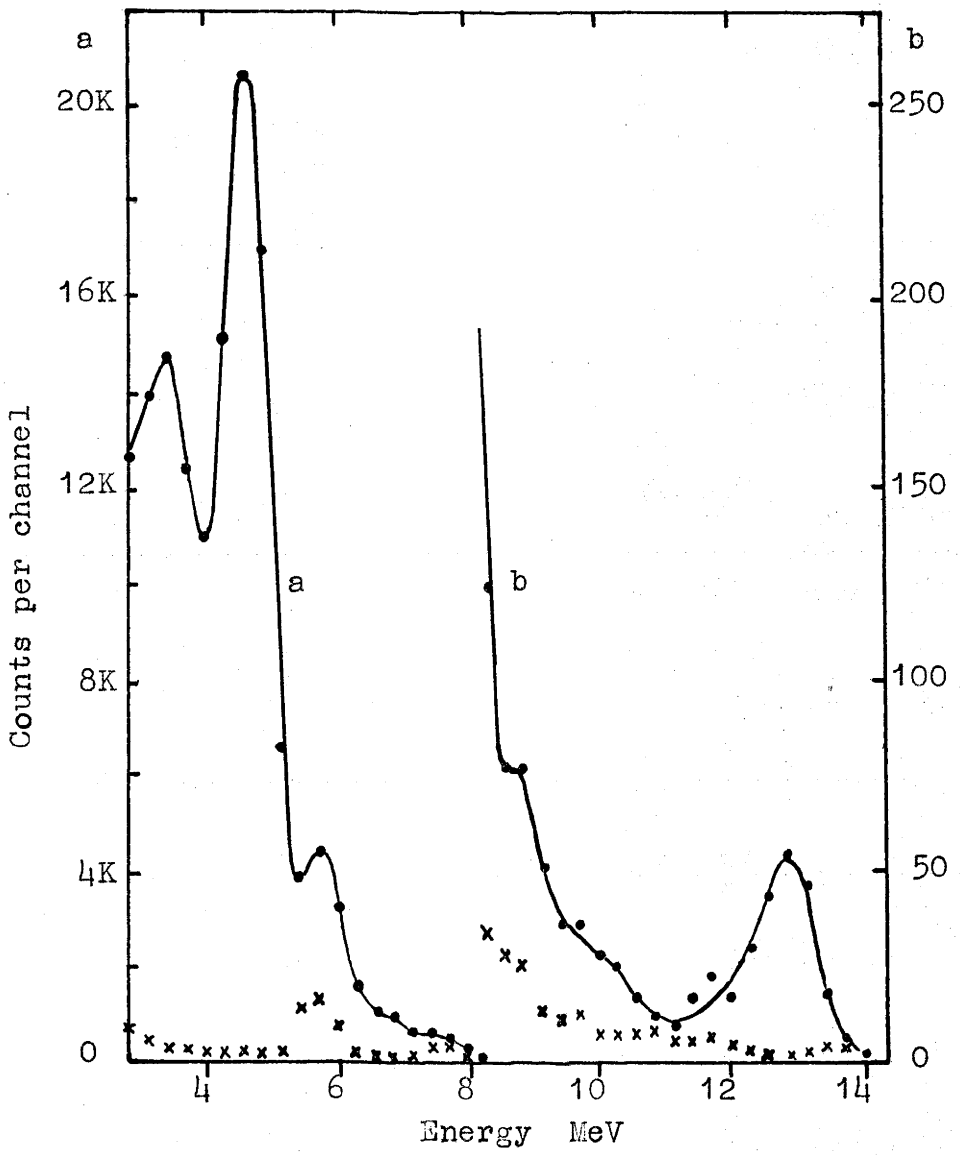

Fig.7.1 Spectrum from 9 hours operation of the gridded ionisation chamber.

• with radiation

× background

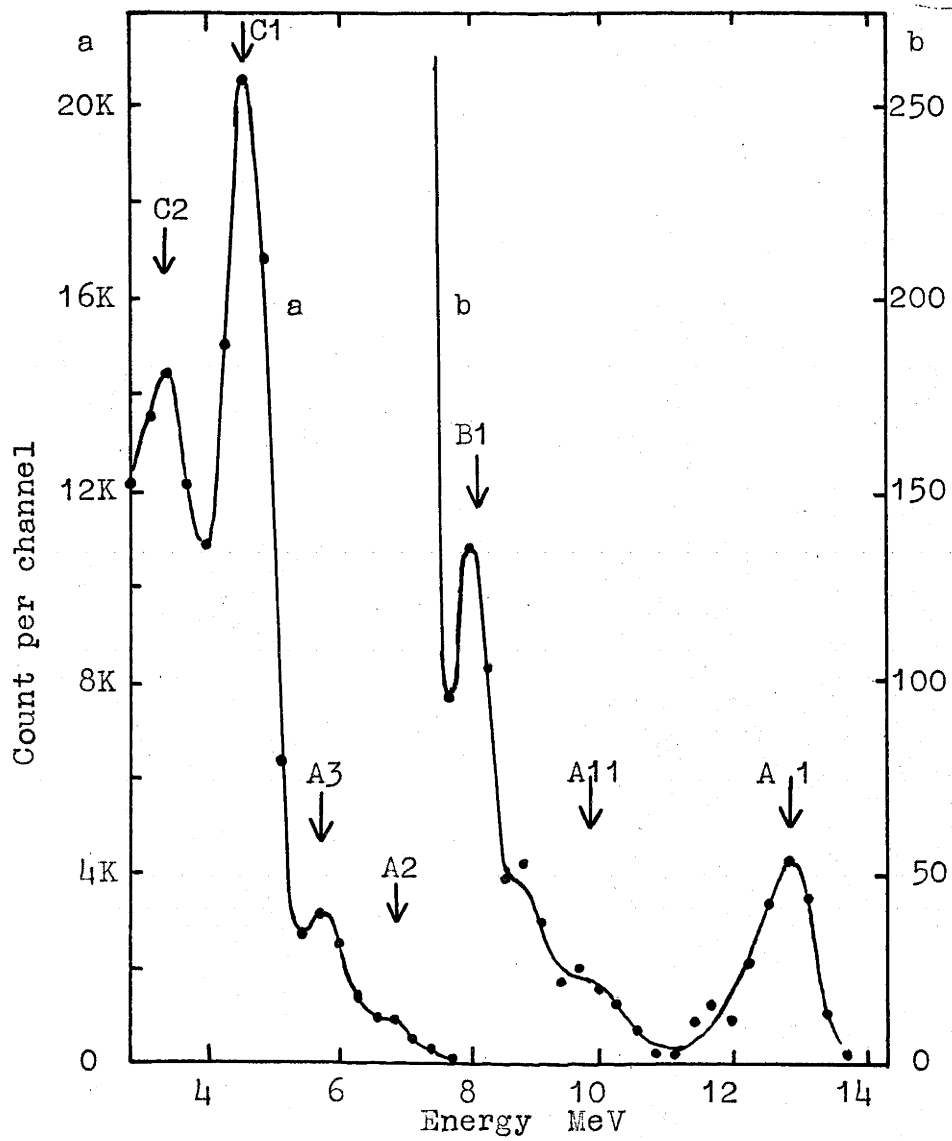

Fig.7.2 The spectrum above 3 MeV resulting from the photodisintegration of Neon.

While there is little danger of ambiguity in the assignment of the appropriate reaction to the higher energy peaks, this is not the case with the lower energy part of the spectrum, which is shown in greater detail in Fig.7.3. First, the strong peak marked C2, which is attributed to $Ne^{20}(17.6,p)F^{19}$, is centred at 3.38 MeV corresponding to a transition to the 1.35 MeV state of F^{19}. There is no marked spread of this peak towards lower energies as might be expected if there was a similar intensity transition to the 1.57 MeV state of F^{19}. Secondly, the filling in between C1 and C2 in Fig.7.3 would seem to arise from reaction A12 i.e.$Ne^{20}(14.8,\alpha)O^{16}$, the residual O^{16} nucleus being left in either the 6.04 or 6.14 MeV state. It could also arise from $Ne^{20}(17.6,p)F^{19}$ if the doubtful state at 0.9 MeV in F^{19} actually exists[98]. Finally, the distribution shows evidence for other groups at 2.93(A5?), 2.4(A6?), 2.0, 1.84 and 1.6 MeV(C4&/or C11?) which might be identified with some of the reactions listed in Table 7.1, but for which no reliable cross section can be estimated. The yields from reactions A5 and A6 are expected to be small because of the low barrier penetrabilities. Most of the counts between about $2\frac{1}{2}$ and 3 MeV will therefore probably be due to reaction A13 i.e. $Ne^{20}(14.8,\alpha)O^{16}$, the transitions being

98.Seale,R.L. Phys.Rev.92:389 (1953).

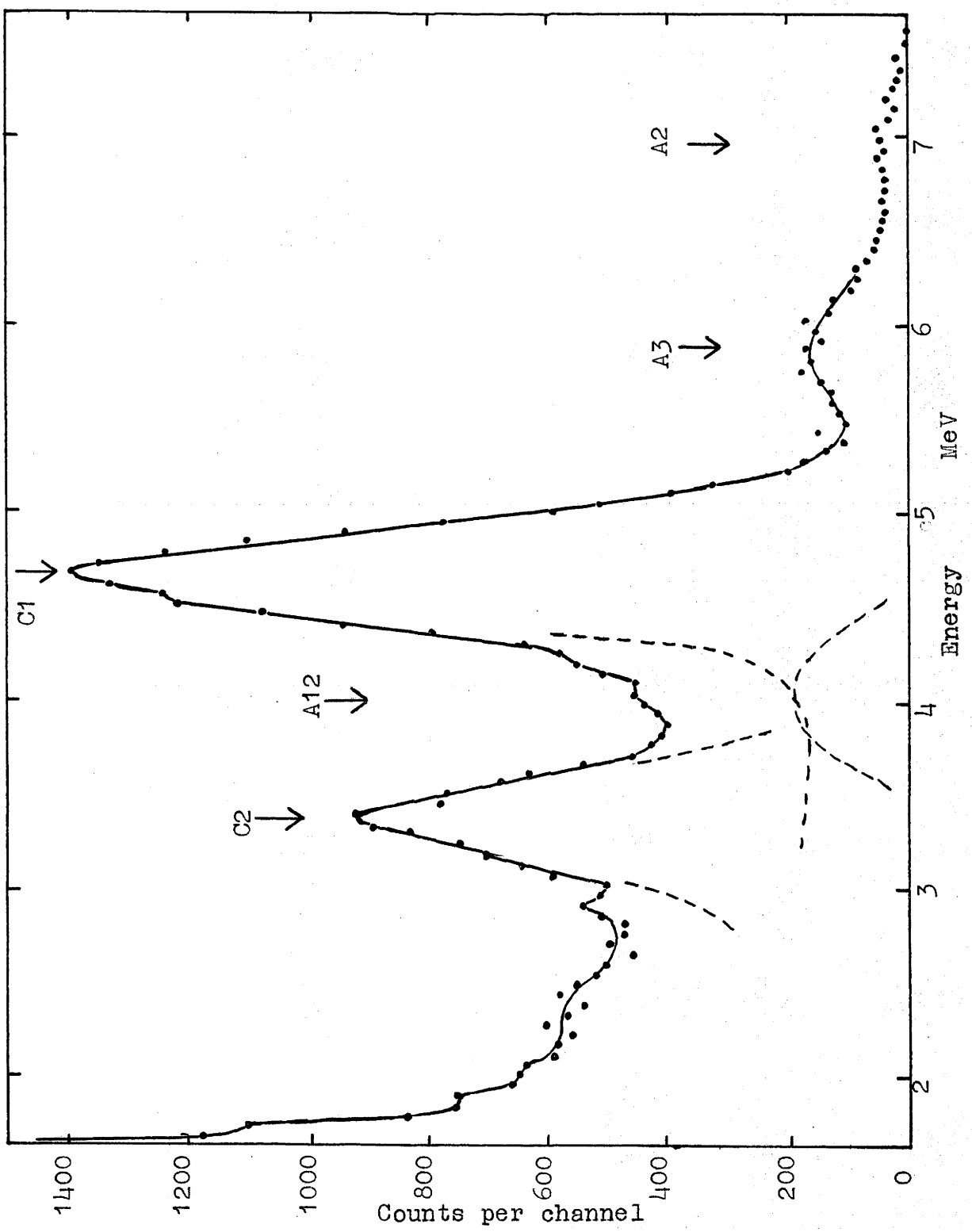

Fig.7.3 Detail of the low energy photodisimtegration spectrum from Neon.

to the O^{16} levels near 7 MeV.

The large proton peak corresponding to reaction C1 was examined under high kicksorter resolution and with reduced gamma ray intensity, as it appeared that this peak was rather broader than the others. The stability and resolution of the apparatus were hardly adequate to produce convincing evidence, yet, as can be judged from Fig.7.4, which consists of the addition of four separate runs, it appears that this peak is a multiple one and could be resolved into three similar intensity components separated by 100 keV. This would suggest that the reaction $Ne^{20}(\gamma p)F^{19}$ proceeds in roughly equal proportions to the ground state and the two low lying levels at 110 and 197 keV in F^{19}.

The cross sections for the reactions have been estimated from the areas under the peaks. In the low energy region where the groups overlap, the areas were estimated by drawing in curves of the expected width, and the values so deduced are only approximate. A wall correction, based on the range of the alpha particle or proton, was applied to the observed yields; it is shown in Table 7.1 in the 'loss' column as the fraction of events not counted. The gamma flux was estimated from the counts recorded by the standard Geiger counter, corrections being made for absorption by the chamber walls,

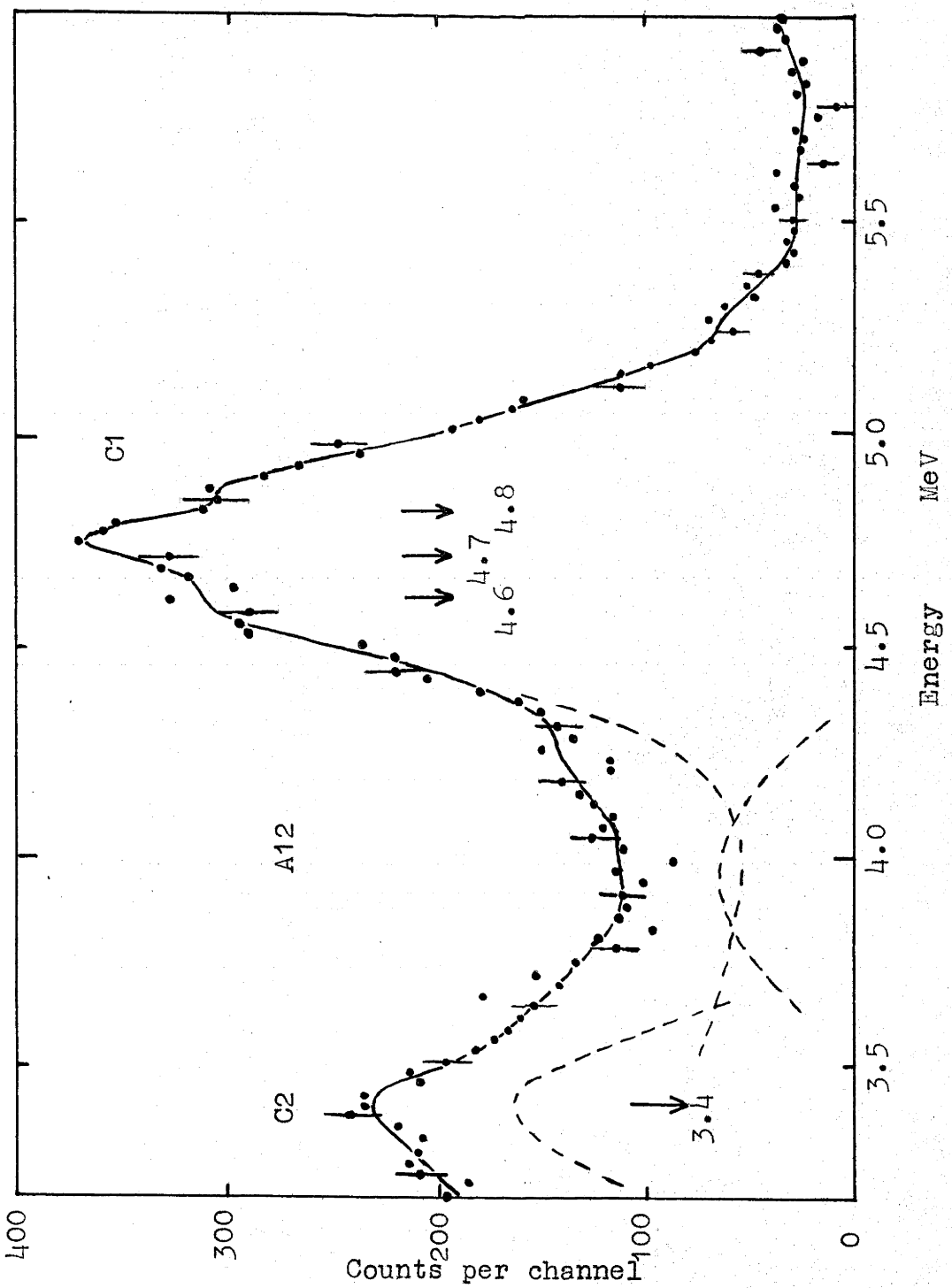

Fig.7.4 The photoproton peak at 4.7 MeV.

about 8% per single wall thickness, and for the inverse square law. Hence finally

$$\sigma(E) = \frac{\text{events observed + wall loss}}{\left(\begin{matrix}\text{quanta(E MeV)/cm}^2\text{ at}\\ \text{the mean distance}\end{matrix}\right) \times \left(\begin{matrix}\text{No. of atoms of isotope}\\ \text{in the sensitive volume}\end{matrix}\right)}$$

The cross section values for the higher energy peaks are considered to be accurate to ±20%, while the relative values should be considerably better. The data obtained with the gridded chamber is displayed in Table 7.1. The smaller proportional counter containing pure neon at a lower pressure was used only for determining the cross sections of those ($\gamma\alpha$) reactions which release more than 5 MeV in the counter; the cross sections obtained were within 20% of the values given in the table.

7.3.2. Non-resonant radiation, E_p = 400 to 900 kV.

Once the various reactions had been identified in the pulse height distribution produced by the resonance radiation, changes in the yields of three reactions were followed as the bombarding proton energy was varied from 400 to 900 kV. Thin targets, of 10 to 40 kV, were used, so that the energy of the sharp gamma ray line was taken from 17.59 to 18.03 MeV, while the energy of the wide 14.8 MeV line was not shifted appreciably. The parts of the pulse spectrum which were studied were: between 2.5 and 3 MeV, the reaction $Ne^{20}(14.8,\alpha)O^{16}$; the 4.7 MeV group, reaction $Ne^{20}(17.6,p)F^{19}$; and the 6MeV group,

reaction $Ne^{20}(17.6,\alpha)O^{16}$.

The variations in the relative yields from these reactions is shown in Fig.7.5. The most important result is the factor two change in the ratio of the proton and alpha particle yields from the high energy gamma line. The shapes of the curves arise from two causes: the change in the ratio of intensities of the radiations at 0^{o}, and changes in the photodisintegration cross sections. The former change has not yet been measured throughout the entire energy range, but an estimate of the trend can be made from the data if some simple assumptions are made about the cross sections. It may be assumed reasonably that the cross section for $Ne^{20}(14.8,\alpha)O^{16}$ does not change appreciably since the line is 2 MeV wide and the mean energy changes by only $\frac{1}{2}$ MeV; the further assumption that either $\sigma(17.6,\alpha)$ or $\sigma(17.6,p)$ is constant permits the change in the ratio of the gamma ray intensities to be calculated. The results of the calculations are shown in Fig.7.6. The difference between $\sigma(17.6,\alpha)$ or $\sigma(17.6,p)$ constant is immaterial below 500 kV, both assumptions giving the same dip in the ratio I_{14}/I_{17} at 470 kV when the ratio is normalised to unity at 440 kV. Devons and Hine[44] have also observed the minimum in the intensity ratio in measurements at 90^{o} to the proton beam; the narrower and shallower dip observed here is probably due

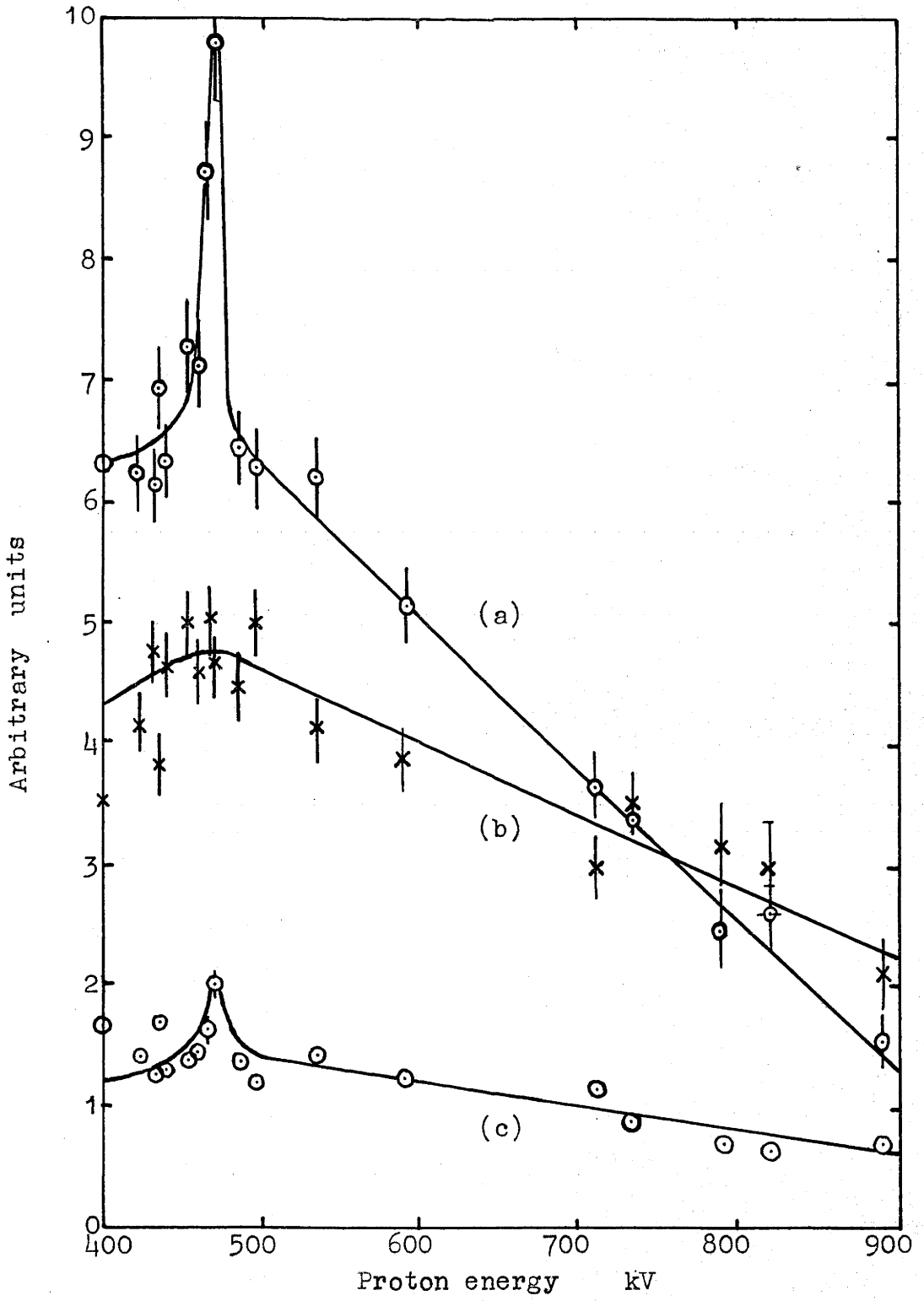

Fig.7.5 Relative yields from the (γp) and ($\gamma\alpha$) reactions in Neon.
(a) (γp) at 17 MeV/($\gamma\alpha$) at 14 MeV
(b) (γp) at 17 MeV/($\gamma\alpha$) at 17 MeV
(c) ($\gamma\alpha$) at 17 MeV/($\gamma\alpha$) at 14 MeV.

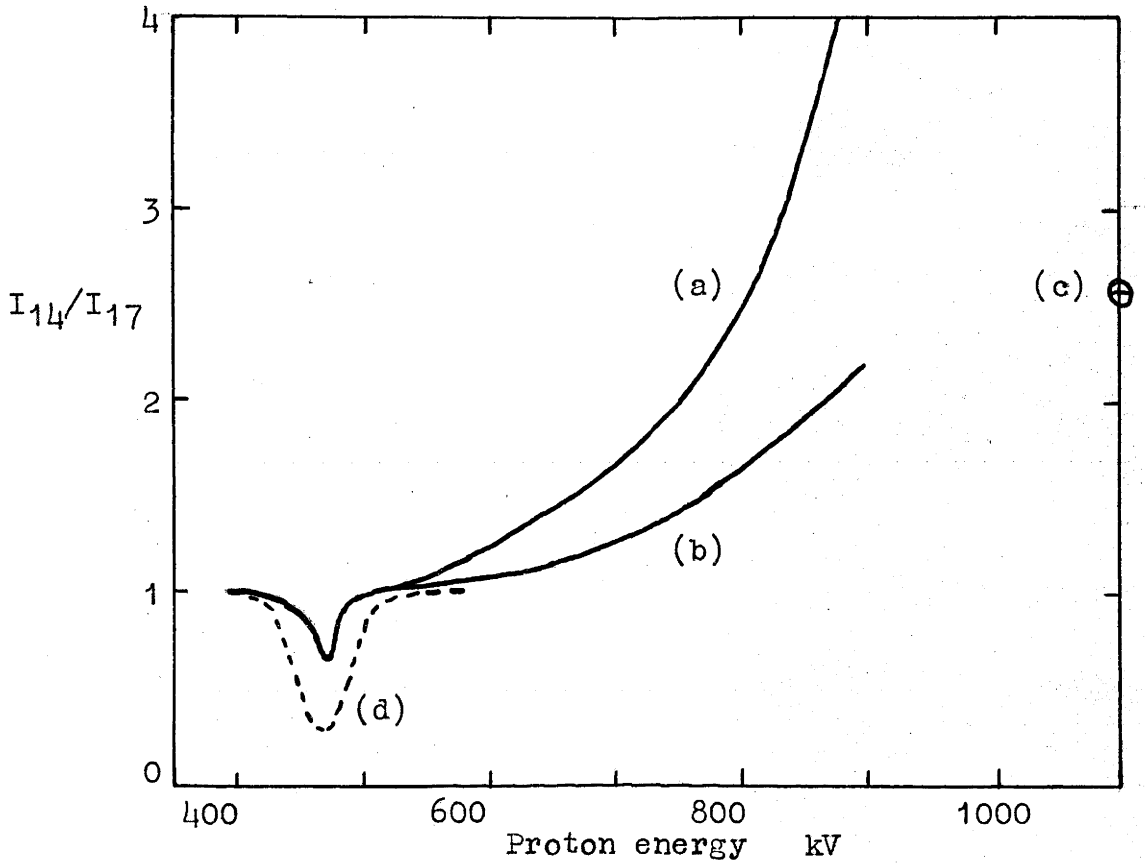

Fig.7.6 Ratio of intensities of the low and high energy components of the $Li^7(p\gamma)Be^8$ radiation.

(a) deduced assuming $\sigma(\gamma p)$ is constant
(b) deduced assuming $\sigma(\gamma\alpha)$ is constant
(c) measured by Stearns and McDaniel[46], normalised to 1,0 at 440 kV.
(d) measured by Devons and Hine[44] at 90°.

} at 0°.

to the fairly thick targets which were used, but could also be due to some $Ne^{20}(17.6,\alpha)O^{16}$ contributions to the photodisintegration spectrum near 2.5.MeV. Above 500 kV, $\sigma(17.6,\alpha)$ constant appears to be the better assumption as it gives a more reasonable trend towards the intensity ratio measured by Stearns and McDaniel at 1100 kV. The trend is to higher values than the 1100 kV figure, so it is likely that the $(\gamma\alpha)$ cross section actually decreases above 17.6 MeV, and the (γp) cross section falls more rapidly still.

7.4. Discussion of Results.

The results for the $Ne^{20}(\gamma\alpha)O^{16}$ cross sections are in good accord with the selection rules deduced by Gell-Mann and Telegdi[6] for the photodisintegration of an even-even nucleus in which the ground state is 0^+. The very low $(\gamma\alpha)$ cross section leading to the ground state of O^{16} would be expected as a result of the isotopic spin selection rule which forbids electric dipole absorption in this case, and from conservation of angular momentum which prohibits magnetic dipole absorption. This transition must proceed by electric quadrupole absorption through a compound state 2^+. The transitions to the excited states at about 6 and 7 MeV respectively may proceed via magnetic dipole absorption, the factor three higher intensity of the transitions to the 7 MeV states

resulting from the smaller orbital angular momentum of the ejected alpha particles[99]. The mean $(\gamma\alpha)$ cross sections for the broad 14.8 MeV component of the radiation show the same trend and are of similar magnitudes to those for the narrow 17.6 MeV component, despite any possible sharp variations of the cross section with gamma ray energy in the 14 to 18 MeV region. The $Ne^{22}(\gamma\alpha)O^{18}$ ground state transition from electric dipole absorption is not forbidden by the isotopic spin selection rules, and the observed cross section is an order of magnitude larger than that for the ground state transition from Ne^{20}.

The $Ne^{20}(\gamma p)F^{19}$ cross section is 25 mb. at 17.6 MeV, decreasing to less than half this value at slightly higher energies. Willard et al. find a resonance in the yield of gamma rays from the proton bombardment of F^{19} at a Ne^{20} excitation of 17.59 MeV. From the reciprocity theorem in the form $\sigma(\gamma p)/\lambda_\gamma^{\,2} = \sigma(p\gamma)/\lambda_p^{\,2}$, at this excitation one would expect $\sigma(p\gamma) = \sigma(\gamma p)/30$, and with a possible weighting factor of $\frac{1}{2}$, this gives $\sigma(p\gamma) = 0.4$ mb. The capture radiation from such a small cross section would be very hard to detect among all the other radiations from competing processes. At the 1.431 MeV resonance in

99. The cross section to the 7 MeV levels in O^{16} might be augmented by the ground state transitions from the reaction $Ne^{20}(17.6,2\alpha)C^{12}$, but as this is isotopic spin forbidden, the cross section will be even smaller than the $Ne^{20}(\gamma\alpha)O^{16}$ ground state transition.

$F^{19}(p\gamma)Ne^{20}$ (Ne^{20} excitation 14.23 MeV) Sinclair[100] finds that the capture radiation is only 1.5% of the total radiation even though the reaction $F^{19}(p,\alpha\gamma)O^{16}$ is not resonant at this energy. The change in the $Ne^{20}(\gamma p)F^{19}$ cross section near 17.6 MeV can not therefore be identified definitely with the resonance in the gamma ray yield seen by Willard et al.

The cross section found for the (γp) reaction in Ne^{20} is about ten times larger than the total $(\gamma\alpha)$ cross section, a factor which is similar to the average in other light nuclei. Since the ratio $\sigma(\gamma p)/\sigma(\gamma\alpha)$ is not constant as the photon energy alters from 17.6 MeV, the reactions must result from different absorption processes. It is therefore likely that the large (γp) cross section arises from electric dipole absorption, and presumably is matched by a similar (γn) cross section. No electric dipole absorption is possible for a system composed of tightly bound alpha particles, so that a simple alpha particle model is not suitable to account for the (γp) cross section. A shell model of the type suggested by Wilkinson[9] may be more appropriate.

---

100. Sinclair, R.M. Phys.Rev. 93:1082 (1954).

APPENDIX 1.

The Wall Effect in a Cylindrical Counter.

Suppose gamma rays are incident at right angles to the axis of an infinitely long cylinder of radius 'r', and produce disintegrations uniformly throughout the volume of the cylinder. Let $f = l/2r$, where 'l' is the residual track length within the cylinder. We shall first find $p(f)$, where $p(f)df$ is the probability that an infinitely long track has a length $(f,f+df)$ inside the cylinder, and then we shall find $P(f)$, where

$$P(f) = \int_0^f p(f)df$$

is the probability that a track of length f strikes the wall of the cylinder, i.e. it represents the fraction of disintegrations corresponding to a particular energy release which do not dissipate all of their energy in the counter.

Consider tracks passing through an element of area dS at Q on the surface of the cylinder, with length f, and coming from a direction specified by the angles (ϕ,ψ). The incident beam makes an angle γ to the diameter through Q and is perpendicular to the axis of the cylinder. The probability of a track in the direction (ϕ,ψ) will be taken as proportional to $g(\cos^2 X)$, where X is the angle

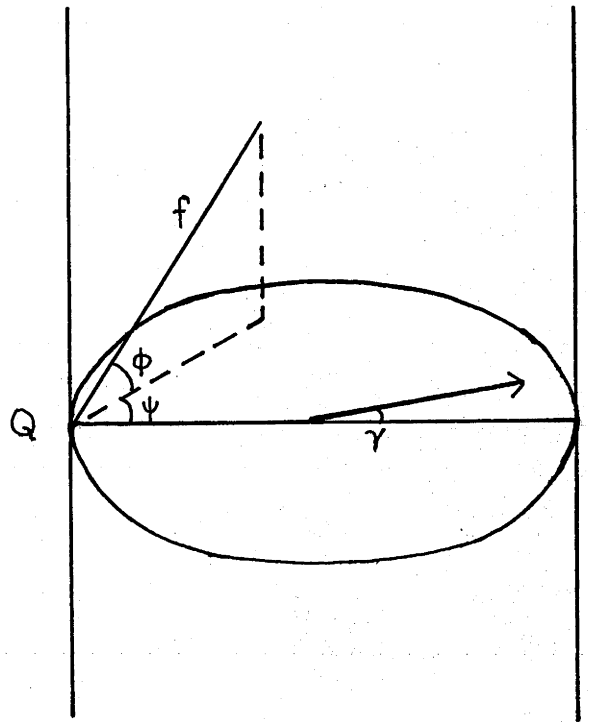

between the gamma ray and track directions, so that

$$\cos X = \cos\phi\cos\psi\sin\gamma + \cos\phi\sin\psi\cos\gamma$$
$$= \cos\phi\cos(\psi-\gamma).$$

Integration will then be over all values of γ with equal weight.

The element of volume at the start of a track is

$$f^2\cos\phi\,d\phi\,d\psi\,df,$$

and the solid angle subtended by dS at the origin of a track is $\cos\phi\cos\psi\,dS/f^2$.

Hence the probability of a track of length (f,f+df) passing through dS is

$$p(f)\,df\,dS \propto \left[\int_{-\pi}^{\pi} d\gamma \int d\phi \int d\psi\, dS\cos^2\phi\cos\psi\, df\, g(\cos^2 X)\right]_{f\leq F},$$

where the limits of integration are to be found from the condition:

$f \leqslant F$ = distance to far wall along the track from Q

$= \cos\psi/\cos\phi$

i.e. we must take ψ in the range for which $\cos\psi \geqslant f\cos\phi$.

By symmetry, ϕ and ψ may both lie between the limits 0 and $\pi/2$;

for $f \leqslant 1$, and $0 < \phi < \pi/2$, then $0 < \psi < \arccos(f\cos\phi)$, and

for $f \geqslant 1$, if $0 < \phi < \arccos(1/f)$, then $\psi = 0$,

or if $\arccos(1/f) < \phi < \pi/2$, then $0 < \psi < \arccos(f\cos\phi)$.

Hence $$p(f) \propto \int_{-\pi}^{\pi} d\gamma \int_{\substack{0, \\ \arccos 1/f}}^{\pi/2} d\phi \int_0^{\arccos(f\cos\phi)} d\psi \; g(\cos^2 X)\cos^2\phi\cos\psi.$$

Substituting $g(\cos^2 X) = \sum_{n=0}^{\infty} a_n \cos^{2n} X$ and $\phi = \pi/2 - \beta$

gives $$p(f) = c\sum_{n=0}^{\infty} a_n \frac{(2n-1)!!}{2n!!}\int_0^{\beta_0} \sin^{2n+2}\beta\sqrt{1-f^2\sin^2\beta}\; d\beta$$

with $\beta_0 = \pi/2$ for $f \leqslant 1$, or $\beta_0 = \arcsin(1/f)$ for $f \geqslant 1$,

and $(2n-1)!! = (2n-1)(2n-3)....3.1$, the coefficient of a_0 being 1.

This integral for p(f) gives a solution in terms of complete elliptic integrals of the first and second kinds (see e.g. Jahnke and Emde[101]). The constant c may be evaluated from $\int_0^{\infty} p(f)df = 1$, and the fraction of events lost for a given maximum f is found from

$$P(f) = \int_0^f p(f)df \quad \text{for } f \leqslant 1$$

$$= 1 - \int_f^{\infty} p(f)df \quad \text{for } f \geqslant 1.$$

---

101. Jahnke, E., and Emde, F. 'Tables of Functions', Dover Publications, N.Y. (1945).

For the case of an isotropic angular distribution, $g(\cos^2 X) = 1$ i.e. $a_0 = 1$, $a_n = 0$ for $n \geq 1$,

hence
$$p(f) = \frac{4}{\pi}\int_0^{\beta_0} \sin^2\beta \sqrt{1-f^2\sin^2\beta}\, d\beta,$$

and
$$P(f) = \frac{4}{3\pi f}\left[(1+f^2)E - (1-f^2)K\right] \quad \text{for } f \leq 1$$
$$= \frac{4f^2}{3\pi}\left[(1+\frac{1}{f^2})E - (1-\frac{1}{f^2})K\right] \quad \text{for } f \geq 1$$

where
$$E(f) = \int_0^{\pi/2} (1-f^2\sin^2\alpha)^{\frac{1}{2}} d\alpha$$
$$K(f) = \int_0^{\pi/2} (1-f^2\sin^2\alpha)^{-\frac{1}{2}} d\alpha.$$

The asymptotic expansions for the elliptic integrals give rapidly converging series expressions for P(f), and for all values of f the first three terms of the series give sufficient accuracy for experimental purposes. The same series expressions for P(f) may be obtained by direct integration of p(f) after a binomial expansion of $(1-f^2\sin^2\beta)^{\frac{1}{2}}$, but in this case the divergence error at $f = 1$ can not be determined.

The functions P(f) have been determined explicitly for the cases of isotropic, $\cos^2\theta$, and $\sin^2\theta$ angular distributions; they are listed in Table I. The same results for a $\sin^2\theta$ distribution have been given previously by Barnes et al.[48] for $f < 1$ and $f > 1$. It is seen that even at $f = 1$ the series error is immaterial, and the relatively small differences resulting from the very different angular distributions should be noted.

Table I. Loss Functions for an Infinite Cylinder.

Angular Distribution	f	P(f)	P(1)
Isotropic	<1	$f(1-f^2/8-f^4/64)$	.8594
	>1	$1-(1/8f^2)(1+1/8f^2+5/128f^4)$	.8545
	=1	$8/3\pi$	.8488
$\cos^2\theta$	<1	$f(9/8-5f^2/32-21f^4/1024)$	.9482
	>1	$1-(1/16f^2)(3/4f^2+5/32f^4)$	.9434
	=1	$44/15\pi$	.9337
$\sin^2\theta$	<1	$f(15/16-7f^2/64-27f^4/2048)$	.8149
	>1	$1-(1/16f^2)(3+5/128f^4)$	.8101
	=1	$38/15\pi$	.8064

When the range-energy relation for the particles and gas in the counter is known, it can be combined with the function P(f) to give the fraction of tracks lost as a function of energy, P(E).

The energy distribution which will result from monoenergetic disintegrations in the counter could be derived from the track length distribution, p(f), and the Bragg curve for the particles concerned. However, when the range-energy relation has already been combined with P(f), it is usually more convenient to derive the energy distribution in the way described below. The P(E) vs. E curve for the counter can be simply turned into P(E) vs. E', where $E' = (E_{max} - E)$. The maximum energy value is usually that of the emitted particle, since for photodisintegration events the recoiling heavy

nucleus has such a short range its loss can be neglected. Differentiation of the new curve will give a p(E) vs. E curve which allows for the variation in ionisation density along the tracks. The spectrum shape for a group of particles releasing the energy E_{max} in the counter will be the same as the p(E) curve up to the maximum energy, and there it will have a peak containing 1 - P(E) events, with a width governed by the resolution of the counter.

Examples of the P(E) and p(E) curves are given in Chapter 3, section 3.7.

APPENDIX 2.

A Note on the Maximum Voltage of a Cockcroft-Walton Generator under Load.

A simple method for deriving the ripple voltage and the depression of the maximum voltage in a Cockcroft-Walton voltage multiplying circuit was given by Bouwers and Kuntke (1937)[102]. For a circuit of n stages, i.e. consisting of 2n rectifiers and 2n condensers each of capacity C, the results obtained were:

ripple $$\delta v = \frac{i}{fC}\frac{n(n+1)}{2} \qquad (1)$$

depression of H.T. $$\Delta V = \frac{i}{fC}\left(\frac{2}{3}n^3 + \frac{1}{2}n^2 - \frac{1}{6}n\right) \qquad (2)$$

where f is the frequency of the alternating input voltage, and i is the mean current drawn from the output terminal. These results have been quoted frequently in the literature, e.g. by Bouwers (1939)[103], Craggs and Meek (1954)[104], and Heilpern (1955)[105]. In practice, the effects of stray capacitances, resistive rectifiers, etc., also contribute to the effective internal impedance of the generator and reduce the voltage efficiency still further (e.g. see Everhart and Lorrain (1953)[106]), so that only the leading

102. Bouwers, A., and Kuntke, A. Z. Tech. Physik 18:209 (1937).
103. Bouwers, A. 'Elektrische Hochstspannungen', Springer, Berlin (1939).
104. Craggs, J.D., and Meek, J.M. 'High Voltage Laboratory Technique', Butterworth, London (1954).
105. Heilpern, W. Helv. Phys. Acta 28:485 (1955).
106. Everhart, E., and Lorrain, P. Rev. Sci. Inst. 24:221 (1953).

term in (2), $2n^3/3$, is important. However, the coefficients of n^2 and n in relation (2) are incorrect. In their derivation, Bouwers and Kuntke omitted to allow for the fact that half of the rectifiers are conducting 180° out of phase with the others. When allowance for this is made, then we find

$$\Delta V = \frac{i}{fC}\left(\frac{2}{3}n^3 + \frac{1}{4}n^2 + \frac{1}{12}n\right) \qquad (3).$$

These relations are for perfect components, so that there is no loss of energy in the multiplying circuit. The output voltage is

$$2n\sqrt{2}V_o - \Delta V$$

where V_o is the r.m.s. input voltage. For ΔV given by (3), the power drawn by the load is equal to the input power to the generator. If ΔV is given by (2), then this equality does not hold.

The same type of circuit analysis can be readily applied to the full-wave generator discussed by Heilpern. The result is

$$\Delta V = \frac{i}{fC}\left(\frac{1}{6}n^3 + \frac{1}{4}n^2 + \frac{1}{12}n\right) \qquad (4).$$

Considering only the first terms in (3) and (4), it is seen that the voltage depression is 4 times smaller in a full-wave generator, not 8 times as suggested by Heilpern. The disagreement may arise from a misunderstanding, because Heilpern does not state explicitly how he defines an

'n-stage' generator. If the definition is the same as that used here, then he has used incorrectly an equation derived by Everhart and Lorrain for the output voltage depression $\Delta V'$ caused by capacitive circulating currents in the generator. Everhart and Lorrain define an N-stage generator as one containing N rectifiers and N condensers, i.e. $N = 2n$, so that

$$\Delta V' = N\sqrt{2}V_o\left(1 - \frac{1}{N\sqrt{C_s/C}}\,\mathrm{tgh}\left(N\sqrt{C_s/C}\right)\right)$$

becomes $$\Delta V' = 2n\sqrt{2}V_o\left(1 - \frac{1}{2n\sqrt{C_s/C}}\,\mathrm{tgh}\left(2n\sqrt{C_s/C}\right)\right).$$

From the PHILOSOPHICAL MAGAZINE, Ser. 7, vol. 46, p. 841,
August 1955.

Cross Sections for the Reaction $^{12}C(\gamma 3\alpha)$ *in the Energy Range* 12–18 MEV

By J. H. CARVER, H. J. HAY and E. W. TITTERTON
Australian National University, Canberra*

[Received March 17, 1955]

ABSTRACT

By combining results obtained from a methane counter with those from nuclear emulsions the cross-sections for the $^{12}C(\gamma 3\alpha)$ reaction at 17·6, 14·8 and 12·3 MEV are found to be $(1{\cdot}70\pm0{\cdot}24)$, $(0{\cdot}33\pm0{\cdot}07)$ and $(1{\cdot}15\pm0{\cdot}6)\times10^{-28}$ cm^2 respectively. Analysis of the data suggests a strong resonance in the excitation function near 12·3 MEV and possible resonances near 15 and 16 MEV.

§ 1. INTRODUCTION

CONSIDERABLE attention has been given to the reaction $^{12}C(\gamma 3\alpha)$ and the position has been reviewed recently by Titterton (1955). Many observers have determined the cross section for the $^7Li(p\gamma)$ resonance radiation by the photographic plate method, a knowledge of this being important since it is often convenient to determine cross sections for other, rarer, reactions occurring in the emulsion in terms of it. The wide spread of values which have been reported (table 1 and fig. 3) is unsatisfactory and makes a redetermination of the cross section at 17·6 MEV desirable; at the same time it was hoped that by using other lines in the $^7Li(p\gamma)$ spectrum, particularly the broad one at 14·8 MEV, information could be obtained on the resonance absorption of radiation by states of ^{12}C, evidence for which had been presented by Goward and Wilkins (1953).

To determine the cross section at 17·6 MEV a methane filled proportional counter was used since this enables data to be collected more quickly and with better energy resolution than is possible by the emulsion method. However, the information obtained is less definite; only the total disintegration energy is measured and it is impossible to distinguish between events where one particle strikes the counter walls and events due to γ-rays of energy lower than the main line, although appropriate corrections can be applied. For this reason the proportional counter was used to obtain the absolute cross section at 17·6 MEV while the photographic plate method was employed to investigate the reaction at lower energies and to determine cross section values at 14·8 and 12·3 MEV relative to the 17·6 MEV measurement.

* Communicated by the Authors.

§ 2. Description and Performance of Counter

The counter is cylindrical, of length 30 cm and internal diameter 9·1 cm. A tungsten wire of diameter 40 μ is taken through a Kovar-glass seal inside a 1·5 mm diameter copper capillary tube, hangs along the axis of the counter and is kept taut by a nickel weight; 18 cm of wire is exposed within the counter. The outer pressure chamber is made from stainless steel 1/16 in. thick and lined with a graphite cylinder and end-plates, also of 1/16 in. thickness, which form the cathode surface of the counter. This lining prevents charged particles, produced in the steel walls, from entering the sensitive region. The only important reaction occurring in the graphite at these energies is the reaction under study and consideration of the maximum depth at which a photodisintegration event could occur and still lead to the dissipation of more than 5 Mev in the active volume shows that $<0{\cdot}1\%$ of observed pulses are due to reactions occurring in the graphite walls. Attached to the main chamber is a gas purifier of the circulation type containing evaporated sodium metal. This reacts strongly with water vapour and oxygen, the two most objectionable of the common electronegative counter gas contaminants, but does not react with methane. Gas is pumped in and out of the counter through two needle valves, the moving parts of which are enclosed in bronze sylphon bellows to prevent grease from coming into contact with the gas.

The filling procedure was as follows: the air in the counter was replaced by methane and a pellet of sodium dropped into the purifier. The methane was then pumped out until a pressure of $\sim 10^{-4}$ mm Hg was obtained when the sodium was evaporated on to the walls of the purifier tube. Pumping was then continued for half a day, the chamber being outgassed periodically by heating with a flame. Methane was then allowed to pass slowly through a copper coil immersed in solid carbon dioxide and acetone to freeze out water vapour and was admitted to the counter until the pressure reached 2·38 atmospheres.

At this pressure and at the working voltage of 2·4 kv the gas multiplication of the counter was found to be 3 times. The counter pulses observed on an oscilloscope had rise times between 10 and 100 μsec—a rather greater spread than expected. According to measurements by English and Hanna (1953) of electron mobilities in methane, the spread due to electron straggling would have been expected to be ~ 3 μsec; this difference was not investigated and is not understood. To handle the long pulses satisfactorily rise and clipping time constants of 80 μsec were used in the amplifier, the output of which was fed to a 120 channel pulse amplitude analyser.

An energy calibration for the counter was obtained using the spectrum of α-particles from Th-X and its daughter products decaying with a half-life of 3·65 days. A small amount of polonium was included in the counter to give a continuous check on the calibration. The energy scale was found to be linear to within 1%.

§ 3. The Counter Experiment

Resonance radiation from the $^{7}Li(p\gamma)$ reaction was excited by bombarding a thick lithium metal target with 500 kv protons, the counter being situated with its axis perpendicular to the proton beam, and centre 10·8 cm from the target at 0°. Irradiation was carried out in 8 hour runs, alternating with background runs of similar duration; the $^{12}C(\gamma 3\alpha)$ counting rate was small ($\sim$140 per hour) necessitating a careful measurement of the counter background. Actually the $^{12}C(\gamma 3\alpha)$ peak produced by the 17·6 Mev γ-rays yields α-particles with a total energy of 10·3 Mev, well above the energy of the background due to radioactive contamination, and in 44 hours no background pulses over 9·2 Mev were observed. However, a knowledge of the background, mainly from polonium (100 counts/hour) and radium (20 counts/hour), was important in an analysis of the tail of the 17·6 Mev peak and of peaks due to lower energy γ-rays.

The radiation was monitored using a thick-walled brass Geiger-counter identical in construction with that described and calibrated by Barnes *et al.* (1952). Readings of pulse counts were recorded at one hour intervals. The relative photodisintegration yield per quantum in the four runs was 1·00 : 1·00 : 1·06 : 0·96.

§ 4. The Cross Section at 17·6 Mev

The pulse spectrum resulting from 31 hours irradiation is shown in fig. 1 (*a*) which, after subtraction of the background given in 1 (*b*), leads to the curve of 1 (*c*). The high energy peak contains approximately 2900 counts, has a half-width of 0·8 Mev, and centres at $10{\cdot}30 \pm 0{\cdot}06$ Mev as expected from the mass data which gives the reaction threshold as 7·28 Mev. Contributions to the spectrum below the main peak come from γ-ray pile-up pulses, α-particles from 17·6 Mev events which are not contained entirely within the counting region, and $^{12}C(\gamma 3\alpha)$ events induced by γ-rays of energies less than 17·6 Mev. The contribution from γ-ray pile-up pulses was estimated by extrapolating the low energy tail measured with the kicksorter bias at a reduced value. The 'pile-up' pulse contribution, although small was significant, amounting to 130 counts per channel at 5 Mev, decreasing to 10 counts per channel at 8 Mev for a 31 hour run.

To allow for losses to the walls a knowledge of the ranges and directions of the α-particles is necessary. The correction applied assumes the disintegrations to be two-stage:

$$^{12}C \rightarrow \alpha + {}^{8}Be\,; \qquad {}^{8}Be \rightarrow 2\alpha$$

and to be isotropic, with 93% of the transitions through the 2·9 Mev level of ^{8}Be, and the remaining 7% through the ground state. A range–energy relation for α-particles in methane was deduced from the curves of Livingstone and Bethe (1937) and correction factors were derived from

those for single α-particles to give the fraction of events in which one or two α-particles of a star intercept the boundaries of the counter. The energy distribution of the resulting degraded pulses was calculated and amounts to approximately 42 counts per channel between 6 and 9·5 MeV. The shape of the distribution has little effect on the magnitude of the peak at 17·6 MeV, but makes the yield at lower energies uncertain and it is for

Fig. 1

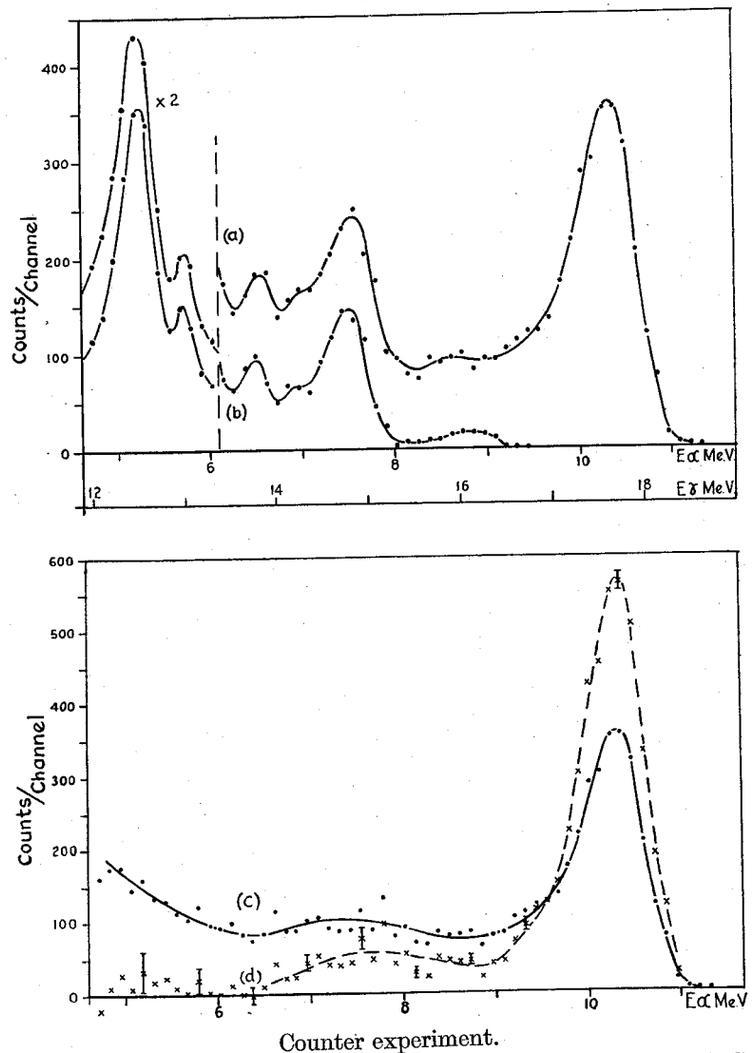

Counter experiment.

(*a*) Pulse spectrum obtained in 31 hours irradiation of CH_4 counter. (*b*) Counter background spectrum normalized to 31 hours running time. (*c*) Pulse spectrum resulting from disintegration of ^{12}C (difference of (*a*) and (*b*)). (*d*) Corrected distribution.

this reason that the cross section at 17·6 MeV only has been calculated from the counter data.

The final distribution fig. 1 (*d*) was derived from fig. 1 (*c*) by subtracting the ' pile-up ' pulse distribution and the pulse distribution arising from wall losses and then adding the loss corrections at the appropriate energy to the 17·6 MeV peak. The peak is asymmetrical probably because the amplifier time constants were shorter than the rise-times of some of the pulses ; the value 80 μsec was chosen for the time constants to give the best compromise between lack of uniformity in pulse height and difficulties due to the γ-ray ' pile-up ' pulses.

A small correction for absorption of radiation in the counter walls was calculated from data given by Heitler (1949). The intensities of the γ-ray lines were assumed to be in the ratio 17·6 : 14·8 : 12·3 :: 0·62±5% : 0·36±12% : 0·02±50%, the first two being based on data of Stearns and McDaniel (1951) the last figure being based on Inall (1954) and Titterton (1953).

The final value for the cross section at 17·6 MeV is

$$\sigma_{17\cdot6}(^{12}C\gamma 3\alpha)=(1\cdot70\pm0\cdot24)\times10^{-28}\ \text{cm}^2.$$

Table 1. Absolute measurements of the cross section for $^{12}C(\gamma 3\alpha)$

Author	σ_{mean}	$\sigma_{17\cdot6}$
Wäffler and Younis (1949)	$0\cdot8\pm0\cdot3\times10^{-28}$ cm^2	
Glattli, Seippel and Stoll (1952)	$1\cdot75\pm0\cdot25$	$2\cdot4\times10^{-28}$ cm^2
Goward and Wilkins (1953)*	$1\cdot4\ \pm0\cdot26$	$1\cdot70\pm0\cdot34$
Greenberg, Taylor and Haslam (1954)†		1·7
Present work	$1\cdot19\pm0\cdot20$	$1\cdot70\pm0\cdot24$

* Combination of lithium γ-rays and bremsstrahlung measurements.
† Bremsstrahlung measurement.
The value for $\sigma_{17\cdot6}$ from Li γ-rays depends on the relative intensity assumed for the 17·6 MeV line which is not the same in the experiments listed.

§ 5. Photographic Plate Measurements

Incidental to another investigation some 1000 $^{12}C(\gamma 3\alpha)$ ' stars ' were measured in Ilford 200 μ type E_1 boron-loaded emulsions which had been exposed to $^7Li(p\gamma)$ resonance radiation. The stars were identified by the usual method of momentum balance and the number-energy histogram is given in fig. 2 (*a*). Three peaks are resolved, the main one at 17·6 MeV contains 742 events, the broad 14·8 MeV group has 86 events while the group centring on 12·5 MeV has 17 events. These numbers may be compared with 2160, 300, 35 observed by Nabholz *et al.* (1952) and 390, 50, 12 observed by Goward and Wilkins (1953).

Loss corrections were made by the geometric method of Goward and Wilkins (1953) and the smooth distribution (full line of fig. 2 (*a*)) obtained. The final result is compared with the methane chamber data in fig. 2 (*b*), the curves being normalized by the area of the 17·6 MeV peaks.

Fig. 2

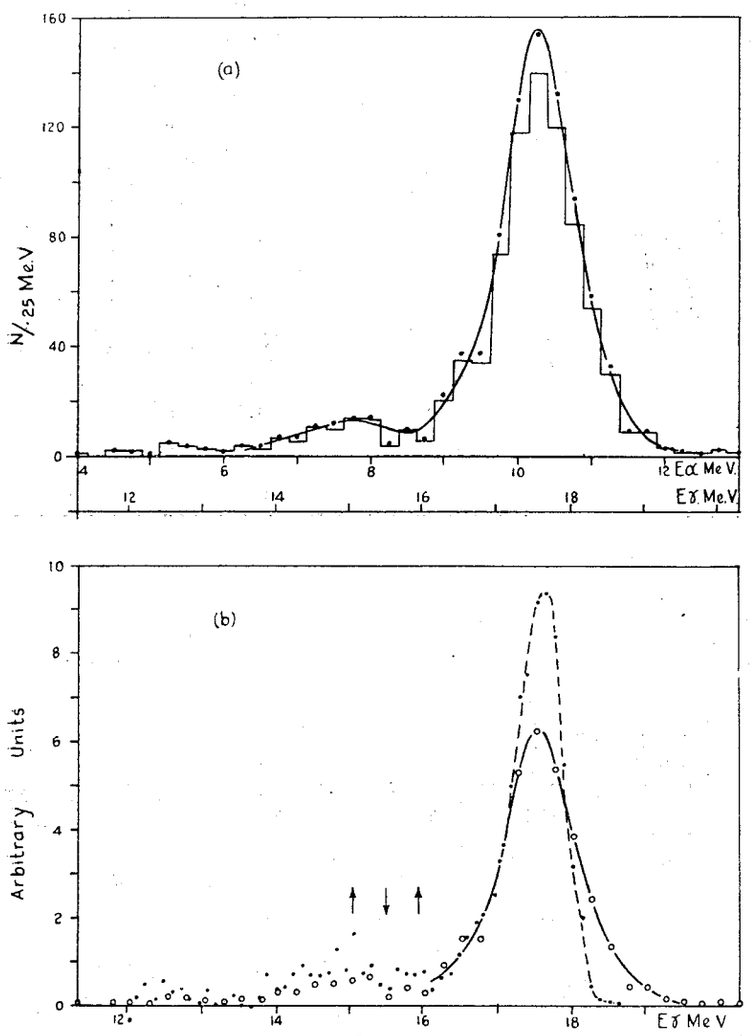

Photographic plate.

(*a*) Histogram of energy released in 845 $^{12}C(\gamma 3\alpha)$ ' stars ' with corrected curve superimposed. (*b*) Comparison of results from methane counter and photographic plate normalized by areas of the high energy peak. • counter, ∘ plate.

§ 6. Cross Sections at 14·8 and 12·3 MeV

Taking the cross section at 17·6 MeV to be $1{\cdot}70\times10^{-28}$ cm² and the relative intensities of the 17·6 and 14·8 MeV lines to be as given in § 4 the photographic plate data gives :

$$\sigma_{14\cdot8}(^{12}C\gamma 3\alpha)=(0{\cdot}33\pm0{\cdot}07)\times10^{-28}\ \text{cm}^2.$$

The group centring on 12·5 MeV in fig. 2 (*a*) could be due to a reaction of the type $^{12}C(\gamma\gamma')3\alpha$, if a level of ^{12}C is available at the appropriate energy. However there is strong evidence from experiments in this laboratory (Titterton 1953, Inall and Boyle 1953, Inall 1954) that there is a weak line at 12·3 MeV corresponding to a transition to a state of ^{8}Be at 5·3 MeV. We therefore discard the possibility that the group may be due to the inelastic scattering of γ-rays and calculate the cross section for the $^{12}C(\gamma 3\alpha)$ reaction at 12·3 MeV taking the intensity of these γ-rays to be $(2\pm1)\%$ of the total radiation. The figure obtained is :

$$\sigma_{12\cdot3}(^{12}C\gamma 3\alpha)=(1{\cdot}15\pm0{\cdot}6)\times10^{-28}\ \text{cm}^2.$$

Using the same set of conditions and normalizing all cross sections to our 17·6 MeV figure, cross sections at 14·8 and 12·3 MeV have been calculated from the histograms published by Nabholz *et al.* (1952) and Goward and Wilkins (1953) and are presented in table 2. It will be seen that there is good agreement among the three experiments for the cross section at 14·8 MeV but considerable differences at 12·3 MeV.

Table 2. Cross section for $^{12}C(\gamma 3\alpha)$ at 14·8 and 12·3 MeV, normalized to $\sigma_{17\cdot6}=1{\cdot}70\times10^{-28}$. The lower two sets of results were calculated from the published histograms. The relative γ-ray intensities used are :

I(17·6 MeV)$=0{\cdot}62\pm5\%$ I(14·8 MeV)$=0{\cdot}36\pm12\%$ I(12·3 MeV)$=0{\cdot}02\pm50\%$

Source	Cross section × relative γ-ray intensity			Cross section in 10^{-28} cm²			Mean
	17·6 MeV	14·8 MeV	12·3 MeV	17·6 MeV	14·8 MeV	12·3 MeV	
Present work, CH_4 counter	1·05			1·70±0·24			
Present work	1·05±2·3	0·118±7	0·023±16		0·33±0·07	1·15±0·6	1·19±0·20
Nabholz *et al.*	1·05±1·4	0·144±3·7	0·015±11·5		0·40±0·8	0·75	1·21±0·20
Goward and Wilkins	1·05±3·2	0·130±9	0·032±20		0·36±0·07	1·6	1·21±0·20

The high value of $\sigma_{12\cdot3}$ implies the presence of a ^{12}C level in this region and the resonance absorption of radiation of this energy. Such an interpretation is supported by some of the bremsstrahlung data and by results obtained in a study of the reaction $^{12}C(nn')3\alpha$ by Livesey and

Smith (1953). Excitation functions over the region 12–18 MeV have been measured with poor agreement by five groups and are presented in fig. 3 ; the present three points have been plotted for comparison.

Inspection of both the methane chamber and the photoplate data over the width of the 14·8 MeV line, fig. 2 (*b*), shows elevation of the points near 15 and 16 MeV and a trough at 15·5 MeV as indicated by the arrows. Taken separately little weight could be placed on either result, but the two sets of data support each other. Moreover, examination of the photoplate results of Goward and Wilkins (1953) and Nabholz *et al.* (1952) show the same features to be present in each of these experiments. Taken together these results lend support to the presence of peaks in the cross section at 15 MeV and 16 MeV as observed by Goward and Wilkins (fig. 3) but suggest that the resonances are more marked than their excitation function indicates.

Fig. 3

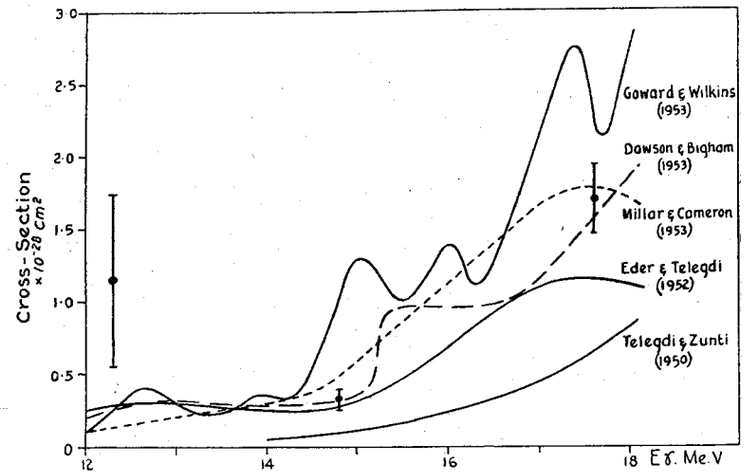

Cross sections for the reaction $^{12}C(\gamma 3\alpha)$ over the region 12–18 MeV. ∓ present results plotted.

The present experiment therefore gives strong evidence for the resonance absorption of γ-radiation by the ^{12}C nucleus near to 12·3 MeV and suggests the presence of other resonances near 15 and 16 MeV.

References

Barnes, C. A., Carver, J. H., Stafford, C. H., and Wilkinson, D. H., 1952, *Phys. Rev.*, **86**, 359.

Dawson, W. K., and Bigham, C. B., 1953, *Canad. J. Phys.*, **31**, 167.

Eder, M., and Telegdi, V. L., 1952, *Helv. Phys. Acta*, **25**, 55.

English, W. N., and Hanna, G. C., 1953, *Canad. J. Phys.*, **31**, 768.

Glattli, H., Seippel, O., and Stoll, P., 1952, *Helv. Phys. Acta*, **25**, 491.

Goward, F. K., and Wilkins, J. J., 1953, *Proc. Roy. Soc.* A, **217**, 357.

Greenberg, L. H., Taylor, J. G. V., and Haslam, R. N. H., 1954, *Phys. Rev.*, **95**, 1540.

Heitler, W., 1949, *The Quantum Theory of Radiation*, 2nd Ed. (Oxford : University Press).

Inall, E. K., and Boyle, A. J. F., 1953, *Phil. Mag.*, **44**, 1081.

Inall, E. K., 1954, *Phil. Mag.*, **45**, 768.

Livesey, D. L., and Smith, C. L., 1953, *Proc. Phys. Soc.* A, **66**, 689.

Livingston, M. S., and Bethe, H. A., 1937, *Rev. Mod. Phys.*, **9**, 245.

Millar, C. H., and Cameron, A. G. W., 1953, *Canad. J. Phys.*, **31**, 723.

Nabholz, H., Stoll, P., and Waffler, H., 1954, *Helv. Phys. Acta*, **25**, 153.

Stearns, M. B., and McDaniel, B. D., 1951, *Phys. Rev.*, **82**, 450.

Telegdi, V. L., and Zunti, W., 1950, *Helv. Phys. Acta*, **23**, 745.

Titterton, E. W., 1953, *Aust. J. Science*, **15**, 174 ; 1955, *Progress in Nuclear Physics IV* (London : Pergamon Press).

Waffler, H., and Younis, S., 1949, *Helv. Phys. Acta*, **22**, 614.

From the PHILOSOPHICAL MAGAZINE, Ser. 7, vol. 44, p. 1191,
October 1953.

The Cross Section for ^{181}Ta (γ, n) ^{180}Ta *at* 17·6 MEV

By J. H. CARVER and H. J. HAY
Research School of Physical Sciences, Australian National University, Canberra*

[Received July 28, 1953]

THE apparent ' resonance ' character of many photo-nuclear reactions is now well known. In the main these processes have been studied with the aid of the bremsstrahlung produced by betatrons and synchrotrons and the reaction identified by activation techniques (a number of references has been given by Carver, Edge and Wilkinson 1953). One of the reactions which has been most thoroughly investigated by this technique is the ^{181}Ta (γ, n) ^{180}Ta reaction. The figure shows the cross section for this reaction as determined by Haslam, Smith and Taylor (1951). Using the gamma-rays from the ^{7}Li (p, γ) reaction, Carver, Edge and Wilkinson (1953) showed that competing reactions did not destroy the ' resonance ' character of the gamma-ray absorption. They found the ratio of the cross sections for ^{181}Ta (γ, 2n) ^{179}Ta at 17·6 MEV to ^{181}Ta (γ, n) ^{180}Ta at 14·6 MEV to be $0{\cdot}29 \pm 0{\cdot}11$.† Taken at their face value these measurements indicate that, at gamma-ray energies of the order of 18 MEV and greater,

* Communicated by Professor E. W. Titterton.

† This result agrees with the neutron yield measurements obtained by Halpern, Nathans and Mann (1952) and Whalin and Hanson (1953) using betatron bremsstrahlung and with the indirect estimate made by Eyges (1952).

the gamma-ray absorption occurs almost entirely by means of direct interaction rather than by the immediate formation of a compound nucleus. The (γ, 2n) cross section at 17·6 MeV (Carver, Edge and Wilkinson 1953) is only slightly larger than the (γ, n) cross section at 17·6 MeV (Haslam, Smith and Taylor 1951) whereas calculations based on the statistical theory (Blatt and Weisskopf 1952) indicate that the (γ, 2n) cross section at 17·6 MeV should be some 16 times the (γ, n) cross section at 17·6 MeV.

In order to determine whether or not the high energy tail in the ^{181}Ta (γ, n) ^{180}Ta cross section is indeed as large as is indicated by the bremsstrahlung results we have measured the ratio of the cross sections for this reaction at gamma-ray energies of 14·6 and 17·6 MeV using the

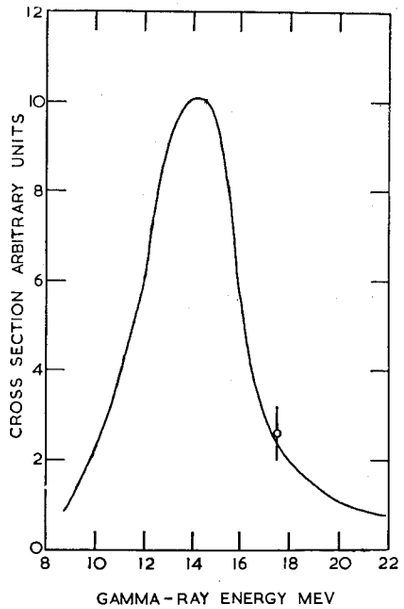

The cross section for ^{181}Ta (γ, n) ^{180}Ta at 17·6 MeV compared with the curve obtained by Haslam, Smith and Taylor (1951).

radiation from the ^{7}Li (p, γ) reaction. The principle of the method was the same as that used by Carver, Edge and Wilkinson (1953) except that a measurement of the induced ^{180}Ta activity (half life 8·15 hr) replaced the total neutron yield measurement.

The proton bombardment of lithium produces gamma-rays of 17·6 MeV (negligible width) and 14·6 MeV (2 MeV width) and the relative intensity of these gamma-rays depends on the proton energy. At a proton energy of 500 keV (thick target) the ratio of the intensity of the 17·6 MeV line to that of the 14·6 MeV line is 1·70$\pm$0·20 ; at 1·15 MeV (target thickness 250 keV) this ratio is 0·45$\pm$0·06 (Stearns and McDaniel 1951). These ratios apply to radiation emitted at an angle of 75° to the proton beam. We have

irradiated a tantalum Geiger counter under these conditions and determined, at both proton energies, the relative induced ^{180}Ta activity per incident quantum. Throughout the irradiations (which were for periods of about eight hours) the gamma-ray yield was monitored continuously by a NaI (Tl) crystal which was biased so that none of the $\sim$0·5 MeV quanta, due to inelastic scattering at the higher proton energy, was detected. Several irradiations were performed at both proton energies and corrections were made for fluctuations in the gamma-ray yield assuming the half-life of ^{180}Ta to be 8·15 hr. It was found that the ratio of the ^{181}Ta (γ, n) ^{180}Ta cross section at 17·6 MeV to that at 14·6 MeV was 0·26$\pm$0·06.* As shown in the figure this result agrees with the bremsstrahlung results and therefore confirms the conclusions drawn by Carver, Edge and Wilkinson (1953) concerning the importance of direct effects at gamma-ray energies above the ' resonance '.

References

Blatt, J. M., and Weisskopf, V. F., 1952, *Theoretical Nuclear Physics* (Wiley).
Carver, J. H., Edge, R. D., and Wilkinson, D. H., 1953 a, *Phil. Mag.*, **44,** 404 ; 1953 b, *Phys. Rev.*, **89,** 658.
Eyges, L., 1952, *Phys. Rev.*, **86,** 325.
Halpern, J., Nathans, R., and Mann, A. K., 1952, *Phys. Rev.*, **88,** 679.
Haslam, R. N. H., Smith, L. A., and Taylor, J. G. V., 1951, *Phys. Rev.*, **84,** 840.
Stearns, M. B., and McDaniel, B. D., 1951, *Phys. Rev.*, **82,** 450.
Whalin, E. A., and Hanson, A. O., 1953, *Phys. Rev.*, **89,** 324.

* This result applies to a monochromatic gamma-ray of 14·6 MeV and not to the broad line used in the experiment. We have corrected our result for the width of this line (and for the 0·6 MeV increase in gamma-ray energies at the higher proton energy) by assuming that near 14·6 MeV and near 17·6 MeV the shape of the (γ, n) cross section is as given by Haslam, Smith and Taylor (1951) but no assumption as to the relative magnitudes of the 14·6 and 17·6 MeV cross sections has been made.

† Communicated by the Author.